Electromagnetic Penetration of Structures Considering High-Altitude Electromagnetic Pulse

A Thesis Presented for the
Master of Science
Degree
The University of Tennessee, Knoxville

David P. Mignardot
May 2024

DEDICATION

This work is dedicated to my parents Henry and Elise Mignardot, who have taught me the value of hard work and unbounded aspiration.

"If we knew what it was we were doing, it would not be called research, would it?"
— Albert Einstein

"Almighty God, Who hast created man in Thine own image, and made him a living soul that he might seek after Thee, and have dominion over Thy creatures, teach us to study the works of Thy hands, that we may subdue the earth to our use, and strengthen the reason for Thy service"
— James Clerk Maxwell

"I start where the last man left off"
— Thomas A. Edison

"Go as far as you can see; when you get there, you'll be able to see farther"
— J. P. Morgan

ACKNOWLEDGEMENTS

I would first like to thank electromagnetic and power system subject matter experts DaHan Liao, Benjamin McConnell, and Lawrence Markel for their guidance and assistance with the work contained in this thesis. I have learned a tremendous amount from the experience of these individuals and am very appreciative of their willingness to share it.

I would also like to thank my advisor Yilu Liu who always challenged me to think critically and from a variety of perspectives. Her support throughout my graduate education has been invaluable.

ABSTRACT

The electric power system is undergoing transformation in the 21st century. Generation is becoming more distributed, more electronic equipment is utilized for operation and control, and load demand is increasing with society's electrification. As this transformation occurs, both new and old threats to the system's resilience are of concern. Of the old threats, and a critical component when studying resilience, is high-altitude electromagnetic pulse (HEMP). In this thesis, weaponized electromagnetic pulse and its interaction with the power system is revisited with an emphasis on structure shielding effectiveness against both radiated and conducted energy. Computational electromagnetic plane wave simulations are carried out to analyze many variables associated with a structure's shielding effectiveness. The variables fall into three main categories including radiation incidence, structure design characteristics, and cable coupling. As a result of this work, a structure's attenuation behavior is identified as highly frequency dependent, especially for the electric field. Parameters associated with the incident radiation, which constitute a worst-case response are identified. A structure's architecture is influential towards the building's electromagnetic shielding effectiveness, especially when large apertures and reinforced concrete are present. Penetrating cables which couple electromagnetic energy are realized as a significant radiation infiltration pathway into a structure's interior. Length of conductor, cableshields, and grounding are identified as the most influential variables regarding cable coupling. The results obtained serve as a collection of general observations which can be extended to more specific, detailed studies.

TABLE OF CONTENTS

LIST OF TABLES

LIST OF FIGURES

LIST OF ABBREVIATIONS

AoI – Angle of incidence
E – Electric
E1 – Early time component of high-altitude electromagnetic pulse
EM – Electromagnetic
EMI – Electromagnetic interference
EMP – Electromagnetic pulse
FDTD – Finite difference time domain
HEMP – High-altitude electromagnetic pulse
HOB – Height of burst
HPM – High power microwaves
IEMI – Intentional electromagnetic interference
LEMP – Lightning electromagnetic pulse
M – Magnetic
MoM – Method of Moments
NEMP – Nuclear electromagnetic pulse
PEC – Perfect electric conductor
RF – Radio frequency
SPD – Surge protection devices

Chapter 1

Introduction and Motivation

1.1 Introductory Overview

Power System resilience has become a subject of increasing importance in recent years. Resilience encapsulates the system's ability to maintain operability and recover efficiently after enduring an extreme disturbance. Extreme disturbances typically affect a wide area, and can range from harsh weather events to human-organized malicious acts. Power system engineers study the effects of events such as extreme weather (hurricanes, excessively high/low temperatures, wildfires, widely dispersed lightning events), cyberattacks, and geomagnetic disturbances (GMD) to ensure the design of the system, and its components, is hardened for such events. Although the frequency of occurrence of these extreme disturbances may be low, or unknown, the potential damage posed on the power system can be extensive; as is the case of electromagnetic interference (EMI). In the early years of the atomic age, high-altitude nuclear weapons tests such as the United States' STARFISH PRIME revealed intense electromagnetic (EM) effects produced by such a detonation. The EM effects proved to be much more severe than expected as the theory at the time of these tests did not expect the detonations to be intense EM generators [1]. Impairment to electric components of on-the-ground infrastructure consisted of street light failure, circuit breaker tripping, damage to relays, damage to overhead and buried cables, blown fuses, spark gap breakdown, and surge arrester burnout [1]. The generated electromagnetic pulse (EMP) from nuclear detonations in the upper regions of Earth's atmosphere (30 km or higher above the Earth's surface) is commonly referred to as high-altitude electromagnetic pulse (HEMP). The following section of this document provides a brief review of HEMP.

1.2 Overview of High-Altitude Electromagnetic Pulse

The term "high-altitude" refers to the stratospheric, mesospheric, and thermospheric regions of Earth's atmosphere in this context (approximately between 30 and 500 km above the Earth's surface). Metatech, using theory developed by Conrad Longmire, determined the maximum EMP response is achieved when the height of burst (HOB) is between 50 and 100 km (30-60 miles) above ground level [2]. High energy (greater than 2 MeV) gamma radiation from the nuclear burst interacting via Compton scattering with atmospheric molecules produces relativistic electrons. These electrons then rotate in the Earth's magnetic field which produces a fast-rising transverse electromagnetic plane wave that propagates away from the burst towards Earth. A more detailed explanation of the generation of HEMP can be found in previous studies [2]—[7]. HEMP consists of three components E1, E2, and E3 which are associated with the early, middle, and late time characterization respectively. The E1 component is a strong pulse with a fast rise time in the 5-10 nanosecond range (much faster than typical power system transients). The maximum electric field intensities from the E1 pulse is nominally 50 kV/m or higher [4]. The E2 pulse can be described in a similar manner to the EMP produced from intense lighting strikes; however, it occurs over a large area and follows the E1 pulse. The E3 component produces effects more intense but of shorter duration than the electromagnetic behavior from geomagnetic disturbances such as solar flares and coronal mass ejection. E2 and E3 fields can reach 100 V/m and tens of V/km respectively. Figure 1.1 pictures the time domain behavior of HEMP, and Figure 1.2 displays the spectral density of various EM environments including the E1 component of HEMP. E2 may be protected by lightning surge arrester equipment and possesses weaker field intensity when compared to E1. E3 is similar to effects from geomagnetic disturbances which have been studied extensively. Therefore, the remainder of this work will solely focus on the E1 component which poses significant hazard to electric equipment and remains the least understood electromagnetic threat.

1.3 Motivation

With a new era of electrification, society is further increasing utilization of electrical components and thus increasing electrical power demand. Electronic equipment and digital control systems are less robust against electromagnetic interference (EMI). Resilience and reliability are key aspects to ensure customers get power when they need it most. The previous statement in combination with escalated geopolitical tensions, introduces a need for further understanding of electrical systems' vulnerability considering malicious outside forces. As the last nuclear weapons testing took place in the early 1990s, it is imperative to build upon previous works and discover new methods of studying the effects of HEMP. Little knowledge exists on E1 interaction with structures on a detailed level and therefore this study aims to fill the gap in knowledge. With results obtained from this work, researchers and engineers are able to establish a more complete picture on power system vulnerability associated with HEMP.

1.4 Organization Structure

This thesis provides an analysis of the interaction between HEMP and structures which emulate power plant infrastructure or similar facilities. The contents of this thesis are organized into six main chapters succeeding the introduction. A literature review and

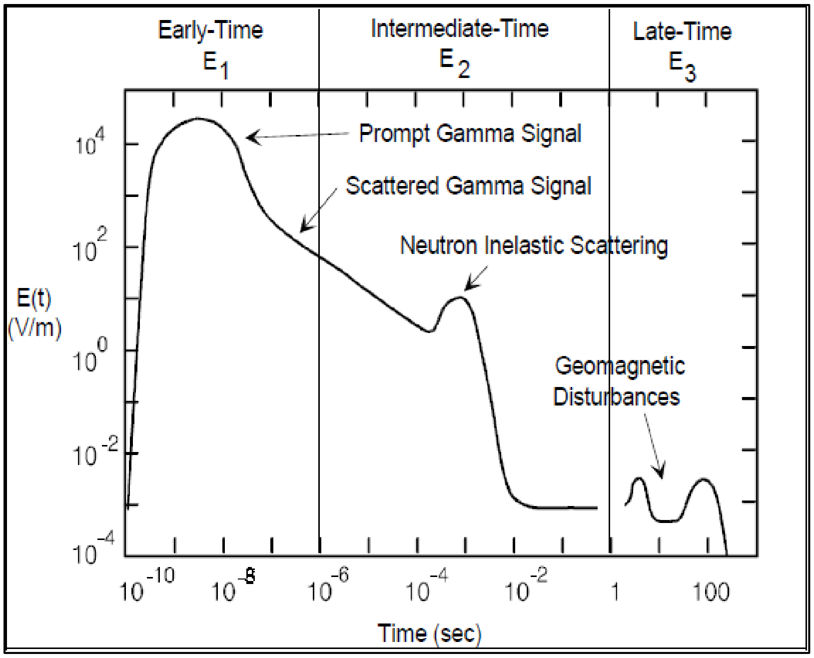

Figure 1.1 Time domain characterization of high-altitude electromagnetic pulse [8].

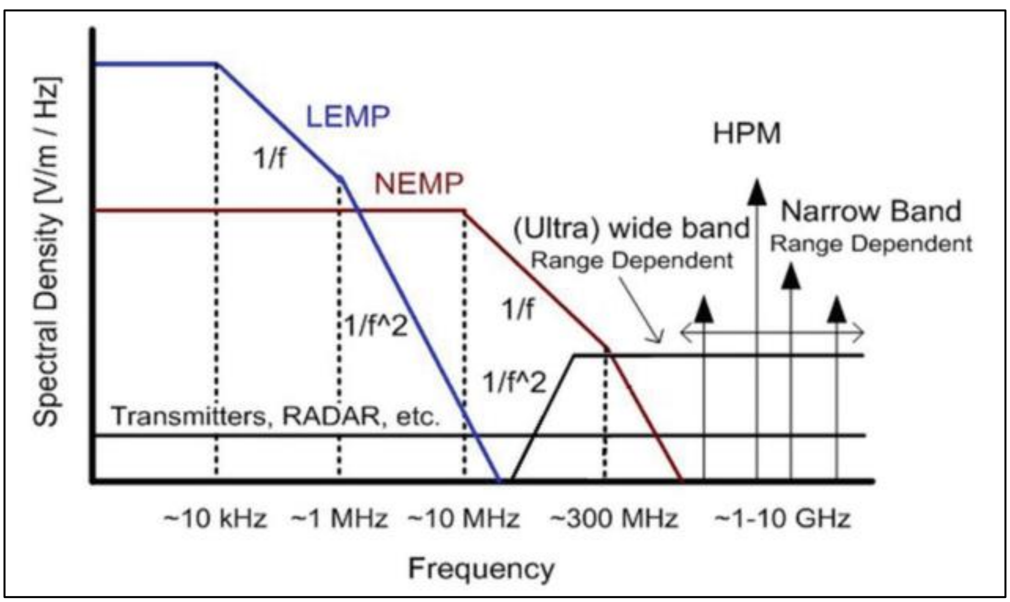

Figure 1.2 Spectral densities of various EM environments including lightning EMP (LEMP) and high-altitude nuclear EMP (NEMP) [9].

a chapter providing background information relevant to the work follows the introduction. Each chapter subsequent to the background review, and leading up to the conclusion, focuses with increasing complexity on the scope of the problem. Chapter 4 will examine the fundamentals of electromagnetic penetration of building structures. Chapter 5 incorporates apertures and composite construction materials into the scope of study. Chapter 6 further increases the level of problem complexity by including structure penetrating cables. Each body chapter discusses the approach, method, and results of associated work. Finally, the seventh chapter concludes the study and provides recommendations for future work.

Chapter 2

Literature Review

2.1 Studies on HEMP Phenomena

Extraordinary scientific achievements such as Heinrich Hertz's discovery of electromagnetic waves in 1888 and Arthur Compton's discovery of the Compton Electron Effect in 1923, paved the way for the science of EMP to unfold decades later. New discoveries and increased understanding of course began to take place in 1945 with the beginning of the atomic era. Carl Baum highlights key points in the timeline of EMP history [10]. For example, at the Trinity Test, Enrico Fermi had predicted intense EM effects resulting from the burst [11]. Throughout the 1950s, and until the Limited Test Ban Treaty was signed in 1963 prohibiting open air nuclear tests, discoveries regarding nuclear EMP continued to be made. At the time, British scientists referred to this new phenomenon as 'radioflash'. Although disruption to instrumentation and measurement systems had been observed since Trinity, the intensity of radioflash was not realized until Operation Fishbowl was conducted by the United States in the early 1960s. Fishbowl consisted of high-altitude nuclear tests, and results from the STARFISH PRIME test indicated significant damage to civilian electric power and communication systems was possible [1]. As a result of the open-air nuclear tests which had been conducted, an abundance of literature regarding nuclear EMP was published including comprehensive works [7], [12]-[14]. Shortly later, work was done to include the study of other EMP environments such as high-power microwaves (HPM) and pulses from intense, indirect lightning strikes.

2.2 Studies on HEMP Interaction with the Power System

HEMP is typically considered a low probability, high risk event. However, this probability may be described as unknown. Systems at the highest risk level include electronically controlled systems and the electric power system. D. Wang et al. provides an overview of power system resilience considering HEMP including topics such as threat identification, EMP detection, and protection strategies [15]. Table 2.1 conveys EMP impact criticality of various infrastructure equipment.

Driven by Cold War era tensions and the knowledge of HEMP's damaging effects, a push to harden military and civilian systems took place. Advanced testing methods were developed after the 1963 Test Ban Treaty took effect. Such methods were designed to evaluate various systems under the strain of EMP environments. Literature

Table 2.1 EMP Impact on Critical Infrastructure [15].

Equipment At Risk	EMP (Nuclear)	Solar Storm	Cyber	Physical Attacks	Radio Frequency Weapons
Generator Stations	DPE	DEU	DPE	DPE	DPE
SCADA/Industrial Controls	DPE	DPE	DPE	DPE	DPE
Utility Control Centers	DPE	DPE	DPE	DPE	DPE
Transformers	DPE	DPE	PPE+CE	DPE	DPE
Telecommunications Including Cellphones	DPE	DPE	DPE	CE	CE
Internet	DPE	DPE	DPE	CE	CE
Radio Emergency Communications	DPE	TE	CE	CE	CE
Emergency SATCOM Communications	DPE	TE	CE	CE	CE
GPS	DPE	TE	CE	CE	CE
Transportation	DPE	CE	CE	CE	CE
Water	DPE	CE	PPE+CE	CE	CE

DPE = Direct Permanent Effects.
DEU = Direct Effects Uncertain.
CE = Cascading Effects (if no backup power).
DPE+CE = Potential Permanent Effects plus Cascading Effects.
TE = Temporary Effect (0.5-36 hours) assuming backup power.

has documented and compared the various EMP test procedures such as EMP simulators, continuous wave testing, and pulsed signal injection [8], [12], and [16]. These methods were utilized to study EMP interactions with the power system. With the advent of The War on Terror and modern geopolitical conflicts, a second push to further understand the impacts of weaponized EMP events ensued. In 2001 the United States Congress allocated resources for the creation of the EMP Commission whose objective was to assess the threat of a weaponized EMP to the United States. The Commission produced a report in 2004 introducing the threat and infrastructure which was at risk [1]. "A single EMP attack may well encompass and degrade at least 70% of the Nation's electrical service" [1]. Such a statistic is alarming, especially when considering the recent upward trend of electrical demand with society's electrification and decarbonization goals. Power system damage and interruption from the E1 pulse can manifest from impaired electronics, triggered protection systems, EM coupling, and flash over incidents. The E2 pulse may also trigger and damage power system protection schemes. E3 may pose damage to transformers, loads and other connected equipment as low frequency currents are coupled onto power lines. Power system damage may be severe when considering a combination of the three pulses as in a real event. In 2010 Edward Savage, James Gilbert, and William Radasky published a report including significant detail on E1 interaction with the power system [4]. More policy was established to prioritize studying the effects of an EMP event with the Critical Infrastructure Protection Act of 2016 and the Coordinating National Resilience to Electromagnetic Pulses Executive Order of 2019. As a result, more literature assessing EMP threats to the Nation's power grid was published, including the comprehensive report from the Electric Power Research Institute (EPRI) in 2019 [17]. The EPRI study performed extensive testing on digital protective relays (DPRs) and determined such devices are able to withstand exposure to an E1 HEMP environment. Communication systems such as supervisory control and data acquisition (SCADA) were deemed susceptible to both radiated and conducted hazards. Additionally, E1 mitigation measures were tested and the study noted hybrid technology surge protection devices (SPDs) performed best. Large scale power system disruption was not expected from the effects of E1 alone. Transformer damage resulting from E3 and the extreme harmonics placed on grid components was predicted to cause large scale system disruption and blackout conditions.

2.3 Studies on Structure Shielding and Electromagnetic Penetration

The previous section presents an abundance of studies which investigated effects of HEMP on the bulk power system. However, fewer studies focus on facility infrastructure which is connected to the bulk power system such as generation plants. As mentioned previously, seminal works on the HEMP topic were produced during the height of the Cold War several decades ago. Large concern of nuclear attacks and nuclear disaster due to power plant failure existed during this time period. Therefore, studies assessing the resilience of nuclear power plants were conducted and some included the threat of HEMP. P. R. Barnes and J. Marable produced a study to analyze surges induced on nuclear power plant cables from HEMP [18]. For the cable study, the researchers assumed a frequency-independent structure shielding effectiveness of 20 dB for both the electric and magnetic fields. This assumption was chosen on the basis of experimental data obtained by measuring field strengths inside and outside of Sequoyah Nuclear Plant. Experimentation was conducted for sources of both FM and AM frequency ranges. (88-108 MHz, and 540-1700 kHz respectively). It is worthwhile to note, the study mentioned the 20 dB value was measured near the exterior walls of the facility while shielding towards the interior center was much greater. Results from the previously discussed study led to another work investigating the possible effects to critical systems within the plant exposed to EMP-induced cable surges [19]. Forced plant shutdown was concluded as the most likely possibility due to these effects. Despite conclusions from the previous studies, safety was still a concern especially regarding the capability of executing a safe shutdown after an EMP event has occurred and potentially damaged certain systems at a nuclear plant. In response to this concern, another study further investigated the interaction of an EMP with a nuclear power plant specifically focusing on the systems required for safe shutdown [20]. Three methods of EMP-facility interaction are mentioned in the report including direct penetration through the structure (diffused fields), coupling into the plant through power system connections, and coupling into the plant via subsystem instrumentation and control cables. High levels of structure shielding effectiveness were noted in the report due to Seismic Class I construction practices of the facility under test. The principal source of EMP energy was predicted to infiltrate the facility through penetrating cables and power lines. Overall, these studies predominantly considered nuclear powerplants. The commonly employed testing methods included direct signal injection and RF continuous wave radiation.

2.4 RF and Microwave Communications

Typical EM/structure interaction studies focus on maximizing radiation penetration in contrast to preventing it. Consideration for effective coverage in radio and cellular communication systems is an important design factor for certain buildings. Alejandro Aragon-Zavala states “These [radio propagation] mechanisms, combined with the complicated structure of real buildings, make the practical prediction of in-building propagation very challenging…” [21]. Although communication systems operate at higher frequencies, general observations and trends may be useful for studying a building’s interaction with E1 HEMP. Aragon-Zavala also points out many depolarizing effects occur when waves pass through a structure's walls and travel interiorly. For simplification purposes, linearly polarized plane waves are studied [21]. Although classical EM theory suggests propagation loss increases with frequency, this conclusion is not always accurate when analyzing indoor propagation. Many variables such as geometry, surface condition, material constitutive properties, and problem frequency complicate the propagation mechanics. Adeseko Ayeni et al. demonstrate how building materials' dielectric and magnetic properties influence building penetration loss [22]. When strong signal coverage is desired inside a structure, the building penetration loss is minimized via the aforementioned variables. The same variables must be considered when a threshold of penetration loss is desired for EMP protection. Military standard 188-125-1 specifies an adequate shielding effectiveness to be in the range of 40-80 dB depending on frequency [23].

2.5 My Contribution

Solely by the nature of HEMP generation, it is impossible to conduct a completely realistic experiment. Continuous wave and signal injection experiments are also difficult to organize as risks exist for operational facilities to be illuminated by potentially damaging, high power RF radiation. Additionally, such experiments are limited in terms of the equipment's variability. Due to the aforementioned reasons, a study utilizing EM simulations addresses impracticalities and variabilities associated with HEMP interaction studies.

Many previous works on HEMP's interaction with structures analyze nuclear powerplants. Due to the inherit safety risks of nuclear powerplants, they are designed and constructed with a larger factor of safety than other plants and structures. Thicker walls, earth berms, and larger-diameter, more finely spaced rebar not only improve structural rigidity and hazard protection, but also provides significant EM radiation shielding. Fewer studies have considered construction attributes reflecting more common structures. Studies focusing on equipment damage risks commonly simplify the scope by assuming a uniform, frequency-independent 20 dB attenuation. Although, as insinuated, the EMP/structure interaction is complex and the attenuation can vary significantly as a factor of many variables.

Chapter 3

Background Information

This chapter provides a review of concepts relevant to the work. The reader may find the information contained in this chapter to be helpful towards understanding the simulations and results discussed later in this thesis. As the nature of this work is heavily reliant on solution of Maxwell's equations of electromagnetism, a section providing background on the Method of Moments (MoM) computational solver scheme is included. Subsequently, a section discussing electromagnetic boundary conditions is included.

3.1 Method of Moments Numerical Solver

Analysis of many electromagnetic problems requires the solution of Maxwell's equations. For problems of high geometric and dielectric complexity, determining analytical solutions of Maxwell's equations becomes increasingly difficult. Computational methods which obtain approximate solutions are favorable especially due to the continuous advancements in digital computing capability achieved over the past several decades. Computational methods discretize the problem into a set of linear matrix equations which can be solved numerically. In general, electromagnetic boundary value problems can be classified with an operator equation as is exemplified in Equation 3.1.

$$L(f) = g \tag{3.1}$$

In Equation 3.1 L represents the system integral or differential operator, f represents the unknown, and g represents the excitation of the system. It is common to express the unknown f into a series of known functions multiplied by complex coefficients as in Equation 3.2. The known functions are referred to as basis functions and the coefficients, which are to be determined, are denoted by α. The formulation in Equation 3.2 is especially common in Method of Moments and finite element method applications.

$$f = \sum_{n=1}^{N} \alpha_n f_n \tag{3.2}$$

The various computational electromagnetic methods differ in the discretization of the problem, choice of basis function, and procedure to determine the unknown coefficients.

The Method of Moments (MoM) is a full wave solution of Maxwell's equations and the method's procedure is outlined in detail by Roger Harrington [24]. As Harrington states, "The name method of moments has been given to the mathematical procedure for obtaining the matrix equations" [24]. A brief overview of the method is presented as follows. The first step, known as pre-processing of Maxwell's equations, is to derive the integral equations which represent the problem. Green's function is utilized for the definition of the integral. The MoM is based on the method of weighted residuals and the residual can be defined using the linearity property and Equations 3.1 and 3.2 [25]. The residual *R* is represented in Equation 3.3 below.

$$R = \sum_{n=1}^{N} \alpha_n L(f_n) - g \tag{3.3}$$

The unknown coefficients can be determined by taking the inner product between the residual and a set of chosen weighting functions *w* one by one. Ramesh Garg points out "The inner product is also called the moment and therefore the name Method of Moments" [25]. Setting the inner product to zero results in a set of simultaneous equations which can be written in matrix form. The set and matrix form are defined is Equations 3.4 and 3.5 respectively [24].

$$\sum_{n=1}^{N} \alpha_n \langle w_m, L(f_n) \rangle = \langle w_m, g \rangle \tag{3.4}$$

$$[l_{mn}][\alpha_n] = g_m \tag{3.5}$$

If the *l* matrix is invertible, then a solution for the coefficients can be determined and thus the solution for *f* can be determined. The MoM is an approximate solution as the number of chosen basis and weighting functions is finite; and the accuracy of the solution is dependent upon the choice of basis functions, weighting functions, and the discretization size [25]. Various approaches for choosing the weighting functions exist such as Point Matching and Galerkin's Method. More details regarding such approaches can be found in references [25] and [26].

Many Computational EM software packages incorporate the MoM as a solver especially for radiation and scattering problems. Altair HyperWorks FEKO is a computational EM software and is used for the majority of work presented in this thesis. FEKO utilizes MoM as its default solver. Some advantages outlined in the FEKO user manual are the fact that MoM is a source method and only the entity being studied is discretized, and boundary conditions do not need to be set by the user [27]. In contrast, a method such as finite difference time domain (FDTD) requires volumetric discretization of the entire computational domain and the setting of an absorbing perimeter boundary condition. One disadvantage is the large memory requirement which results from a full system matrix encapsulating the interaction between each of the basis functions via Green's function [26]. FEKO makes use of the surface equivalence principle which replaces sources with equivalent electric and magnetic currents on the surface of an entity. Radiated field values can be calculated knowing the incident field and induced surface currents.

3.2 Electromagnetic Boundary Conditions

A simple way to define wave propagation is by means of a plane wave. For plane waves, quantities associated with the wave at an instant are constant through a plane defined perpendicular to the direction of propagation. An electromagnetic plane wave is a transverse wave thus the electric and magnetic fields exist perpendicular to each other and oscillate perpendicular to the direction which they are traveling. Figure 3.1 illustrates a plane electromagnetic wave. The magnitude of the electric and magnetic fields is related via the intrinsic impedance of free space or 377 Ω. In this work, a plane wave is an excellent idealization to employ as the interaction studied occurs very far away from the wave source. In other words, it is fair to assume a plane wave when the radiation travels tens to hundreds of kilometers before interacting with an object. The plane wave approximation allows for derivation of simple boundary conditions describing the interaction between a wave and object.

Electromagnetic boundary condition theory is covered in most electromagnetic fundamentals textbooks including [29] and [30]. Despite extensive coverage elsewhere, basic principles of electromagnetic interaction with a perfect conducting surface are discussed in this section due to the benefit of the knowledge when interpreting the results of this thesis. The earth beneath one's feet has a massive abundance of charge. When this earth is damp, or is dense with metallic particles, it can be a good conductor. Therefore, researchers commonly model the Earth's surface as a perfect electric conductor (PEC) to simplify the problem under study. It is important to note; this PEC assumption is rooted in a low frequency approximation. A. Kamra and M. Ravichandran point out the assumption of Earth's surface as a PEC is not always accurate depending on the geological composition and temperature of the ground [31]. However, this study focuses on structures located in moderate climate regions where the soil is primarily composed of sedimentary rock (significant portions of continental U.S.); and therefore, the PEC assumption is employed. The field inside a perfect conductor is zero and thus only exists at the surface. Therefore, consistent with EM boundary conditions, the tangential components of electric field are zero at the surface of a PEC. Consequently, the normal components of magnetic field are zero. The EM boundary conditions at the surface of a PEC are represented in equations 3.6 and 3.7.

$$E_{tan} = 0 \tag{3.6}$$

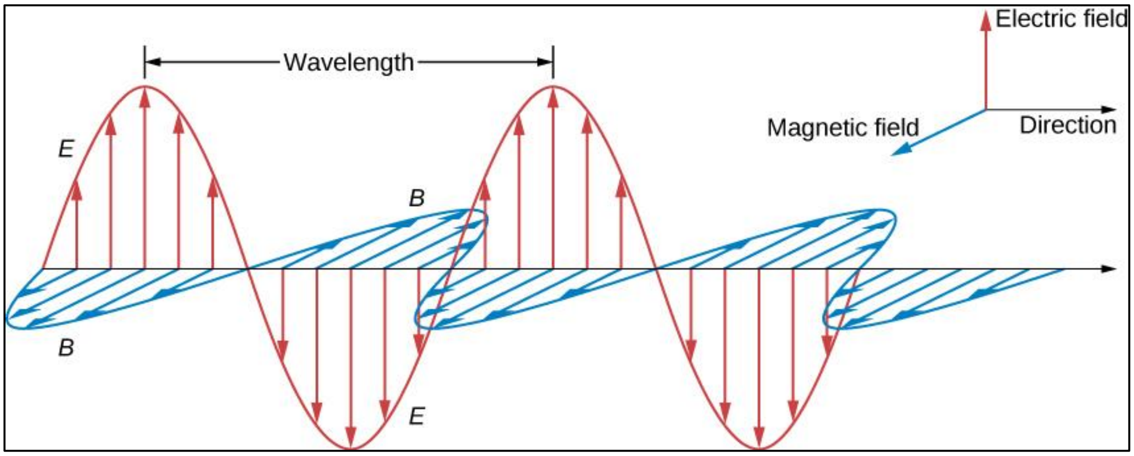

Figure 3.1 Representation of EM plane wave [28].

$$H_n = 0 \tag{3.7}$$

It is worthwhile to note, the above conditions hold approximately true for distances above the PEC surface which are small compared to the wavelength of the problem under study. Field strength vs. height above ground is plotted below in Figure 3.2.

Additionally, the PEC surface has infinite conductivity and zero resistance. Therefore, any incident EM wave will be completely reflected as no absorption is possible. Plane wave EM radiation interacting solely with a PEC surface, produces field values twice that of the incident value encapsulating the incident plus reflected waves. The previous statement refers to a specific scenario dependent upon polarization and angle of incidence of the incoming radiation. The following figures validate the aforementioned statements. When the radiation is horizontally polarized, only tangential components of E field exist regardless of AoI; thus the E field excitation at the surface is zero as plotted in Figure 3.3 (a). H field contains only tangential components when AoI is zero; thus the total excitation is the incident plus reflected wave. The H field excitation diminishes as the AoI approaches 90° and normal component is increased as illustrated in Figure 3.3 (b). However, when the radiation is vertically polarized only tangential components of magnetic field exist, and as AoI approaches 90° the normal component of E field increases, thus increasing the excitation as plotted in Figure 3.4. Notice when field strengths are at their maximum, the value represents twice the incident value due to the reflective property of the PEC ground plane.

It is evident the vertically polarized case enables the most intense excitation as the H field is always present in a tangential manner on the surface. With the horizontally polarized case, the E field is always present in a tangential manner, and therefore the E field excitation is zero. It is worthwhile to note the apparently increasing E field strength in the vertically polarized case is actually an oscillatory behavior as a function of distance. The field strength experiences maxima every quarter of a wavelength above the surface when the angle of incidence is normal to the ground plane. Figure 3.5 pictures the electric field strength plotted against height above ground plane up to one wavelength for various incident angles.

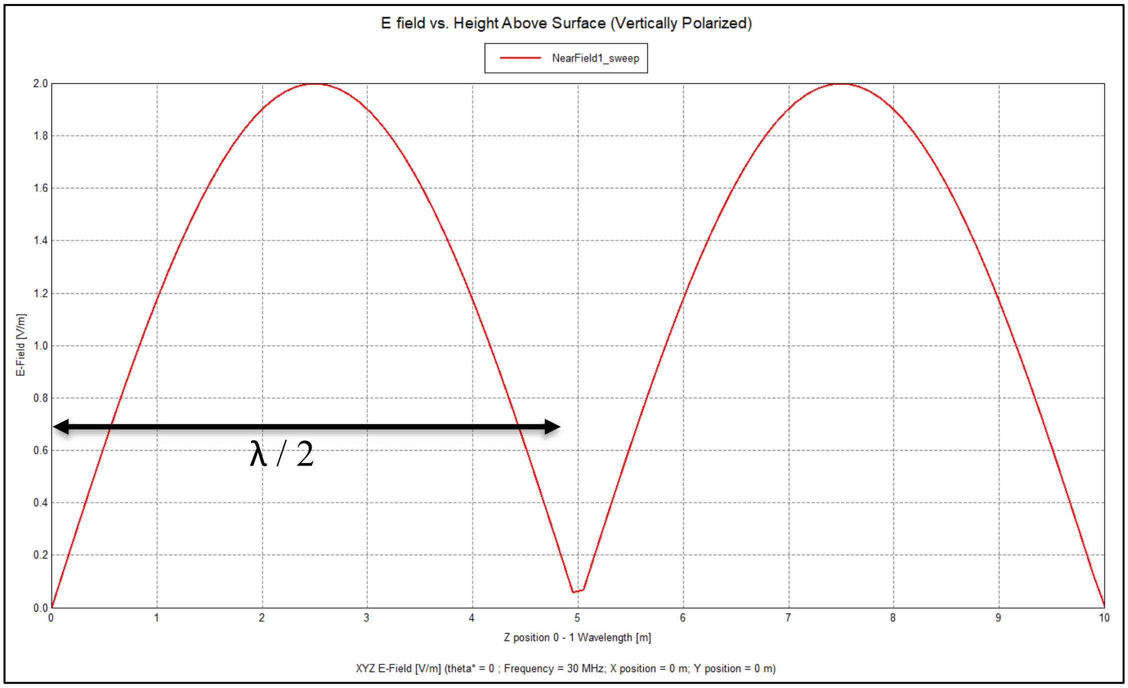

Figure 3.2 Electric field strength vs. height above ground (vertically polarized; zero-degree AoI).

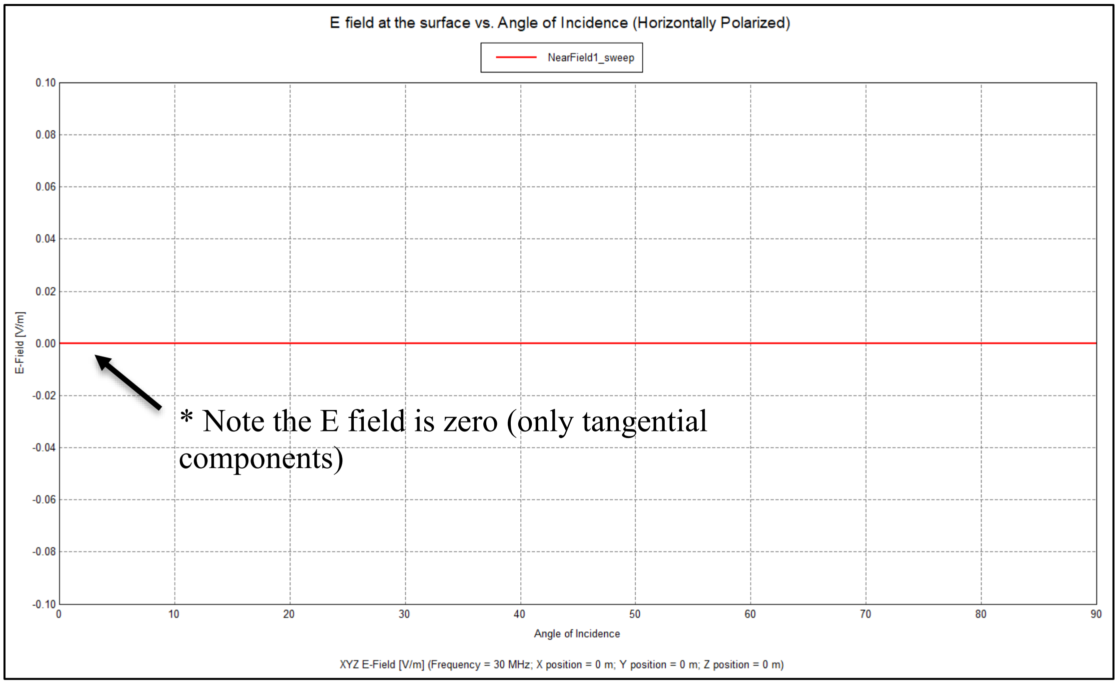

(a)

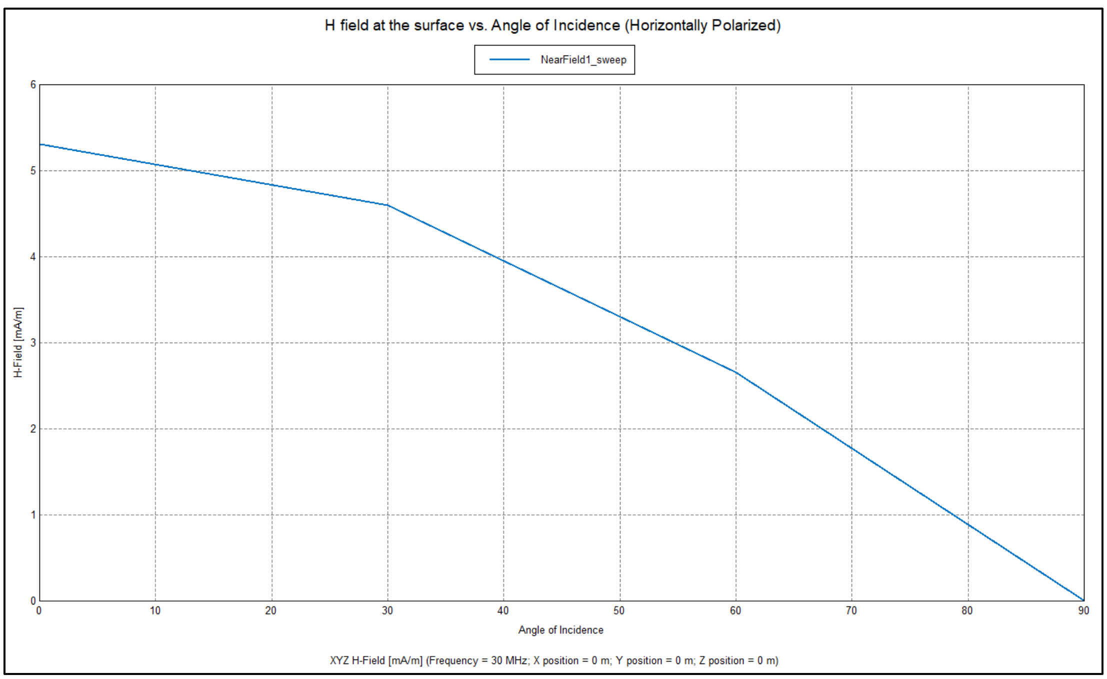

(b)

Figure 3.3 Total electric (a) and magnetic (b) field at the surface for horizontal polarization.

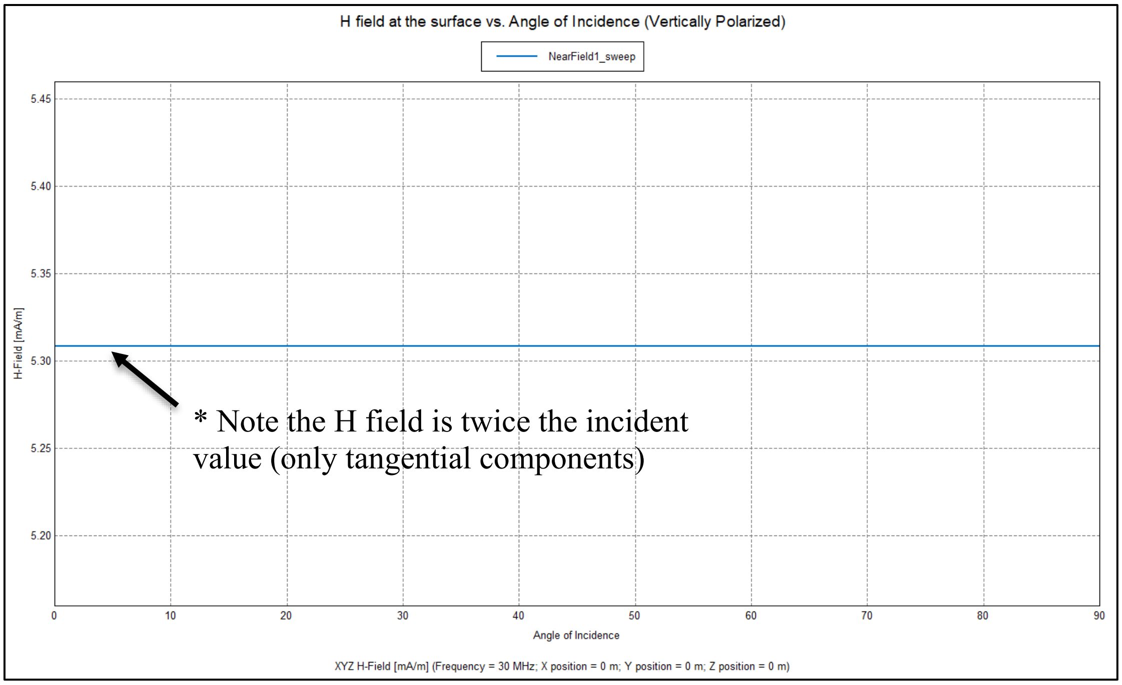

(a)

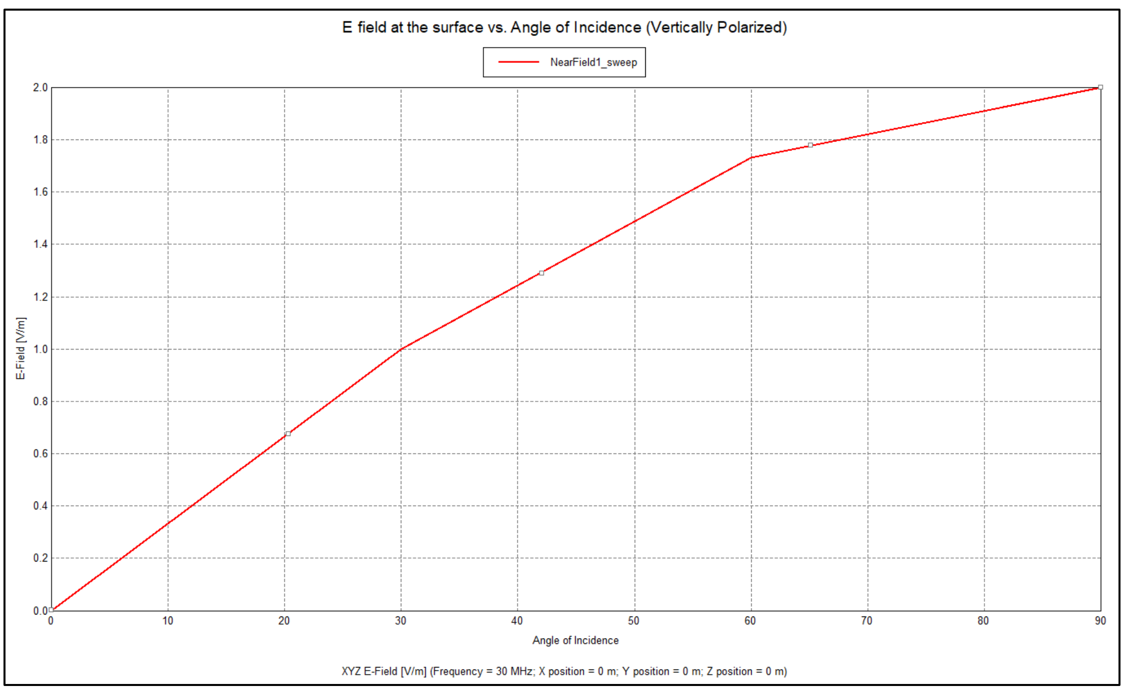

(b)

Figure 3.4 Total magnetic (a) and electric (b) field at the surface for vertical polarization.

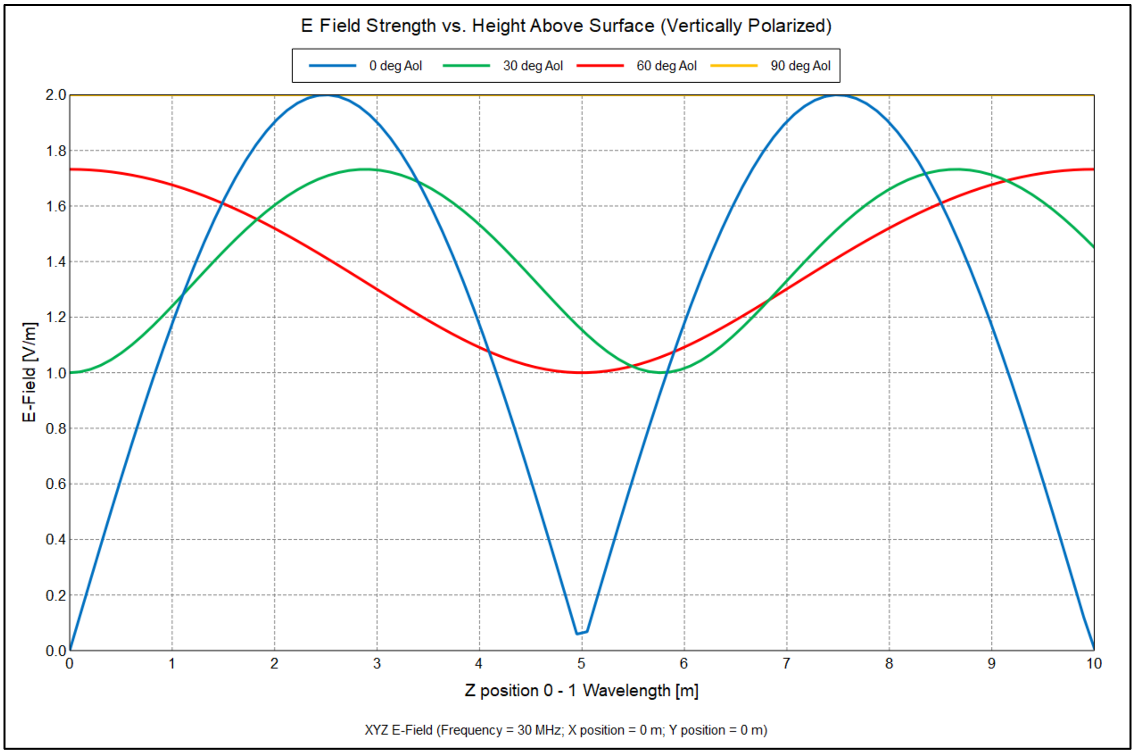

Figure 3.5 Electric field strength vs. height above ground (vertically polarized; various AoI).

Chapter 4

Fundamentals of EMP/Building Interaction

4.1 Overview

This chapter documents the research associated with the fundamental interaction between EMP radiation and building structures. Such an interaction is influenced by many parameters pertaining to the EM radiation, the structure itself, and the ground beneath the structure. Parameters studied in this work include radiation angle of incidence (AoI), radiation polarization, dielectric material properties and their frequency dependence, and the electrical properties of the ground. Understanding the effect such parameters have on the EMP/building interaction is critical because all similar works must consider these basic parameters. Results from the fundamental parameter simulations are considered and implemented for more complicated simulations later in this thesis. Additionally, the results in this chapter provide a baseline structure transfer function which can be compared against for validation of complex simulations. Mignardot's published conference paper [32] summarizes the work on EMP/ building interaction fundamentals and this chapter provides a comprehensive analysis in full detail.

4.2 Approach and Method

Computational electromagnetic simulations are conducted to calculate electric and magnetic fields and furthermore, develop an understanding of the interaction between a building structure and plane wave electromagnetic radiation. Field results are numerically calculated using the MoM. (Details of the MoM numerical scheme can be found in Chapter three of this thesis). Field data points are formulated into a transfer function to determine the attenuation, or 'shielding effectiveness' provided by the structure. IEEE Standard 299-1969 [33] defines the appropriate transfer function as a logarithmic voltage ratio for frequencies within the scope of this work. The transfer function used for the entire work is defined below in Equations 4.1 and 4.2 for the E and H fields respectively. E_p and H_p represent measured field strengths, while E and H represent free space field values (at 1 V/m and 1/120π A/m for electric and magnetic field respectively). Measured field points are taken at both singular locations as well as multitudes of locations and averaged.

$$E_f = 20\log\left(\frac{E_p}{E}\right) \tag{4.1}$$

$$H_f = 20\log\left(\frac{H_p}{H}\right) \tag{4.2}$$

A HEMP must travel up to hundreds of kilometers through the atmosphere from the detonation location to a structure on the Earth's surface. Considering the large distance, and air as nearly a perfect dielectric medium, it can be assumed the EM radiation propagates as a plane wave when reaching the structure. Therefore, the simulation excitation source is modeled as an electromagnetic plane wave propagating from the sky towards the building. Although the magnitude of the source is normalized to 1 V/m, the frequencies of analysis are chosen to represent the broad spectrum of a HEMP event: 100 kHz to 50 MHz. The frequency range is capped between 100 kHz and 50 MHz to ease computational demands; however, significant energy content exists from direct current (DC) up to 100 MHz [4], [17]. It is also worthy to note, frequency components beyond 100 MHz also exist but contain an insignificant portion of energy. A multitude of frequency points are analyzed within the range.

Throughout the work documented in this thesis, two simple geometries are utilized for the building structure three-dimensional model. These geometries include various sized cubical and rectangular prisms. Overall dimensions are maintained between 1 and 10 meters to limit the number of meshed elements, thus reducing computer memory requirements. A free space interior region is separated from the exterior by walls of finite thickness ranging from 10 to 20 cm. The wall material itself is modeled as a dielectric to emulate concrete, and the dielectric properties of the wall are one of the variables within the focus of this work. Overall, the building structure and its characteristics are designed to resemble a power generation facility. As an example, the Chickamauga Hydroelectric Dam is a 100 MW generating facility owned and operated by the Tennessee Valley Authority. Particularly, the generating room is the building where the turbine-generators are housed and serves as an example facility for this work. Chickamauga Dam is pictured below in Figure 4.1.

Scientists assume Earth to be a perfect electrical conductor (PEC) for a wide variety of electromagnetic and geophysical studies such as in [31] and [35]. By making the PEC assumption, the electromagnetic problem is greatly simplified and the Green's functions can be calculated more easily. Thus, the ground plane is considered to be a perfect electric conductor for all simulations in this work except for when studying the effect of a dielectric ground plane.

Figure 4.1 Chickamauga Hydroelectric Dam located in Chattanooga, TN [34].

With the MoM procedure, only surfaces in the model are required for discretization. The software's automated meshing feature is used, which defines the mesh based on 1/12 of the shortest wavelength [27]. In other words, the triangle element edge length is determined accounting for highest frequency in addition to geometric discontinuities and media properties. The discretization setting can also be set finer for convergence studies. An example of the discretization mesh is illustrated in Figure 4.2.

The aforementioned details regarding the problem approach and method refer only to a baseline scenario. Many of the defined characteristics act as variables and are altered and compared to determine criticality. The results obtained from this study serve as a collection of general observations which can be extended to more complicated simulations.

4.3 Angle of Incidence Results

Problems involving HEMP possess many challenges including the uncertainty of multiple variables. For example, the location and orientation of a nuclear detonation and the propagating EMP relative to a facility is likely to be unknown. The orientation, with respect to a reference axis, of the incoming electromagnetic wave is known as the angle of incidence. Approximate calculation assuming the HOB as 100 km and the distance from ground zero (the surface location directly below the burst) to peak field strength as 200 km [17] yields an AoI of 65°. However, the radiation incident upon a particular structure may be significantly altered depending on geography, orientation, and proximity to other objects. The excitation source's angle of incidence dictates the interaction with the structure. Due to the nature of AoI variable uncertainty, the 'worst case' scenario is determined. In this work, the AoI is measured with respect to the vertical axis perpendicular to the ground plane as in Figure 4.3; a straight downward propagation is represented with a zero-degree AoI.

To analyze the effect of AoI, the structure is illuminated with plane wave radiation at various angles of incidence. Electric and magnetic field data is numerically calculated at the geometric center point of a hollow 10 by 3 by 4 m rectangular building. The interior of the building is enclosed by 10 cm thick dielectric walls, floor, and ceiling. A frequency-independent wall material ($\varepsilon_r = 4.5$, $\sigma = 0.02$ S/m) is employed to emulate concrete. Using Equations 4.1 and 4.2 along with the free space field values, a transfer function is developed which characterizes the structure's shielding effectiveness as a function of frequency. Transfer function results for a model employing a PEC and dielectric ground plane are displayed in Figures 4.4 and 4.5 respectively.

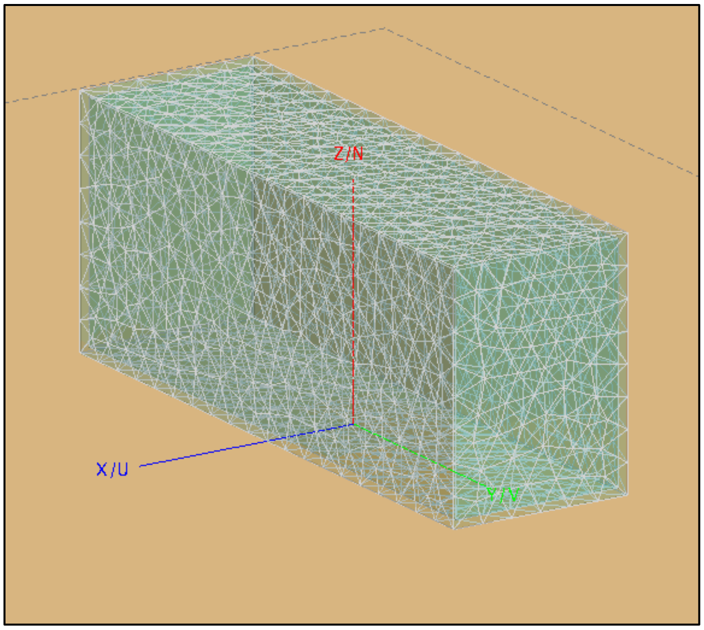

Figure 4.2 Example of discretization mesh with 3,366 elements.

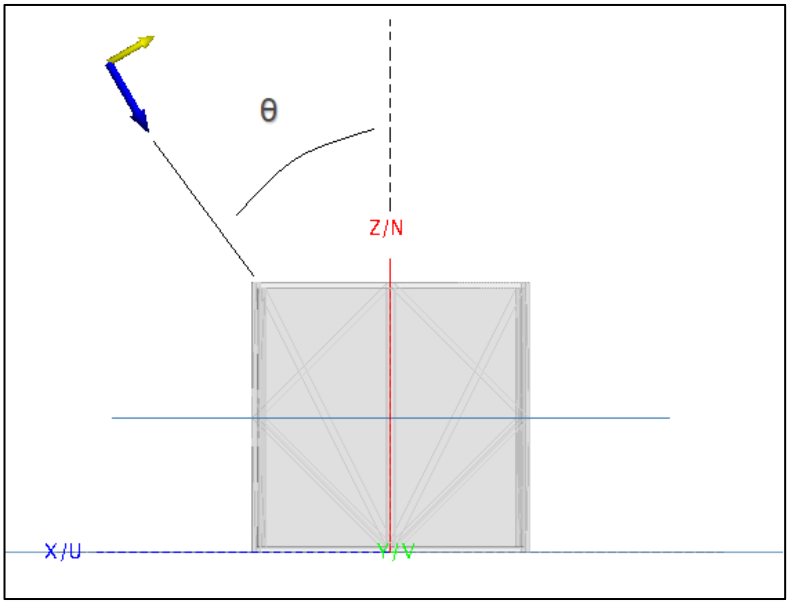

Figure 4.3 Angle of incidence θ measured with respect to vertical axis.

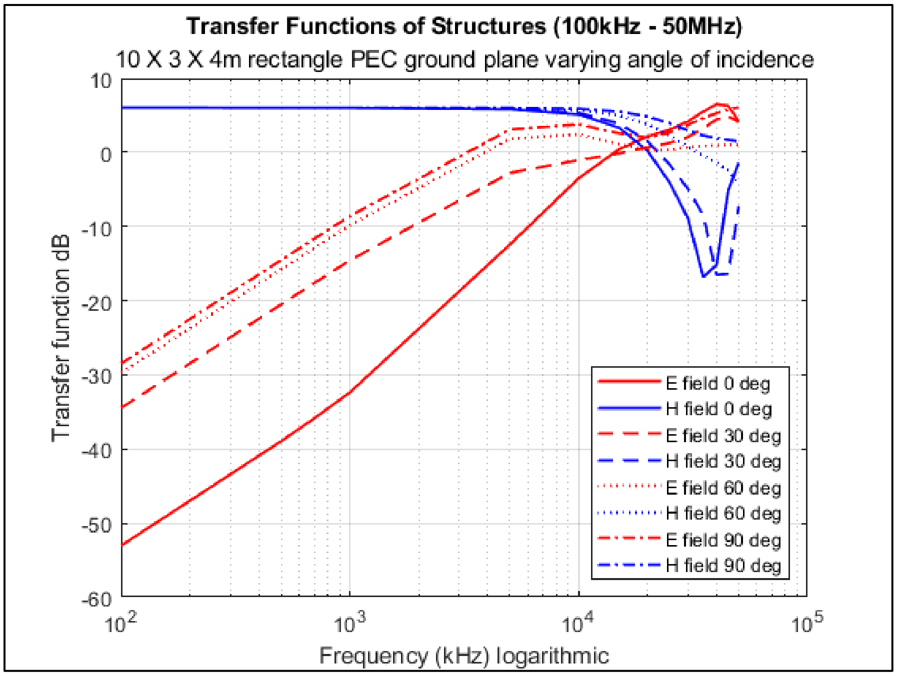

Figure 4.4 Comparison of building transfer functions with varying radiation angle of incidence (PEC ground plane).

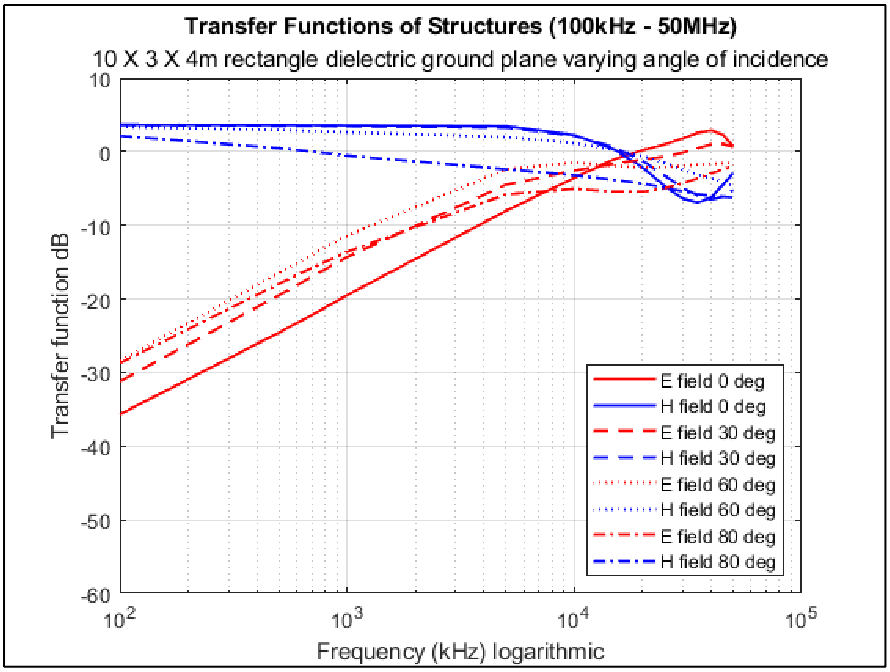

Figure 4.5 Comparison of building transfer functions with varying radiation angle of incidence (dielectric ground plane).

The dielectric ground plane is modeled as a frequency independent ground plane to emulate soil (ε_r = 10, σ = 0 .002 S/m).

Recall the transfer function represents a ratio; therefore, a large negative number implies the inside field data is very small compared to the free space value. Values below zero signify attenuation via the wall penetration loss. The apparent amplification of the magnetic field is not an amplification but rather a result due to the definition of the transfer function. The ratio is taken with respect to the free space field value, and the calculated data includes the free space plus the reflected field values. Due to the magnetic boundary condition, described in section 3.2, the calculated field value is double the free space value hence the ~6 dB gain. If the transfer function was defined with a ratio of the calculated field value and field value outside the wall of the structure, a ~0 dB gain would be expected.

Figures 4.4 and 4.5 indicate the following results. In the low frequency region (below 10 MHz for this particular model), the results indicate little variation with a change in AoI, especially when considering the magnetic field transfer function. The outlying curves are associated with angles at the extreme of the range (either 0° or 90°). It is worthy to note, during an EMP event the AoI will be unknown and is more likely to be a moderate angle closer to the middle of the range. The E field transfer function has more variation with AoI at lower frequencies and converges at higher frequencies; the H field transfer function displays the opposite result. In the resonance region (beyond 10MHz), larger angles appear to result in a less dramatic oscillatory effect. When observing the data in an average sense both ground plane scenarios generate similar results; however, even less variation exists while considering the dielectric ground plane.

4.4 Angle of Polarization Results

Another intrinsic property of electromagnetic radiation is the polarization. The polarization angle characterizes the time-varying orientation of the electric field component of the incident electromagnetic wave. A wave can be vertically or horizontally polarized, which corresponds to the electric field being parallel or perpendicular to the plane of incidence respectively. When considering a plane wave, both fields will propagate along the same axis. The angle of polarization is an important parameter to study because the polarization affects the propagation characteristics of the wave and thus the penetration into the structure.

During an EMP event, the polarization will be unknown. Therefore, it is reasonable to determine a worst-case scenario for simulation efforts. Studying electromagnetic boundary conditions, as in section 3.2, reveals the behavior of a plane wave when interacting with a conducting surface such as the earth. At the surface of a PEC (assuming an infinite half-space model), electric fields consist of only normal components whereas magnetic fields only consist of tangential components [36]. Although the above conditions are observed at the surface, the observations can be extended to locations near the surface for approximate results. When analyzing lower frequencies, wavelengths can be orders of magnitude larger than the structure dimensions. Therefore, in lower frequency conditions, points around the structure are very close to the ground plane surface compared to the wavelength. To further validate the boundary conditions, simulations are carried out to analyze field strength at various polarizations. When the incoming wave is horizontally polarized, the E field contains only tangential components regardless of AoI. The same is true for the H field if the incoming wave is vertically polarized. To illustrate the effect of polarization, field results are numerically calculated and averaged inside the walls of a 3 m cubical concrete structure. Figure 4.6 plots the field results as a function of angle of incidence while comparing vertical (solid line) and horizontal polarization (dashed line).

It is evident the vertically polarized case enables the most intense excitation as the field intensities for all frequencies and AoI are stronger when compared to horizontal polarization. In case of vertical polarization, as AoI approaches ninety degrees, intensities trend higher for most frequencies, which is in accordance with the AoI results from section 4.3. Employing a moderate polarization angle between vertical and horizontal does not constitute a worst-case scenario because for most incidence angles, a combination of tangential and normal field components will always exist. Although the polarization angle of an incoming EMP is likely to be unknown, assuming vertical polarization is a logical and conservative assumption for simulation. Vertical polarization enables a worst-case scenario as field strengths are observed to be most intense for a given frequency and angle of incidence. In the low frequency region, locations within the structure are close to the ground plane surface (with respect to wavelength) and therefore, observations can be expected to replicate that of boundary conditions.

4.5 Frequency Dependence of Wall Materials

The previously discussed simulations employ a frequency-independent wall material with a fixed permittivity and conductivity to emulate concrete. Further studies are conducted to determine if the frequency-independent electrical parameter approximation is reasonable. A 10 by 3 by 4 m rectangular structure with an all-around wall thickness of 20 cm is modeled to test such frequency dependence. Two comparisons are studied; the first comparing a frequency-dependent software-defined

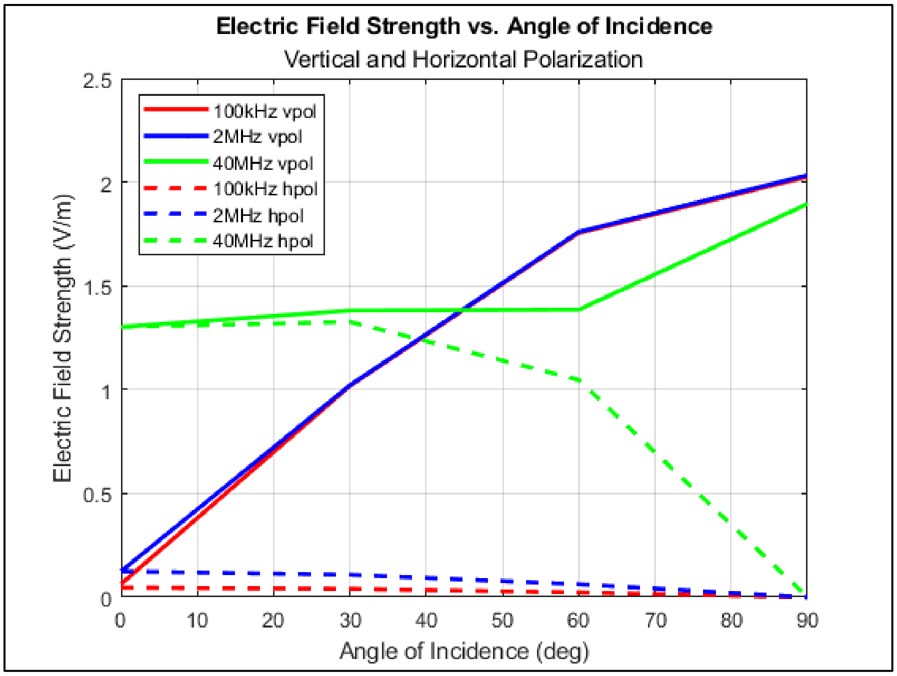

(a)

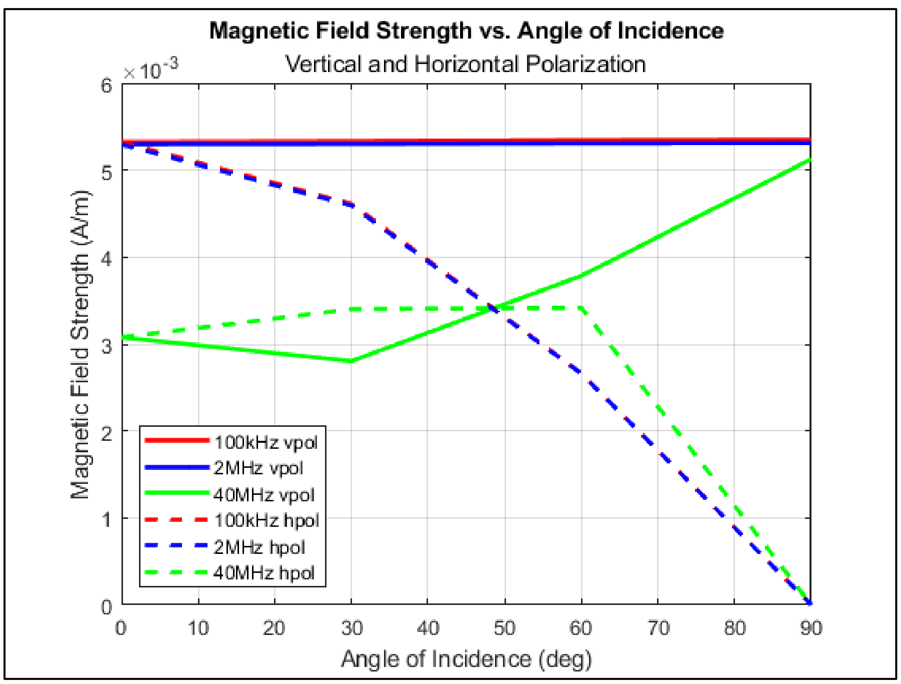

(b)

Figure 4.6 Interior electric (a) and magnetic (b) field strengths comparing radiation polarization.

dielectric media, *construction concrete block*, and the previously used frequency-independent material. The software defined media specifies data for a list of frequencies. Data from frequencies not specified is linearly interpolated [27]. A plane wave source propagates directly down onto the structure (0° angle of incidence) and a frequency range of 100 kHz to 50 MHz is analyzed. Data for the transfer function is averaged from nine points evenly spaced inside the walls of the structure. Results demonstrate a similar excitation behavior regardless of wall material, especially for the magnetic field. The electric field experiences slightly less attenuation throughout the frequency spectrum under the frequency-dependent software-defined media. Figure 4.7 illustrates the transfer function results for this scenario. Although for zero-degree AoI the results appear to match, the frequency-dependent software-defined media was invalidated upon testing with alternate AoI. The inaccuracies are likely because the specified data points are for frequencies well into the GHz range and the linear interpolation down to HEMP frequency range is not sufficient. At an AoI of zero degrees, for vertically polarized radiation, the E field excitation at the surface is zero, thus explaining the similar results for both wall materials.

The second comparison studied the same frequency-independent wall material compared to a frequency-dependent media defined by the Messier Model. The Messier Model provides analytical expressions for conductivity and permittivity as a function of frequency [37]. The expressions are defined in Equations 4.3 and 4.4 below.

$$\sigma(f) = \sigma_{DC}\left(1 + \sqrt{\frac{4\pi f \varepsilon_\infty}{\sigma_{DC}}}\right) \tag{4.3}$$

$$\varepsilon_r(f) = \frac{\varepsilon_\infty}{\varepsilon_0}\left(1 + \sqrt{\frac{\sigma_{DC}}{\pi f \varepsilon_\infty}}\right) \tag{4.4}$$

σ_{DC} is the DC conductivity and is set to 6.5e-3 S/m. ε_∞ is the high frequency limit of the dielectric and is set to 8 times ε_0. In this simulation, a 50° angle of incidence is employed and data for the transfer function was averaged over a volume inside the structure including 96 points. Figure 4.8 illustrates the data point locations and serves as a visualization for all other simulations averaging data from numerous interior points.

The results from the second comparison represent the difference in dielectric media more accurately and can be seen in Figure 4.9 below. The transfer function trend developed little alteration from the frequency dependence of the wall material's electrical properties. The Messier Model defined media demonstrates slightly less attenuation when

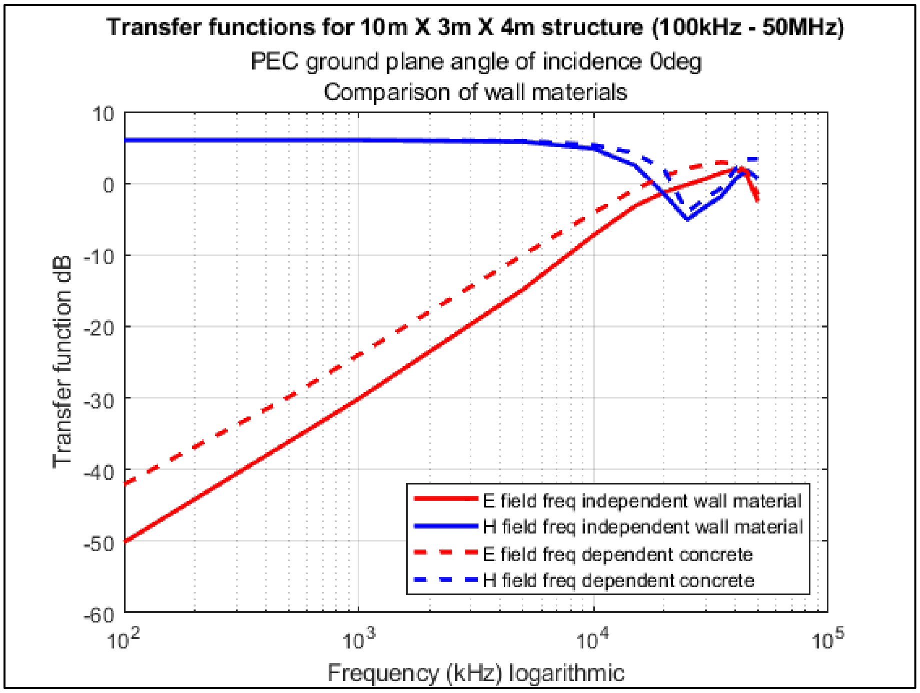

Figure 4.7 Comparison of transfer functions for different structure wall materials with incoming radiation from directly above.

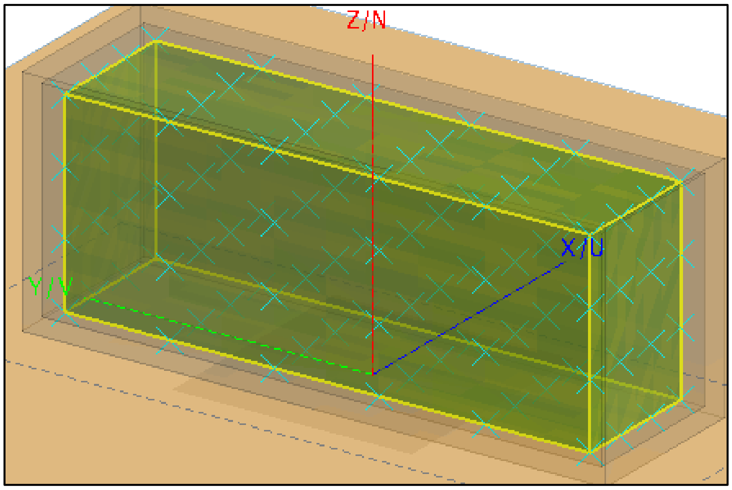

Figure 4.8 Points within structure at which field results are calculated then averaged.

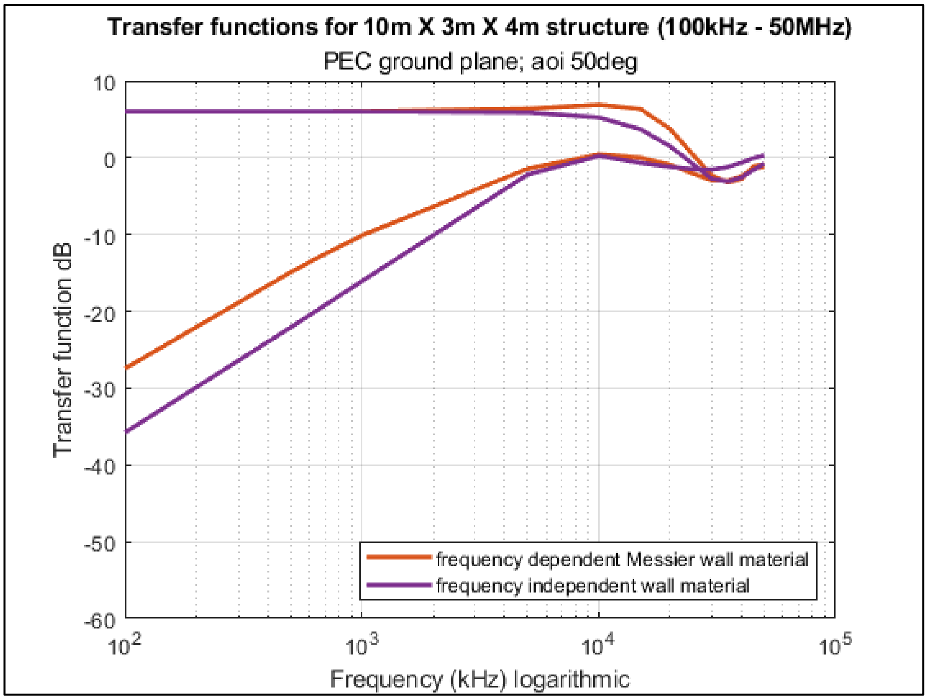

Figure 4.9 Comparison of transfer functions for different structure wall materials with incoming radiation at 40° above ground plane.

compared to the frequency independent wall material. This effect is greater for the E field at low frequencies and the H field at higher frequencies.

Overall, when assuming the Earth as a PEC, and performing simulations in the 100 kHz – 50 MHz range, frequency dependence of the wall material's electrical properties does not significantly alter transfer function results. It is a reasonable simplification to assume constant permittivity and conductivity for the structure's construction material. However, if a more conservative study is required, using the Messier Model to define dielectric materials may be more appropriate.

4.6 Effect of Dielectric Ground Plane Results

As mentioned earlier in this chapter, researchers often assume Earth to be a perfect electrical conductor for a wide variety of electromagnetic and geophysical studies. This assumption is valid because the earth acts as infinite source of charge. However, earth is not a perfect conductor and maintains some electric field beneath the surface. Many variables influence the earth's electrical properties as Vance points out in [38]. Simulations are conducted to analyze the validity of a PEC ground plane by comparing transfer function results with two dielectric ground plane models. A frequency-independent dielectric ground plane is modeled ($\varepsilon_r = 10$, $\sigma = 0.002$ S/m), as well as a frequency-dependent dielectric ground plane defined by the Messier Model using a DC soil conductivity of 0.002 S/m. [37]. Geology consistent with the Eastern Tennessee region was taken to approximate these electrical properties. This geology consists of rocky hill terrain composed primarily of sedimentary rocks such as limestone and dolomite; and topsoil is considered a mixture of loam and sand. [38]–[43]. A 3 m cubical structure with an all-around wall thickness of 10 cm is modeled for study. Data for the transfer function is averaged over 64 points in a volume centered inside the structure walls. A comparison of the transfer function results is pictured in Figure 4.10 below. A visual representation of electric field results is displayed in Figure 4.11.

Simulation errors were observed when employing a dielectric ground plane. 'Hot spots' of high intensity field appeared near the walls inside of the structure at frequencies around and below 1 MHz. These results are likely erroneous and express a limitation of the MoM solver. One potential contributor to the inaccuracies is the solver's inability to converge accurate solutions of the Sommerfeld integrals at lower frequencies. When data is taken farther away from the walls, towards the center of the interior, results demonstrated precision with the alternate simulations conducted in this study. Transfer function results in Figure 4.11 are formulated with data sufficiently far from the walls. Figure 4.12 pictures the inaccurate 'hot spots'.

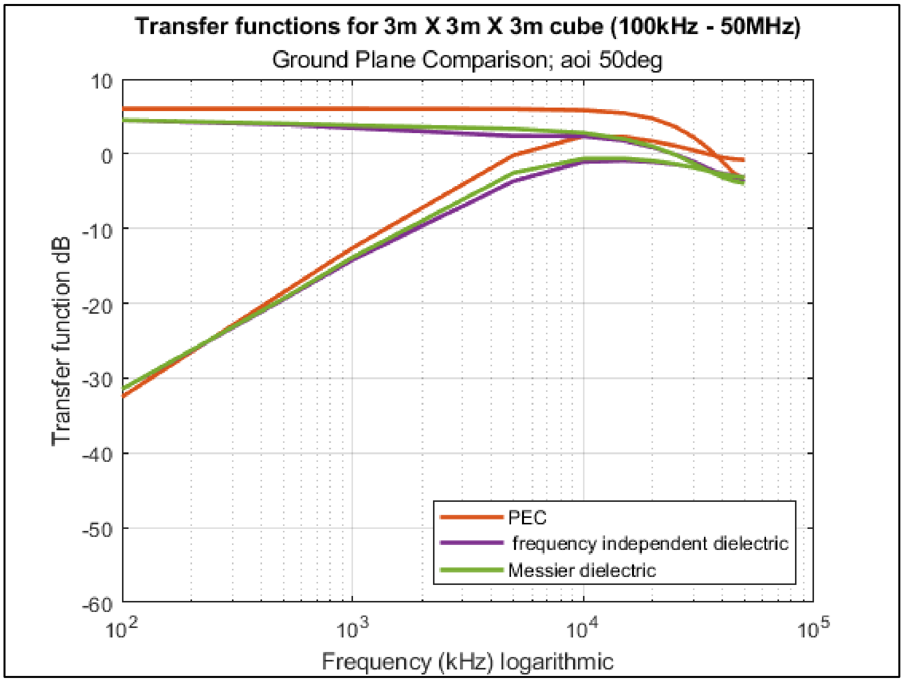

Figure 4.10 Comparison of transfer functions for different ground planes.

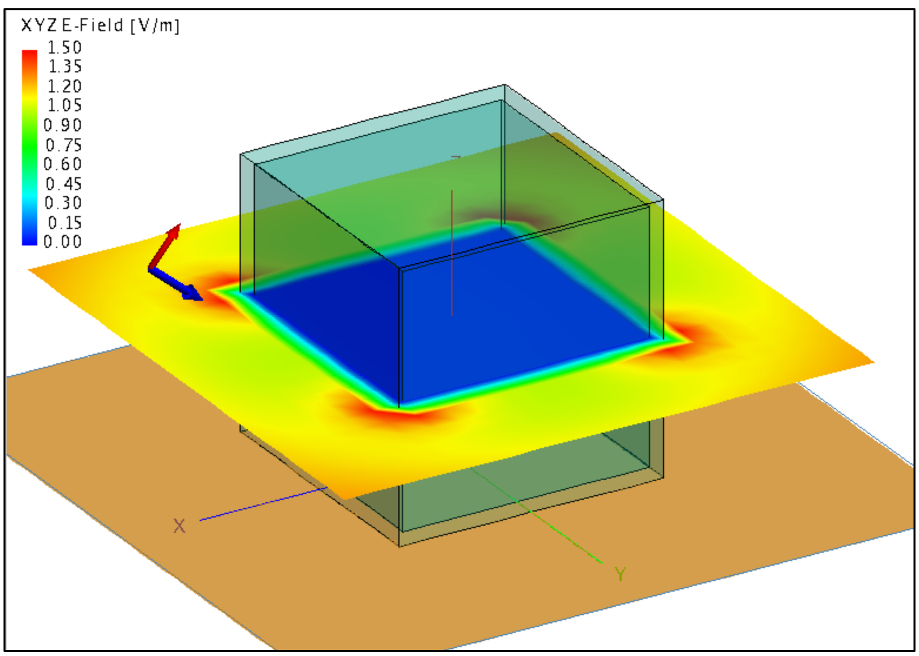

Figure 4.11 Electric field results inside and around structure for PEC ground plane (100 kHz).

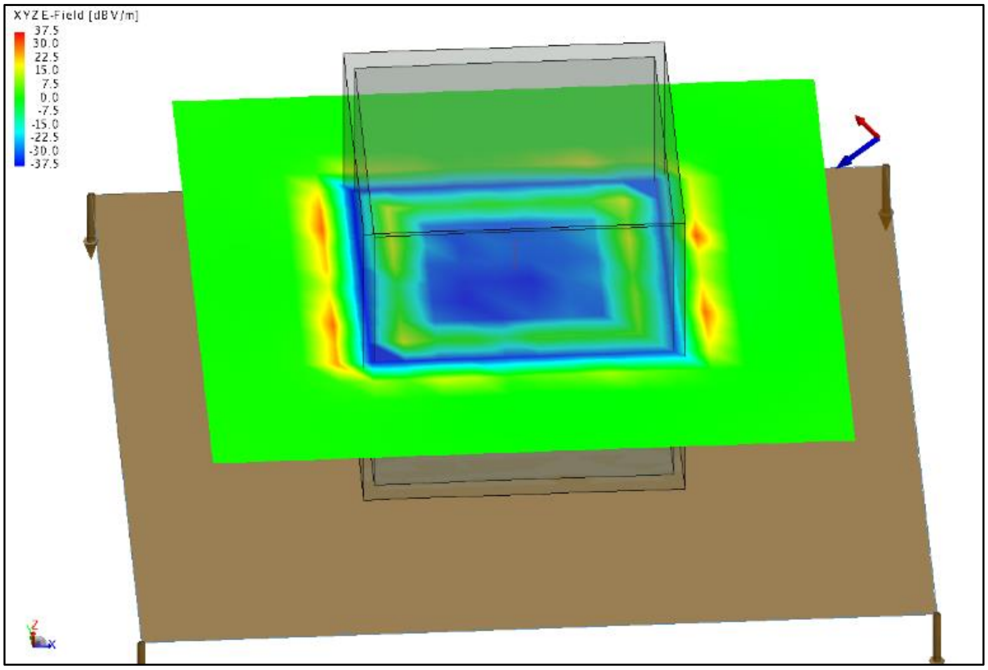

Figure 4.12 Electric field results inside and around structure for dielectric ground plane (100 kHz) (Concluded to be erroneous).

Utilizing a PEC ground plane does not drastically affect results when studying this particular frequency range. In fact, the PEC model provided the lowest attenuation. As the frequency approaches the resonance region, results tend to diverge more. The dielectric ground plane models behaved very similarly throughout the frequency range and thus the frequency dependence of the ground plane is not a significant parameter in this study. For a worst-case scenario, utilizing a PEC ground plane is reasonable. For more accurate studies, a simple frequency-independent dielectric ground plane can be modeled. It is worthy to note the dielectric ground plane models take more computation time due to the solving of Sommerfeld integrals in the MoM.

Chapter 5

Structure Design Characteristics

5.1 Overview

This chapter expands upon the work of the previous by introducing complexities into the scope of study. Previously discussed were the fundamentals of EM interactions with structures, and many variables are directly associated with the EMP propagation. However, this chapter focuses on more details regarding the construction of the structure itself. Effects of apertures, reinforced concrete, shielded concrete, metallic roof construction, and some geometrical considerations are evaluated. Results from Chapter 4 provide fixed conditions related to the incident propagation which constitute a worst-case scenario. Assumptions such as greater angles of incidence and vertical polarization allow analysis of other parameters while maintaining a lower overall variability. Consistent with the rest of this document's work, parameters are developed to emulate power generation facilities. These parameter values can possibly be extended to encompass other large industrial facilities.

5.2 Aperture Results

5.2.1 Windows

Although a completely enclosed area may provide excellent attenuation from electromagnetic signals, points of infiltration can diminish the attenuation effect. Apertures such as glass windows have a huge effect on building penetration loss as mentioned in [21] and [44]. Just as glass is transparent to electromagnetic energy at visible light frequencies but opaque to some ultra violet frequencies, glass windows may be points of infiltration for HEMP. Industrial facilities including power plants often have windows or large bay doors; thus it is critical to determine the effect such apertures have on the overall shielding effectiveness of a structure. Variables of interest include the aperture size (relative to radiation wavelength), number of apertures, and aperture material (glass or free space, or metal door). Similar to previous simulations in this work, the problem is modeled as a 10 by 3 by 4 m rectangular building with all around wall thickness of 10 cm. The excitation is vertically polarized plane wave radiation propagating at 50° relative to the vertical axis. A PEC ground plane is employed and the structure walls are modeled with a frequency-independent dielectric emulating concrete.

The first consideration of study is the window's size. Several windows are placed on each side of the long-dimension building wall. The size is defined by total surface area occupied by windows. The structure without any windows serves as the control. Four different window size configurations are studied as follows: ten 1 by .75 m windows totaling to 7.5 m^2 of area, ten .5 by .375 m windows totaling to 1.875 m^2 of area, ten .25 by .1875 m windows totaling to .5 m^2 of area, and finally six 2 by 1.5 m windows totaling to 18 m^2 of area. For simplicity the thickness of each window is consistent with the wall thickness at 10 cm. Figure 5.1 displays the model with various windows sizes for visualization.

A frequency-dependent dielectric model for glass exists within the software. However, due to the inaccuracy of linear interpolation for lower frequencies, as mentioned in section 4.5, a frequency-independent model is instead employed. Also illustrated in section 4.5, the electromagnetic results for a frequency-independent model proved to be reasonably accurate when compared to alternate models. The frequency independent wall material (ε_r = 7, σ = 10e-9 S/m) is parametrized to emulate silicate window glass [45]– [47]. Figure 5.2 displays the structure transfer functions comparing different window sizes.

The results indicate windows do not alter the general attenuation behavior. For smaller windows, results are as if no windows are present at all. At the lowest frequency analyzed, the largest windows diminish the attenuation by ~8dB and the second largest windows by ~2dB. This relationship appears to be directly proportional to the window surface area. Although, when studying electromagnetic interactions, it is important to consider phenomena such as diffraction and scattering. The median wavelength in this simulation is approximately 12 m (corresponding to 25 MHz). Even the largest window size studied possesses dimensions smaller than the median wavelength. Therefore, side length dimensions may have a more direct influence on attenuation results when the window itself is larger. When the wavelength is much larger than the aperture dimensions, the apertures themselves have less influence on the incident radiation. For higher frequencies, the wavelength is more comparable to the window dimensions studied; however, the attenuation difference between window sizes decreases with increasing frequency. This result is due to the wall penetration loss of the structure which behaves as a high pass filter. At higher frequencies the walls themselves are more electromagnetically transparent and thus behave more like windows.

The focus in Chapter 4 regards parameters associated with the EM radiation itself such as angle of incidence. Results indicated as AoI increased, the electric field attenuation provided by the structure diminished. Another batch simulation is conducted to determine if apertures such as windows have any effect on the previously obtained results. The determination is windows do not alter behavior for various AoI. Figure 5.3

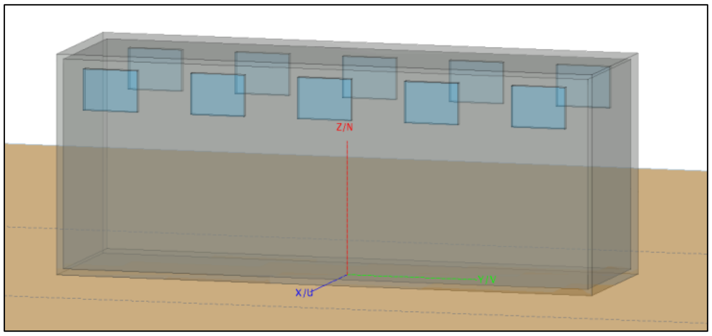

(a)

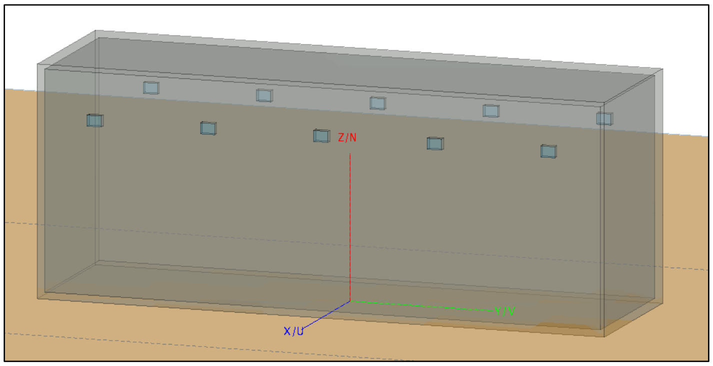

(b)

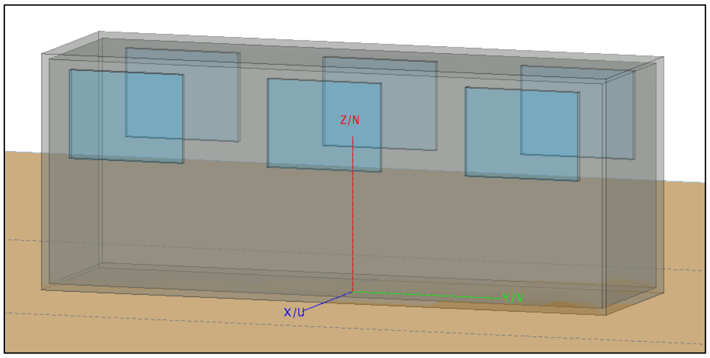

(c)

Figure 5.1 One-meter windows (a), .25 m windows (b), 2 m windows (c).

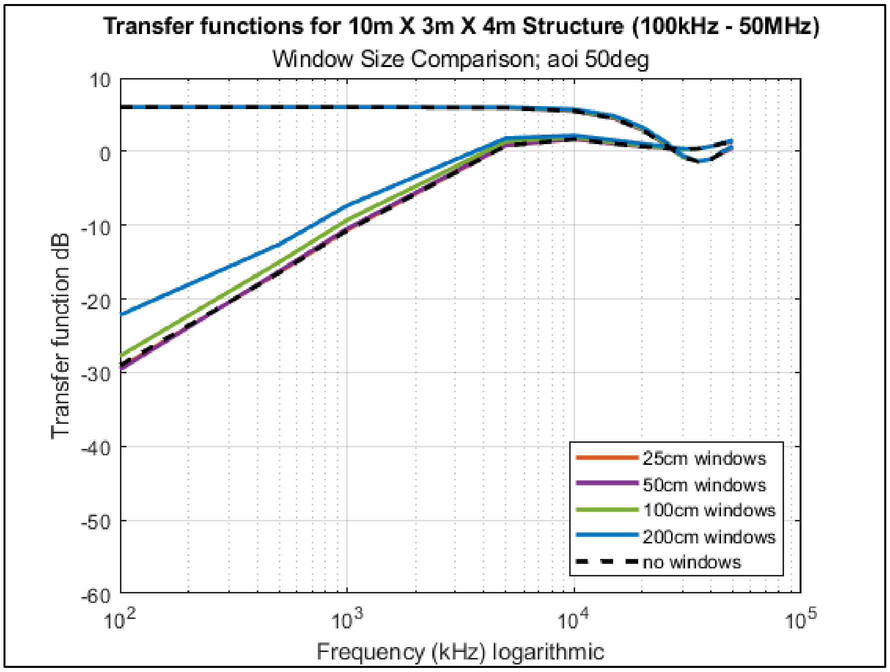

Figure 5.2 Structure transfer functions comparing various window sizes.

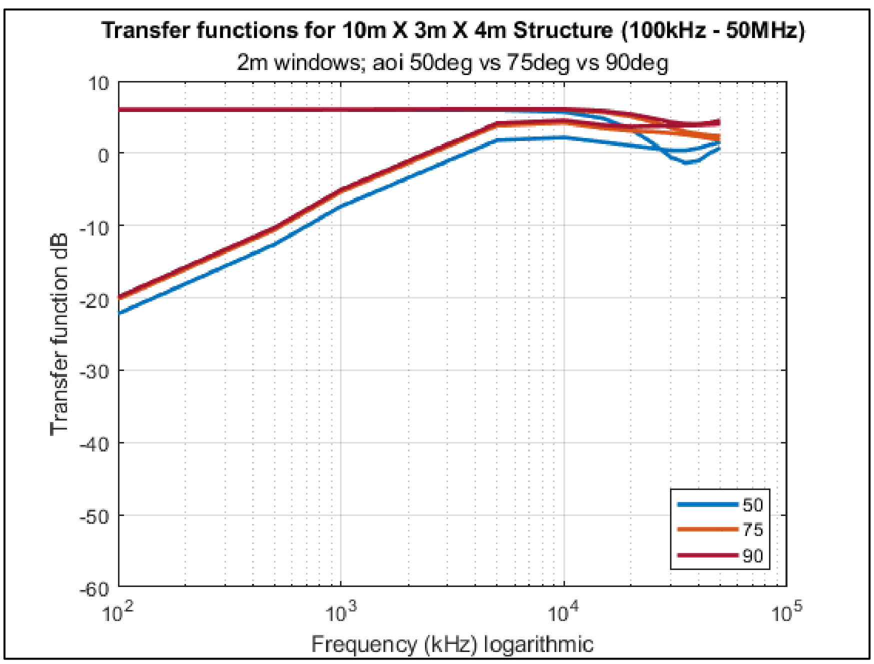

Figure 5.3 Structure transfer functions comparing various radiation AoI for a building with 2 m windows.

plots the transfer function, and as before, E field attenuation diminished with increasing AoI. Also, little change exists when AoI is increased beyond 75°.

Although the results outlined in this chapter thus far indicate no significant change in the structure's average transfer function, attention must also be focused to the areas near the vicinity of the windows. As mentioned previously, the transfer function is averaged from numerous data points evenly spaced throughout the structure. The transfer function near a window or other aperture may be completely different than the average. This is an important consideration as certain critical equipment maybe located near windows and doors. Observing the field values in a contour image is a great method to visualize the leakage points into the structure. Figure 5.4 provides several images which detail the E field throughout the structure. The field strength near the vicinity of the windows is much greater. The windows themselves become secondary radio sources and the re-radiated signal strength depends on the distance from the window. The region of increased field intensity is observed primarily perpendicular to the aperture surface. Field strength is unaffected in the portion of the interior below the windows. A ~10 dB increase in strength is observed directly in front of the window compared to a point directly between windows.

During some operation times, the window apertures may be open. For instance, an opening to transport equipment or provide ventilation may be formed during everyday operations. The question arises whether an open-air aperture is more of an electromagnetic penetration hazard when compared to glass. Again, the rectangular structure with 2 m windows is simulated with plane wave excitation. In this case, the structure's attenuation transfer function is compared for open vs. glass windows. The windows are completely removed for the open case model. A slight decrease in E field attenuation is observed at lower frequencies, and beyond 1 MHz virtually no difference is observed. This is expected as the apertures exhibit a less dominant effect at higher frequencies compared to the structure walls. The result is displayed in Figure 5.5 below.

To further evaluate the performance of glass against EM radiation, a study of the glass electrical properties is considered. Specifically, this simulation analyzes the glass conductivity. Various types of glass possess various conductivities due to the material makeup and the formation process. The range of conductivity for various glass types is several orders of magnitude and thus requires a sensitivity study [45]–[47]. The conductivity will be varied from 10e-11 S/m to 10e-7 S/m within the frequency-independent model, and the same structure average transfer function is observed. Virtually no difference in the overall shielding is affected by glass conductivity. Less than two thousandths of a dB difference exists between 10e-11 S/m to 10e-7 S/m at very

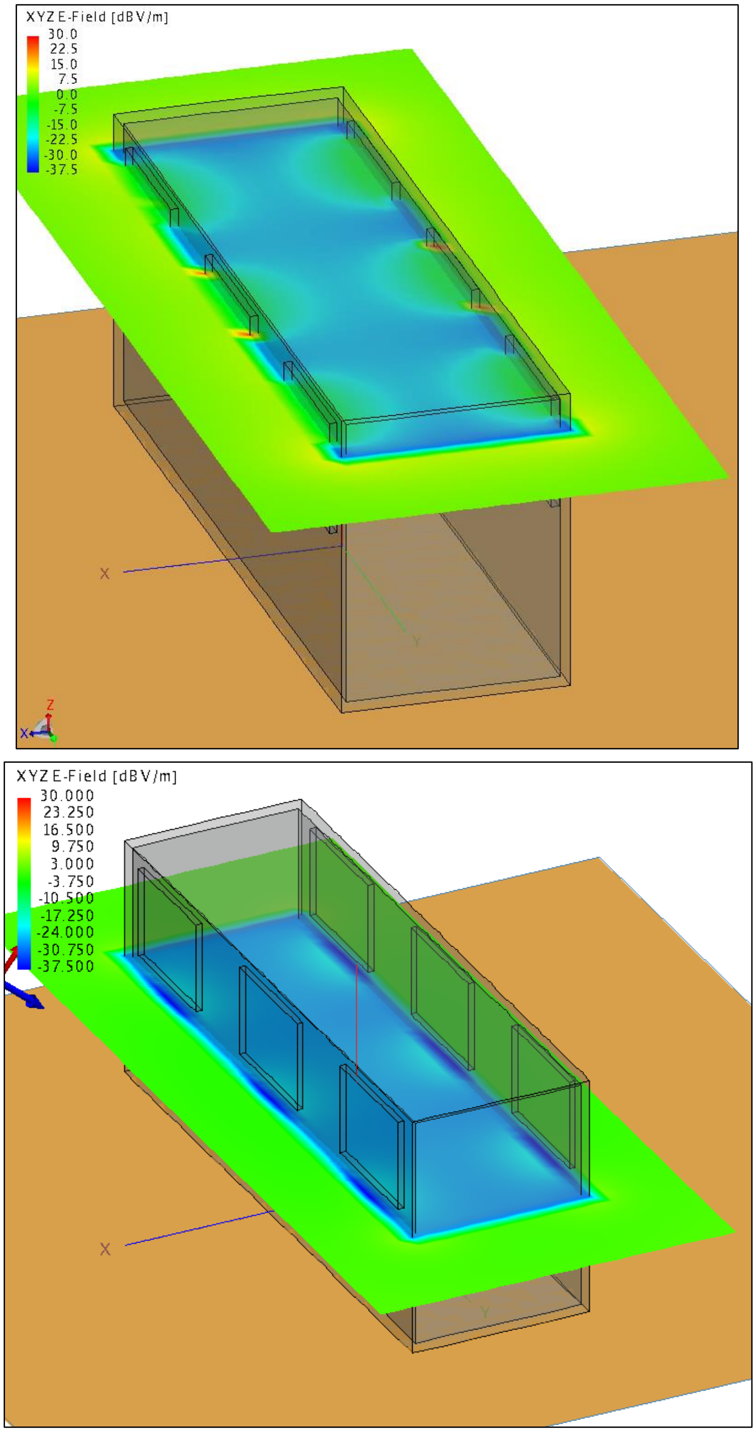

Figure 5.4 Electric field leakage visualization at 100 kHz.

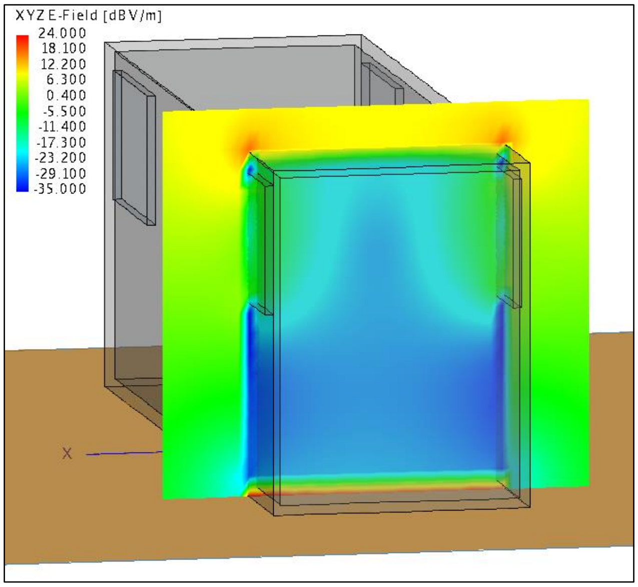

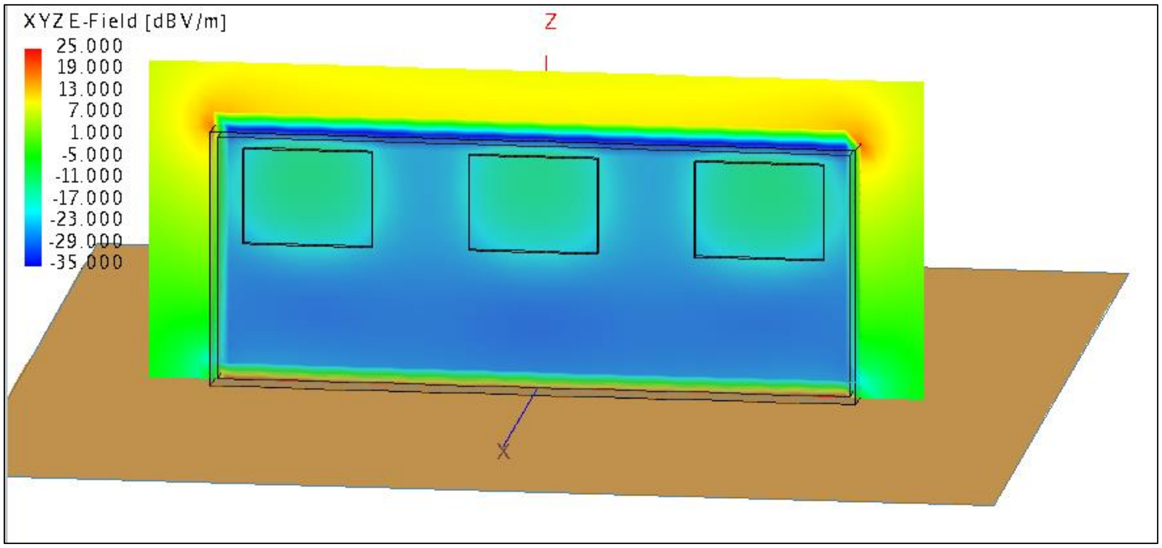

Figure 5.4 Continued

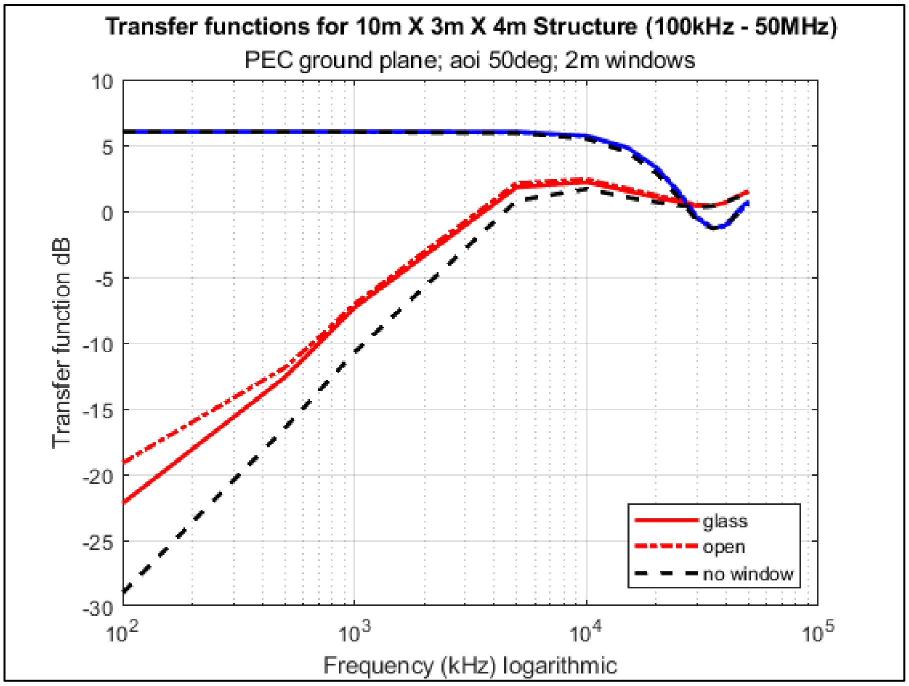

Figure 5.5 Structure transfer functions comparing various open-air and glass windows.

low frequencies. Such a result is likely because the concrete conductivity is still significantly greater than any glass conductivity. Therefore, glass conductivity is not a critical parameter regarding aperture attenuation. Further validation of this result is achieved by performing the same simulation considering a frequency-dependent model for glass where the conductivity changes as a function of frequency, in addition to a lossless material model where the conductivity is zero. The Messier model is utilized and the DC conductivity is parametrized as 10e-9 S/m. Nearly identical results are achieved, and therefore we can reiterate, the glass conductivity is not a significant parameter when studying overall structure shielding effectiveness.

5.2.2 Convergence Study

Convergence of results is a key consideration for numerical solutions such as MoM. Convergence of results is observed when results do not change after increasing the number of meshed elements. In general, using more elements and solving more equations leads to a more accurate solution but will take more computation memory and time. 9,174 meshed elements with an average edge length of 26.8 cm are discretized considering the solved building case with 2 m windows. A convergence study is carried out by increasing the number of discretized elements to 13,944 with an average edge length of 21.8 cm. Average field results are practically identical as seen in Figure 5.6 below. Thus, the obtained results are validated and the original coarser mesh can be used without question of accuracy for a similar size and scope problem.

5.2.3 Garage Bay Door

Another common aperture is a garage bay door. Although similar to a large window, a bay door may have a conductive closure and is often open for long periods of time. Two scenarios are considered to study how the structure's overall shielding is affected by a bay door. The first is when the door is open, and the second when the door is closed. The door is incorporated into the structure model as a 3 by 3.25 m opening as pictured in Figure 5.7. The door itself is modeled as .912 mm (20 gauge) thick sheet steel. The sheet steel is defined as a frequency-independent conductor with a relative magnetic permeability of 100 and conductivity of 3e6 S/m.

When the door is open, EM penetration behavior is similar to the case of an open window as expected. It is worthy to note the total surface area of the door is 9.75 m^2 and the field results are very similar to the simulation with 1 m windows exhibiting a total surface area of 10 m^2. It can therefore be inferred; when considering dielectric structures, the radiation penetration is a function of the total aperture surface area rather than individual aperture size or placement. This result is very beneficial for an estimation of radiation penetration applicable to other

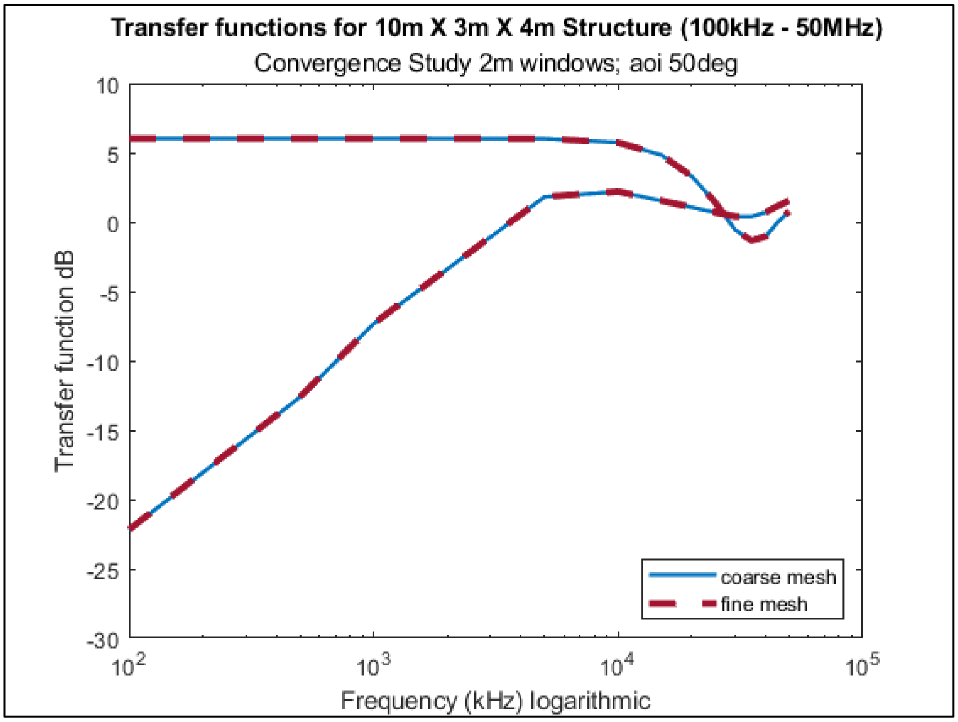

Figure 5.6 Structure Transfer functions illustrating convergence of two problem discretization.

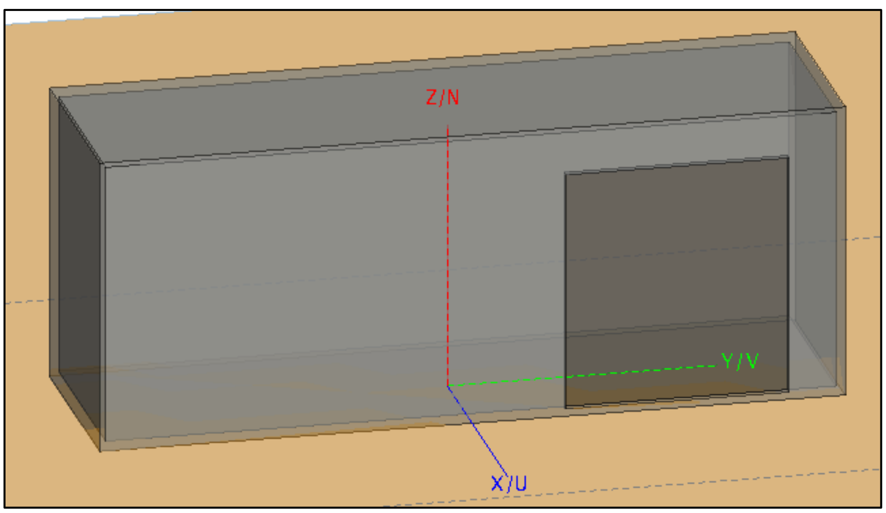

Figure 5.7 Sheet steel garage bay door model.

building architectures. The structure transfer function results for two different angles of incidence, as well as a field visualization result is displayed below in Figure 5.8.

When the door is closed, some shielding is provided but to no significant extent when considering the average. However, the area of intensified field strength behind the door is minimized when the door is closed. The strongest observed field strength is observed along the edges of the bay door.

To test the theory of diffraction a small gap around the door is included varying from 0 – 50 mm. Electromagnetic diffraction is the ability for radiation to bend around corners and is especially significant for short-wavelength radiation. E and H field values are calculated at points near the vicinity of the wall. At lower frequencies, the E and H field strength is not a function of gap width; however, the opposite is true for higher frequencies. At higher frequencies, the gap dimensions are more comparative to the wavelength dimension. Figure 5.9 illustrates the bay door gap in the model and Figure 5.10 plots the field strength against gap width for higher excitation frequencies. The field strength increases with gap width insinuating a more severe diffraction effect.

5.3 Construction Material and Design Results

5.3.1 Reinforced Concrete

In practice it is essential for large concrete infrastructure to be reinforced with material to improve tensile strength. Placement of steel reinforcement rods known as rebar within the concrete provides ductility to the overall composite material. Rebar is not only useful to enhance structural integrity, but also can provide significant electromagnetic shielding. Rebar is typically made from steel which is conductive and magnetic. Such properties enable significant interaction with electric and magnetic radiation. To study the effect rebar has on a structure's shielding effectiveness, a similar 10 by 3 by 4 m structure with 20 cm wall thickness is modeled. A grid of bonded PEC rebar (modeled as finite diameter wires) is placed within the concrete walls all around the structure. To limit the scope of this particular problem, the excitation is modeled as vertically polarized plane wave radiation with an AoI of 75°. Figure 5.11 pictures the meshed model incorporating rebar.

Common construction practice spaces the rebar approximately 24 inches apart and therefore a base case is established with 24-inch rebar spacing in all directions. The structure transfer function is produced for this base case and compared to both finer and coarser spaced rebar. Results suggest the structure gains significant attenuation properties

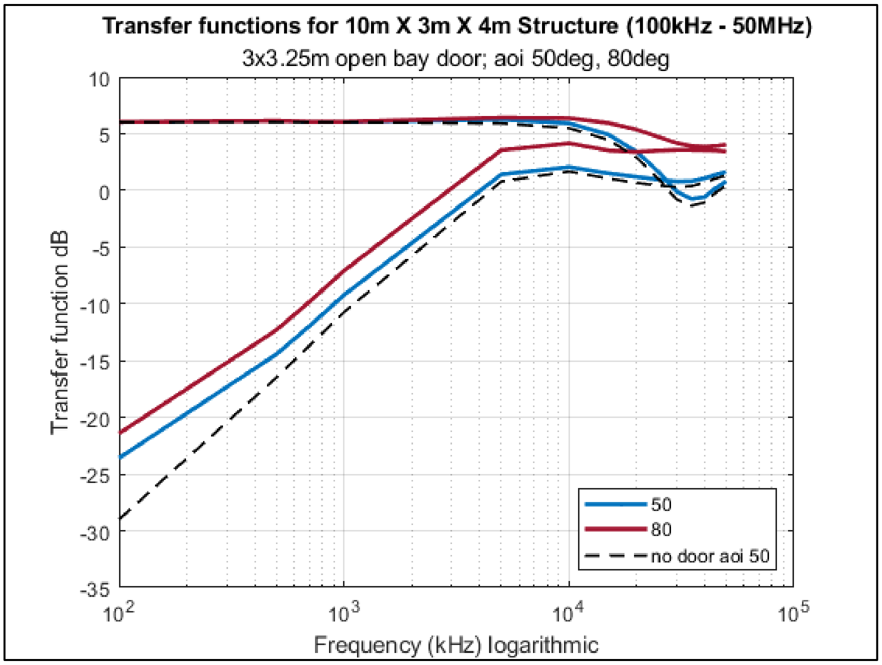

(a)

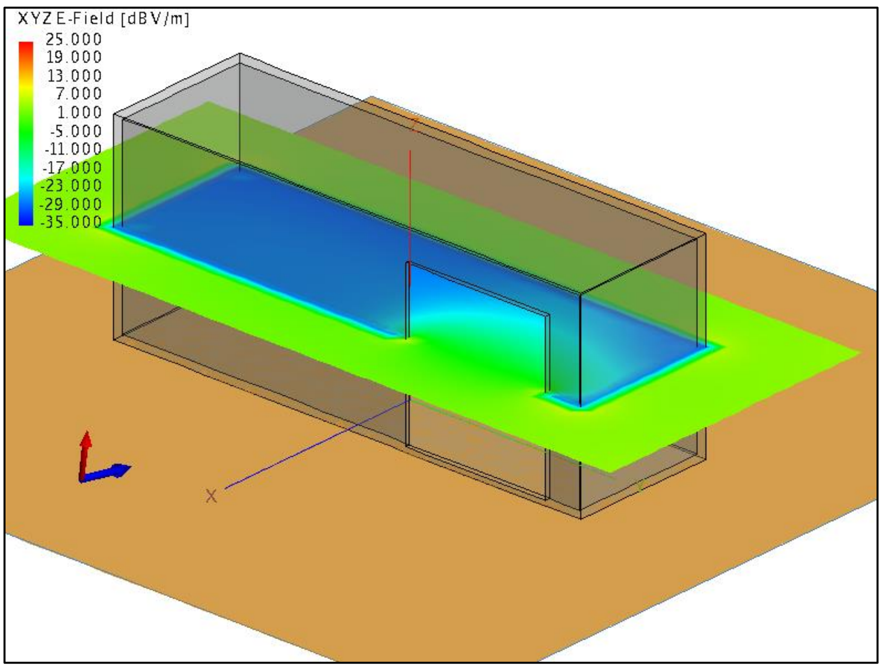

(b)

Figure 5.8 Structure Transfer functions comparing various radiation AoI for a building with large open bay door (a); E field visualization at 100 kHz (b).

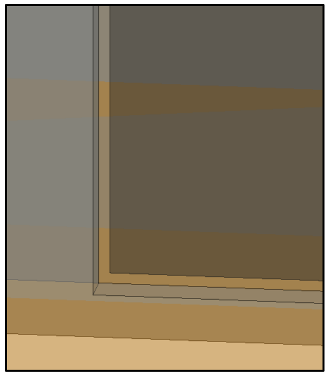

Figure 5.10 Structure bay door edge gap.

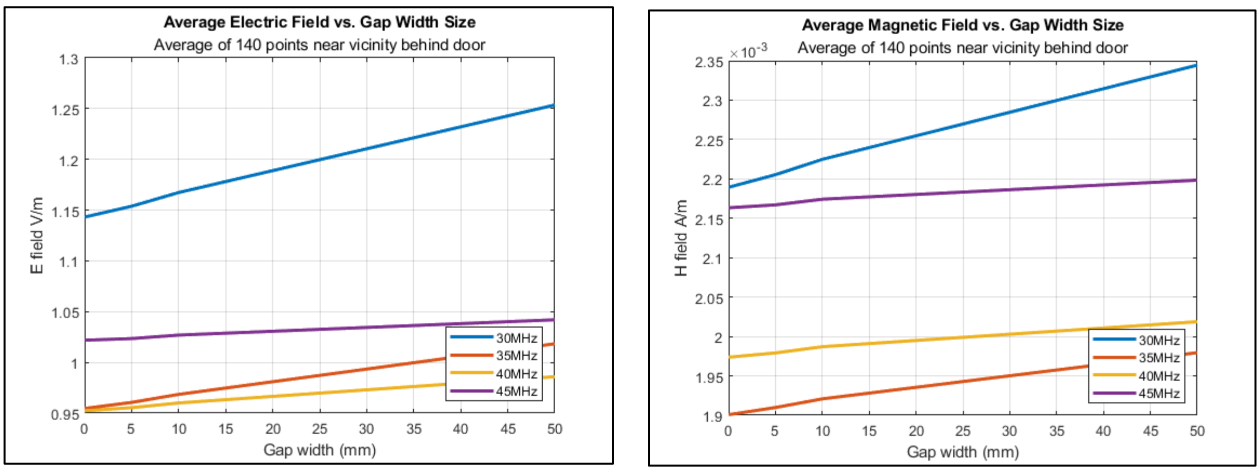

Figure 5.9 Electric and magnetic field strength behind door as a function of gap with around door.

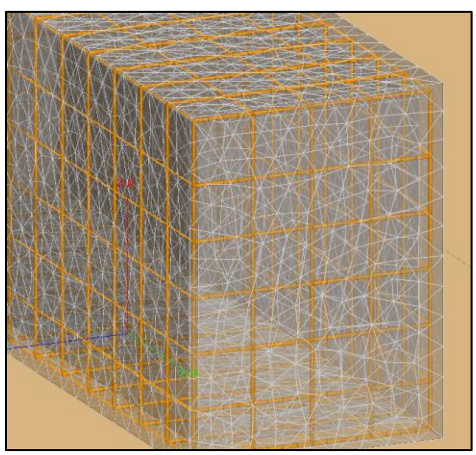

Figure 5.11 Meshed structure model including reinforcement bars.

when rebar is incorporated. Both the E and H fields are shielded significantly throughout the entire frequency range when compared to a structure without rebar. The closer the rebar is placed together, the better the shielding. When the 'window' gaps between rebar are smaller, relatively larger wavelength radiation is restricted from passing through and thus smaller gaps constitute better shielding for higher frequencies. Regarding the base case 24-inch spaced rebar, the H field is attenuated ~6 dB throughout most of the frequency range. The E field is attenuated beyond 40 dB at the lowest simulated frequencies and remains attenuated beyond 10 dB even at 40 MHz. Figure 5.12 plots the reinforced structure's transfer function for various rebar spacing configurations. Figure 5.13 illustrates the effective H field attenuation. It is worthwhile to point out the magnetic field points of higher intensity which appear along the long axis exterior walls of the structure.

Another common construction practice is to ground the reinforcement bars to the earth. A structure's concrete footings lie deep in the earth and are composed of reinforced concrete [48]. In some cases, rebar extends out of the footing into the earth to serve as an electrode [48]. Alternative methods include anchor bolts, concrete enclosed electrodes, and rebar meshes. The simulation model achieves grounding by extending rebar at each corner of the structure down to contact the ground plane. The same simulation is conducted and transfer function results obtained. Virtually no difference is observed in the average transfer function results when the rebar is grounded. To further analyze grounded rebar, a simulation of a pure rebar cage structure (no dielectric) is carried out. Without the concrete the E field is not shielded nearly as well at low frequencies. The interior volume is susceptible to an intense resonance at 40 MHz excitation. Also grounded rebar plays a more drastic role and improves the attenuation of the rebar cage. Both the E and H fields are attenuated by 6 dB within the cage at lower frequencies, and this improves to approximately 12 dB for the E field when the rebar is grounded. However, when the rebar is grounded, another strong resonance is observed at an excitation of 10 MHz. Figure 5.14 plots the aforementioned results.

The last tested variable associated with rebar is the rebar's diameter. The structure's shielding effectiveness is compared with number 8 and number 10 rebar (1 in and 1.25 in). It is determined larger rebar does slightly improve attenuation properties for both the E and H fields. Simulating the same model, attenuation improved by approximately 1 dB. Finally, a convergence study is conducted to validate results under finer mesh conditions. Simulations are done for a model with 9,000 elements, 12,000 elements, and 14,000 elements. In all cases results are nearly identical. It is worthwhile to note, fine meshes are more critical for accurate results at the lower frequencies. The results from these simulations may be found in Figures A1 and A2 of the Appendix.

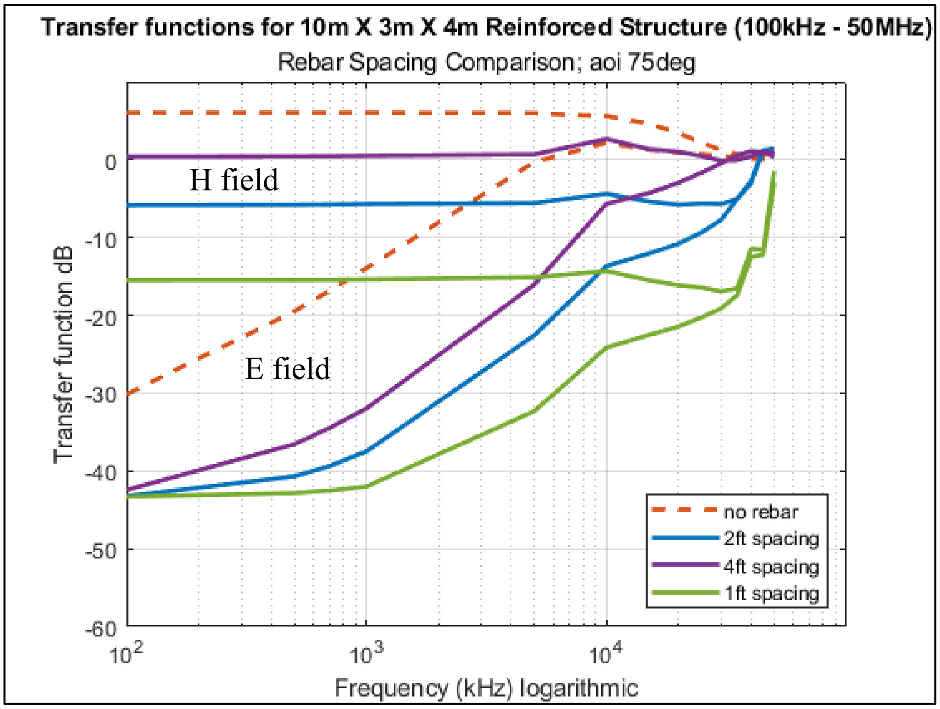

Figure 5.12 Reinforced structure transfer functions comparing various rebar configurations.

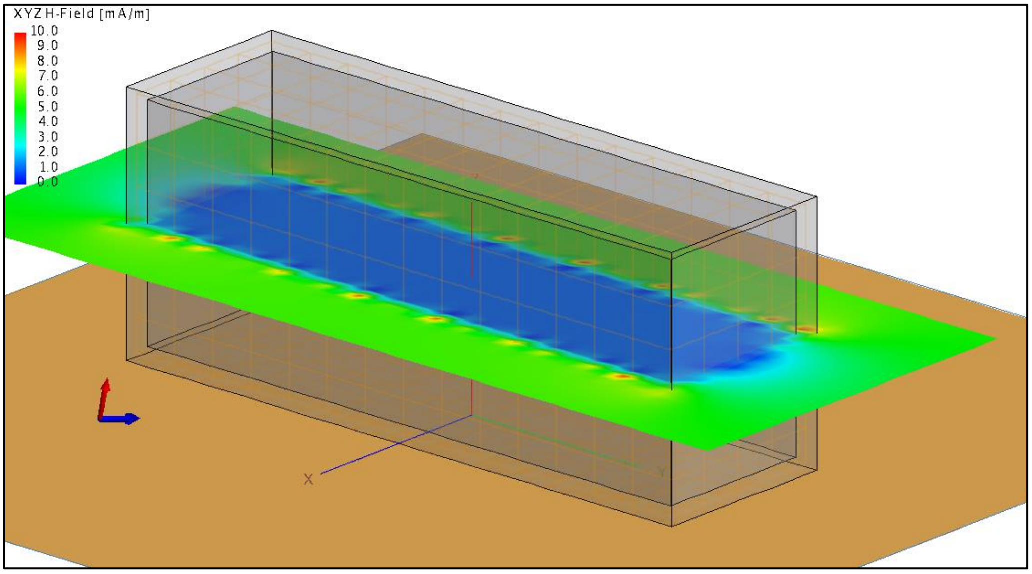

Figure 5.13 Reinforced structure (24-inch spaced rebar) H field results at 1 MHz excitation.

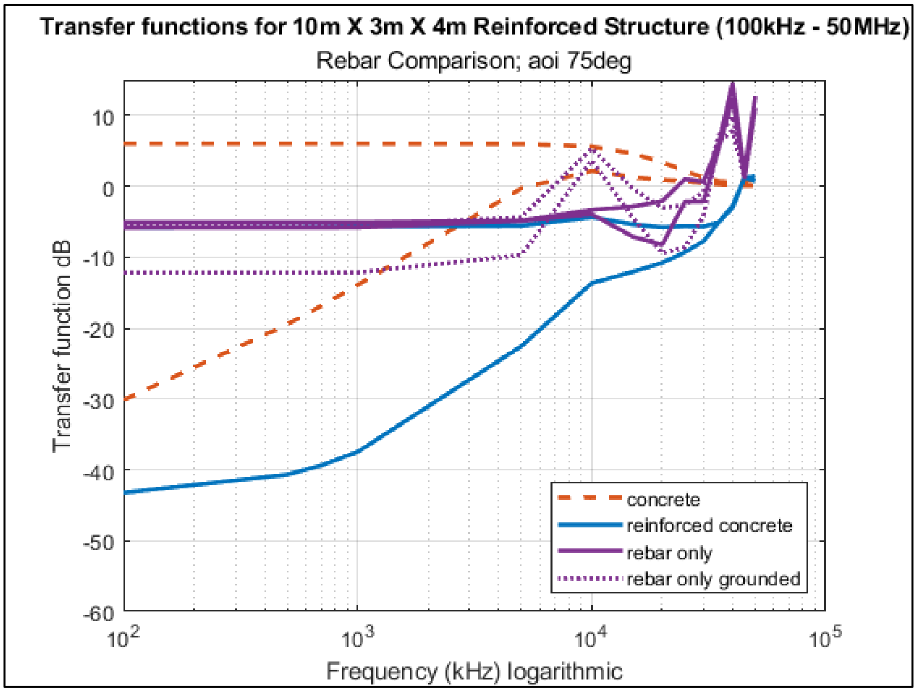

Figure 5.14 Reinforced structure transfer functions comparing various rebar grounding configurations.

5.3.2 Shielded Concrete

Both ongoing and published research [49], is investigating adaptations in building materials for improving their shielding effectiveness against electromagnetic threats. One method is the development and use of shielding concrete. Shielding concrete is concrete containing powder or filings of conductive and magnetic materials such as iron and nickel. A simulation is conducted to test the effectiveness of shielding concrete at HEMP range frequencies. Attenuation transfer functions for a 3 m cubical structure are evaluated for three cases. The three cases are as follows: normal dielectric concrete with a conductivity of .02 S/m; conductive concrete with a conductivity of 2 S/m; and PEC plated concrete. As expected, the plated concrete performs extremely well maintaining attenuation beyond 50 dB for the entire frequency range. The conductive shielding concrete provides excellent E field attenuation greater than 30 dB for the entire frequency range. The H field attenuation improves with frequency. Attenuation for both the plated and shielding concrete increases at frequencies beyond 30 MHz. The comparison can be visualized below in Figure 5.15.

5.3.3 Metallic Roof

Previous simulations are conducted for a building model completely enclosed by concrete. However, many industrial structures are constructed with a metal roof. A structure's roof is a massive design characteristic which can drastically affect the shielding effectiveness. Not only is the roof a huge portion of surface area directly exposed to the open air, it is also a discontinuous feature when non-homogenous with the walls. Figure 5.16 exhibits a view of the roof from the interior of the Chickamauga generator room. This figure is intended to provide the reader with a visualization of a non-homogenous roof construction. This section documents the analysis of metallic roof construction and its effects on a structure's electromagnetic shielding effectiveness.

Two different configurations are modeled and simulated: one with a perfect conducting layer placed on top of the interior volume and walls; the other similar except the PEC layer is placed exclusively on top of the interior volume (not the walls). As this layer is a perfect electric conductor, no thickness is considered. Additionally, no gap between the wall tops and the roof exists. Figure 5.17 illustrates the configuration of the models.

Similar to previous cases, the field results are calculated from many points spread throughout the rectangular structure's interior and then averaged. Transfer function results for both metal roof models are compared with results from an entirely concrete building. Surprisingly, the magnetic field attenuation is nearly unaffected when regarding

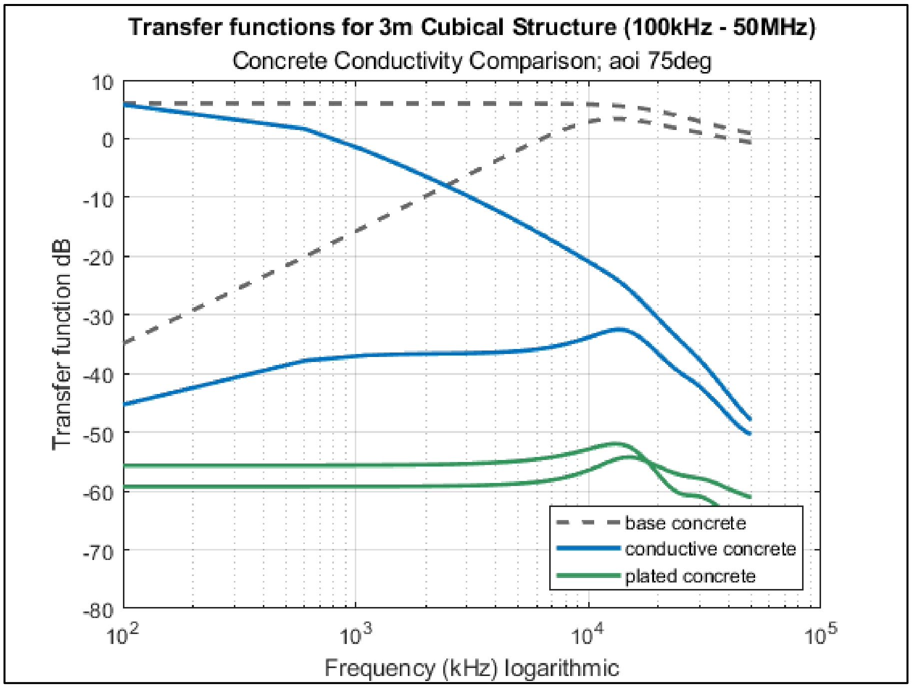

Figure 5.15 Structure attenuation transfer functions for various concrete types.

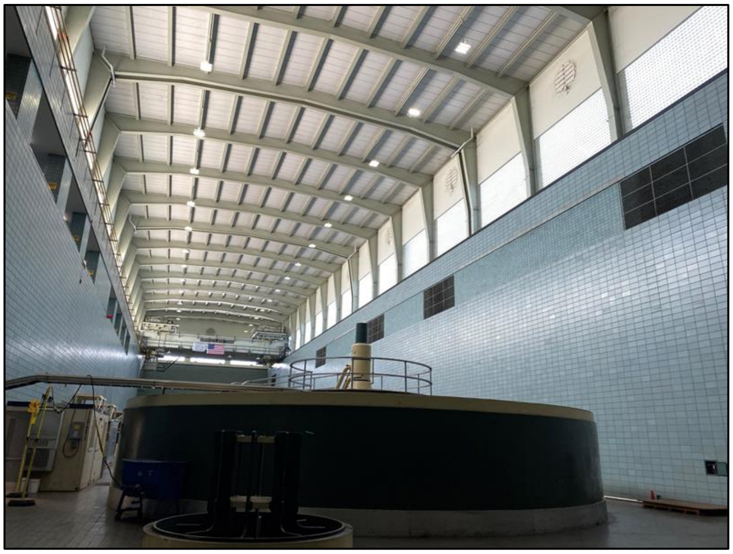

Figure 5.16 TVA Chickamauga generator room interior roof view.

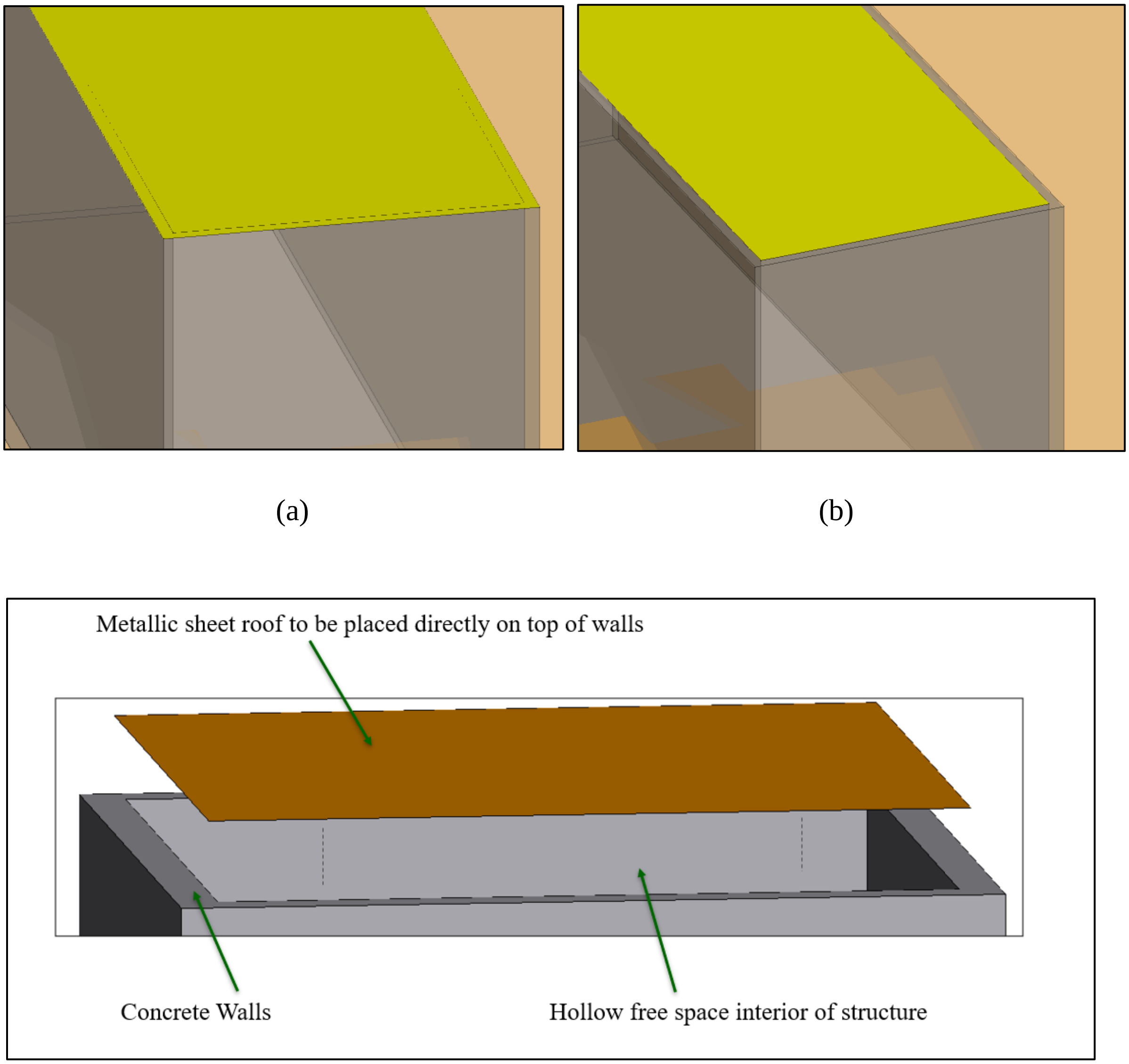

(a) (b)

(c)

Figure 5.17 Metallic roof modeling approach; wall and interior coverage (a); interior coverage (b); isometric visualization (c).

metal vs. concrete roof construction. When considering the metal roof which extends to the exterior wall edge (pictured in Figure 5.17a), slight E field attenuation improvement is observed especially at lower frequencies. The most interesting observation results from the metal roof which only extends to the interior wall edge (pictured in Figure 5.17b). Over 20 dB of attenuation is lost at 100 kHz excitation, and a significant reduction of attenuation is observed up to 5 MHz excitation. Figure 5.18 plots the transfer function results. The full coverage metal roof exhibits shielding very similar to the fully homogenous concrete roof.

To determine the explanation behind the significant reduction in shielding for the interior wall edge extended metallic roof case, more simulations and analysis are conducted. Models are created with a reduced perimeter roof to incorporate a small gap between the roof and walls. Similar results are observed and radiation is infiltrating as if there is a gap between the roof and walls. To understand the physics of this phenomena, it is helpful to introduce some radar terminology. A surface wave, also known as a creeping wave, is an electromagnetic signal which couples and travels on a large flat surface. Whenever this wave hits a discontinuity such as an edge, energy is re-scattered into space in many directions. In the model, this roof edge is directly exposed to the structure's interior without any medial concrete. Therefore, this edge is a significant point of EM infiltration whenever surface currents are induced on the metallic roof. Figure 5.19 pictures the electric field focused on the joint between the roof, walls, and interior.

Although the full coverage metal roof model possesses a similar edge, the space between the edge and the interior volume is filled with concrete thus successfully attenuating the electric field. Up to this point the question of whether the observations are truly from a physical result or a simulation artifact remains. A similar simulation is carried out in a finite difference time domain (FDTD) software to validate the MoM results. The same reduction in attenuation for the partial covered roof is observed in the FDTD results thus validating the case study. Refer to Figure A3 of the Appendix for FDTD result plots.

5.4 Geometrical Considerations

The models studied throughout this work are kept geometrically simple for two primary reasons. The first reason is to minimize the computational demand required for simulation. Studying the HEMP phenomena requires analysis of a wide frequency band and thus significant computational resources. Even small scale and geometrically simple models simulated throughout this work require tens of gigabytes of memory, and can take

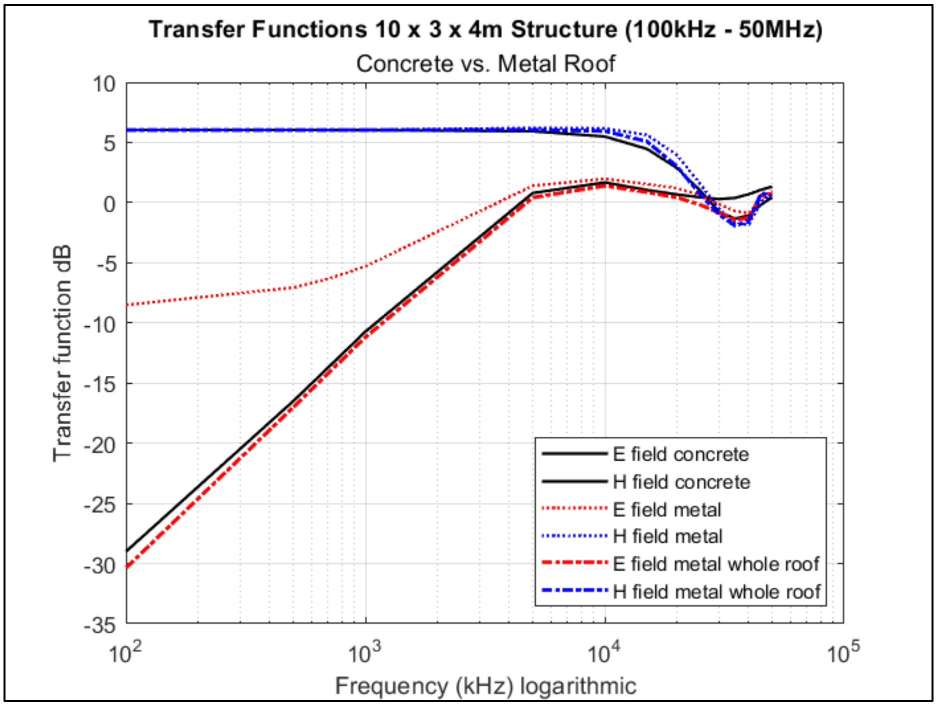

Figure 5.18 Concrete structure transfer functions comparing various roof constructions.

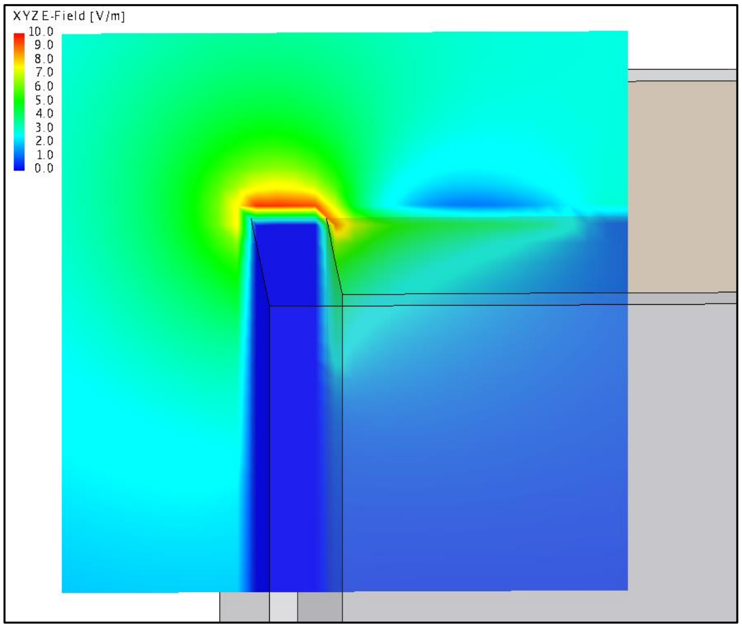

Figure 5.19 Metallic roof edge as E field point of infiltration (100 kHz).

over a dozen hours of run time utilizing six cores. By simulating geometrically simple and relatively small models, the computer memory requirement and solving time can be minimized. The second reason is to obtain generalized results. Power generation facilities and other large-scale industrial complexes are unique in design and layout, and contain many geometrical intricacies. Results from generalized simple models can be applied and extended to a variety of complex facilities. Basic geometrical considerations are studied to broaden the applicability of the results generated from this work in addition to answering some fundamental shielding effectiveness questions.

The first shielding effectiveness question asks how wall thickness effects penetration loss. Basic logic tells us a thicker wall should provide more shielding. But of course, thicker walls constitute more material and thus higher construction costs. Another consideration is that, at certain frequencies, a material may be effectively electromagnetically transparent and thickness wouldn't make much difference. To clear up this question a simple simulation is conducted on two cubical models: one with 10 cm thick walls, and one with 30 cm thick walls. A transfer function is developed and compared from the exact same interior points. The computed transfer functions are compared below in Figure 5.20. The thicker-walled structure provides much better E field shielding; as much as 6 dB for the entire low frequency region and approximately 3 dB throughout the resonance region. The magnetic field propagation loss is indifferent for both structures until frequencies beyond 10 MHz are reached. In the higher frequency resonance region, the thicker-walled structure exhibits improved attenuation. Overall shielding effectiveness is well improved throughout the entire frequency range studied. Considering the overall volume of the cubical structure as 27 m^3, the volume of concrete for 30 cm walls is 13.176 m^3, and the volume of concrete for 10 cm walls is 5.048 m^3. The thicker-walled structure requires over two and half times the amount of concrete.

Two different structure geometries, cubical and rectangular, are considered for all simulations in this thesis. Both exhibit six sides, sharp edges, and significant sections of continuous, flat surface area. The key geometrical difference is that the rectangular structure possesses one dimension considerably larger than the other two. The question arises whether the overall wall propagation loss is different between the two geometries. Large industrial facilities may have closer resemblance to one or the other geometries and thus this comparison is insightful. As many variables as possible are held as control variables to simulate the two geometries precisely. Incident radiation is maintained at a fixed AoI of 50°, ~140 interior points equidistant from the walls are averaged for the transfer functions, the wall thickness is maintained at 10 cm, the wall material dielectric properties are employed as the same, and the overall volume is maintained at ~120 m^3 for both models. The cubical model is constructed with 5 m side lengths and the rectangular

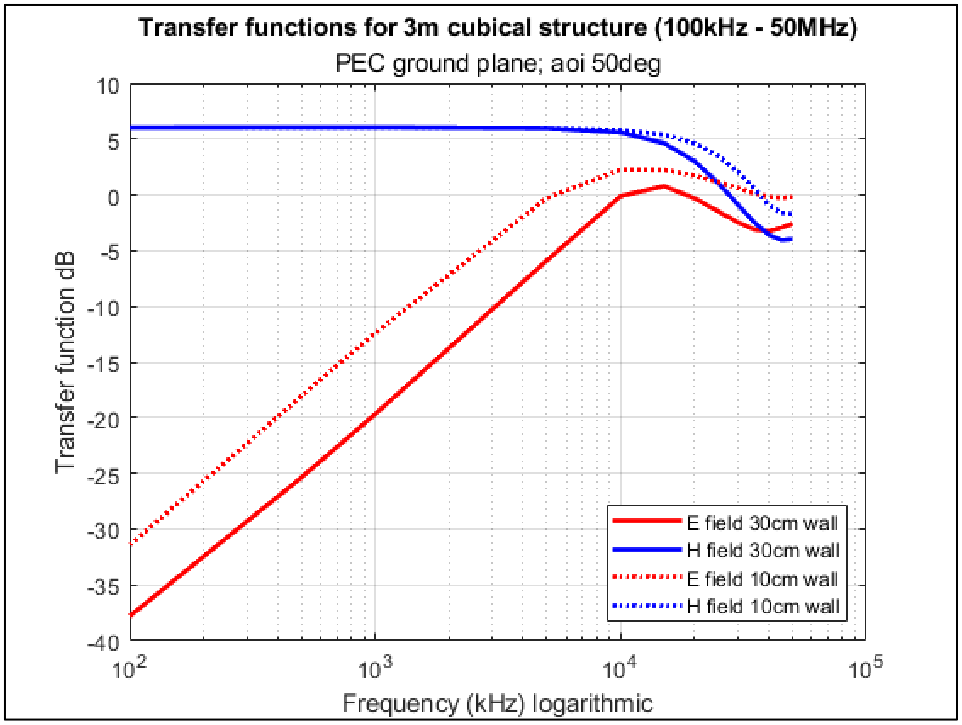

Figure 5.20 Cubical structure transfer functions comparing concrete wall thickness.

model is a 10 by 3 by 4 m structure. The general attenuation trend is similar between the two models; however, the rectangular structure exhibits slightly better E field shielding up to 10 MHz and the cubical model exhibits better E and H field shielding at higher frequencies. Results are compared in Figure 5.21 below.

For completeness, another simulation is conducted on the rectangular structure. Initially the incoming radiation is incident upon the 10 by 4 m wall, which possesses a surface area of 40 square meters. The additional simulation is carried out after modifying the excitation source such that the incoming radiation is incident upon the 3 by 4 m wall. Generator rooms belonging to multi-unit hydroelectric power plants exhibit geometries where one dimension is significantly longer than the other as the length of a dam is often larger than the width. Transfer function results indicate a similar attenuation response for both cases. The field values are very similar and don't diverge for the two models until the upper end of the frequency region. It is unlikely the burst location, and thus the direction of incoming radiation, will be known during a real event. However, from these results, it is reasonable to assume an unaltered structure shielding effectiveness regardless of direction of incidence. It is important to note site-specific infrastructure, topography, and construction may impact the incoming radiation in a significant and unsymmetrical manner.

Site-specific infrastructure is mentioned in the previous paragraph. Such infrastructure may be external to the generator or boiler room facility and thus left electromagnetically vulnerable. For example, motors, relays, breaker panels, and supportive equipment may be placed outside of a primary site building. Most of this research focuses on electromagnetic effects observed inside a building, and thus some knowledge of exterior effects is important. Potentially certain locations exterior to a large facility are more susceptible to intense EM fields. Simulations are conducted to collect E and H field data for a number of points within five volumes. Each volume is adjacent to one of the structure walls and roof and extends 1 m away from the structure. Figure 5.22 pictures the reinforced concrete structure model and data collection volume.

Plane wave radiation is incident upon one of the short dimension walls at an AoI of 75°. The attenuation transfer function is defined exactly as before where the calculated field values are ratioed with the free space field values. The E field is amplified by nearly 15 dB above the structure's roof at low frequencies. In fact, the E fields which develop above the roof are much stronger than anywhere else around the structure. This result is consistent with the electromagnetic boundary condition where E field strength increases with height above a ground plane up to a quarter wavelength height. E and H field levels drop significantly at frequencies beyond 15 MHz. Field values are weakest along the long

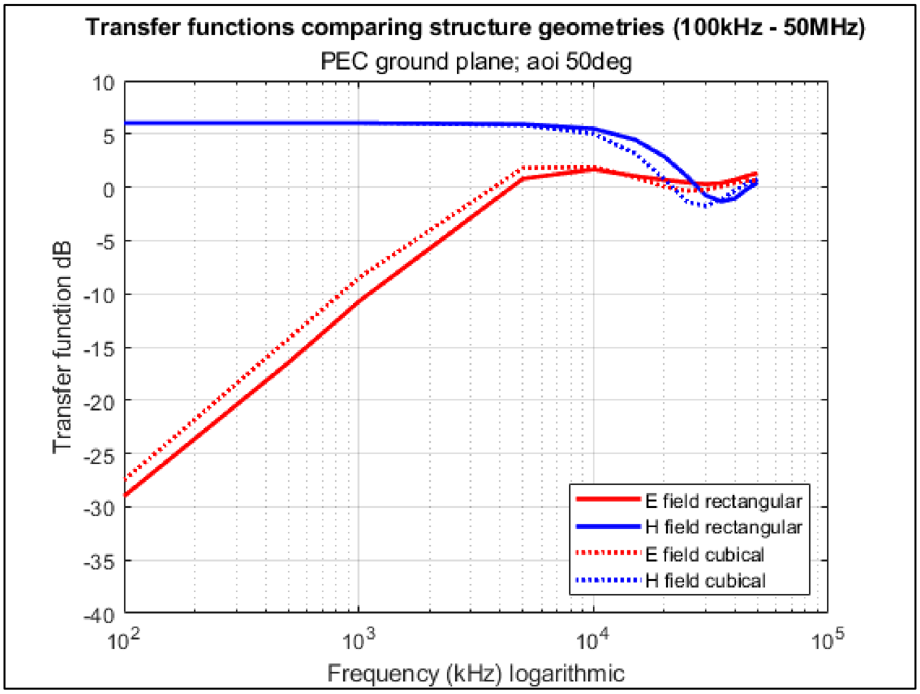

Figure 5.21 Cubical vs. rectangular structure transfer functions.

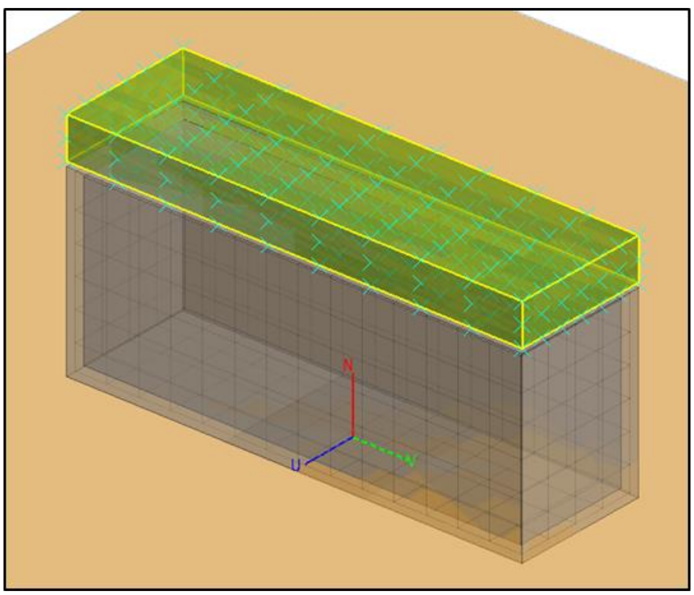

Figure 5.22 Model for exterior field value simulation.

-dimension walls. Results for the short dimension wall incidence field values are plotted below in Figure 5.23. Simulations also are conducted for radiation incident upon the long -dimension wall and the associated field strength transfer function results are plotted in Figure A4 of the Appendix.

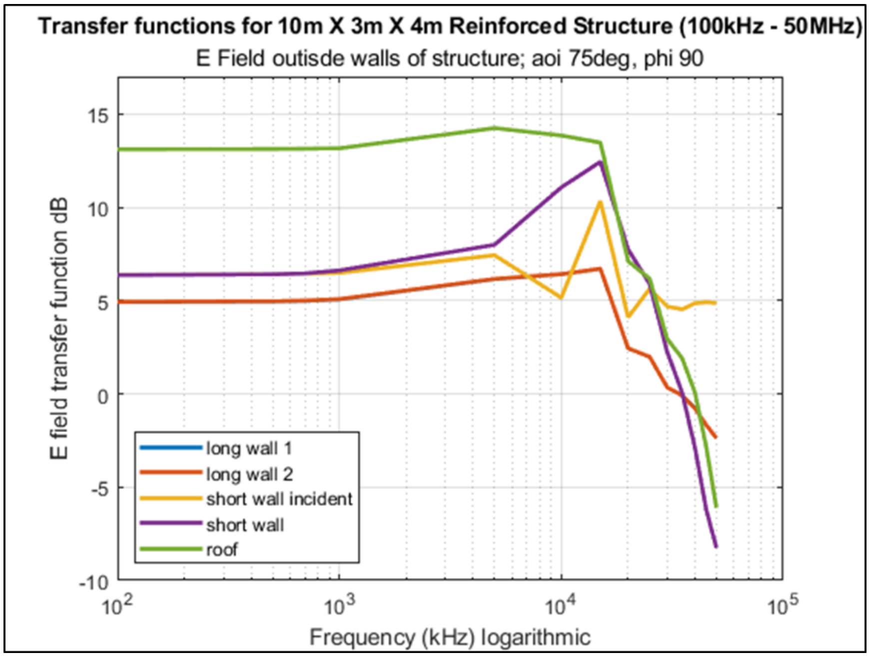

(a)

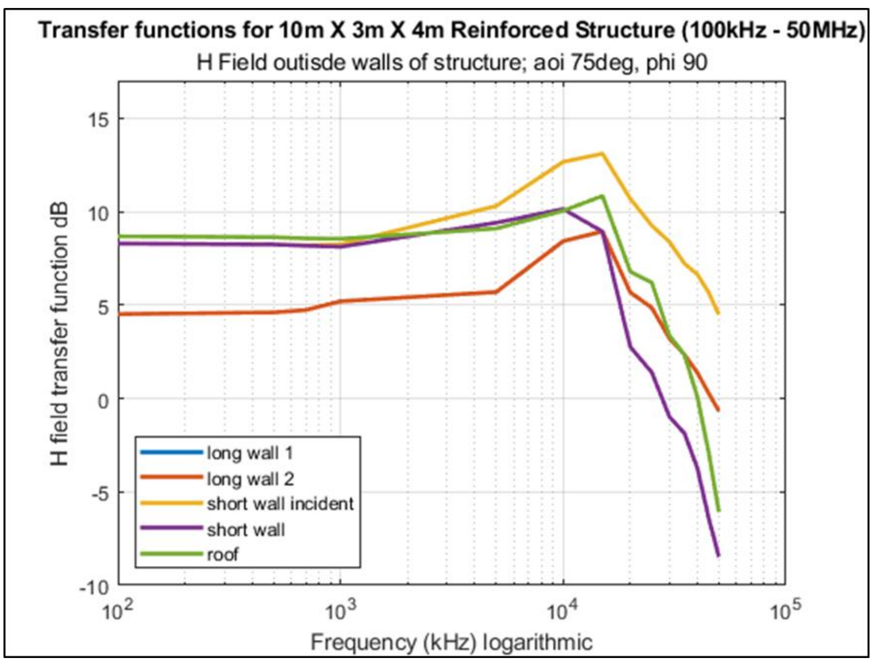

(b)

Figure 5.23 Field strength transfer functions, E field (a), H field (b), for volumes exterior to the structure.

Chapter 6

Line and Cable Coupling

6.1 Overview

In manner similar to the previous research, this chapter expands the scope of work by further complicating the shielding effectiveness problem. A building's walls could be extremely effective shielding against E1 radiation; however, a cable or line which penetrates such walls could be a significant point of infiltration. Previous chapters focused on diffused fields, and the focus will shift now to conducted energy and re-radiated fields. This chapter studies how E1 energy is coupled to, travels on, and re-radiates off lines and cables which penetrate building walls. Additionally, the effectiveness of cableshield and grounding locations as mitigation practices are analyzed. The studied variables include line diameter, height above ground, line termination, and length of line. Induced current magnitudes on the lines, termination voltages, and field values around the lines characterize the coupling results. The structure's transfer function is also calculated to determine the overall shielding effectiveness. Mignardot's published conference paper [50] summarizes the effect of penetrating cables and power generation facility structure shielding effectiveness. Results from Mignardot's work are explained comprehensively in this thesis. Additional works dive deeper into HEMP cable coupling focusing on electromagnetic compatibility (EMC) [18], [51]—[55]. The referenced works either focus on the physical analysis of EMP coupling, or transmission infrastructure. As mentioned in Chapter 2, previous research has not studied the frequency-dependent shielding behavior and how penetrating cables may influence such behavior. A small number of studies have touched on EMP coupling and transient response of cables near and/or penetrating a facility structure [56], [57]. This chapter not only analyzes the induced currents and transient behavior, but also documents the results regarding the effect on penetrating cables as a point of infiltration reducing a structure's shielding effectiveness.

6.2 Approach

Many types of cables, lines, and wires exist at power generation facilities, including both overhead and buried circuits. These lines can vary in size and number depending on the purpose. For instance, high voltage power lines are large and overhead while low voltage instrumentation and control cables are often buried. Many of these lines provide power and communication signals to critical equipment across the facility, and any coupled energy would be delivered to the connected equipment. Buried cables are often encased in plastic or metallic conduits which are laid in concrete or soil up to a few meters beneath ground level. Such buried cables are shielded not only from the conduit and concrete encasing, but also the ground itself. Therefore, the focus of this work is directed towards overhead lines. Figure 6.1. Illustrates the plot plan of Palo Verde Nuclear Generating Station. Major overhead lines and buried cables are labeled on the figure. The plan along with Ericson's descriptions served as guidance for the modeling of the cable coupling problem.

Several solution methods exist for the cable coupling problem. First is the MoM which has been used for the calculation of field values throughout this thesis. Although more computationally intense, the MoM is the most accurate method, being a full wave solver accounting for both common (antenna mode) and differential (transmission mode) mode currents, and radiating effects. The Altair FEKO software also offers a hybrid Multiconductor Transmission Line (MTL) and MoM solver. In this hybrid scheme the cable is solved with MTL and the external fields are solved with MoM. Detailed explanation of the MTL method is described by Weeks in the IBM Journal of Research and Development [58]. Finally, analytical methods such as the fundamental Telegrapher's Equations and the matrix Baum-Liu-Tesche (BLT) equation are also options for computationally expensive problems [59], [60]. To accurately capture the radiative effects of the penetrating lines, the MoM scheme is used to greatest extent possible. The MTL solver is used for more computationally demanding problems such as braided cable shield effectiveness. Although the analytical methods are fair candidates for the overhead line itself, incorporating the effects of the 3D structure would be too complex.

6.3 Transmission Line Model

The line for the base case simulation and all subsequent simulations is a single conductor with earth return path. This model is chosen for its simplicity as the earth return path is easily modeled as a PEC ground plane in the *FEKO* software. Additionally, this model represents a variety of lines which may penetrate a facilities' walls including power, communication, and instrumentation circuits. In this model, a single conducting wire extends up from a ground plane connection to a given height and is extended in a perpendicular direction for a given length before connecting back to the ground plane. Figure 6.2 portrays the transmission line model, where l is the line length, h is the height above ground, and $Zint$, $Zext$ are the interior and exterior termination impedances (interior and exterior of the structure walls). Vance defines an approximated characteristic impedance for a line above a metallic ground plane in Equation 6.1 [61]. The characteristic impedance is a real quantity dependent upon the cable's radius, a and height, h and is valid for cases when $h>>a$.

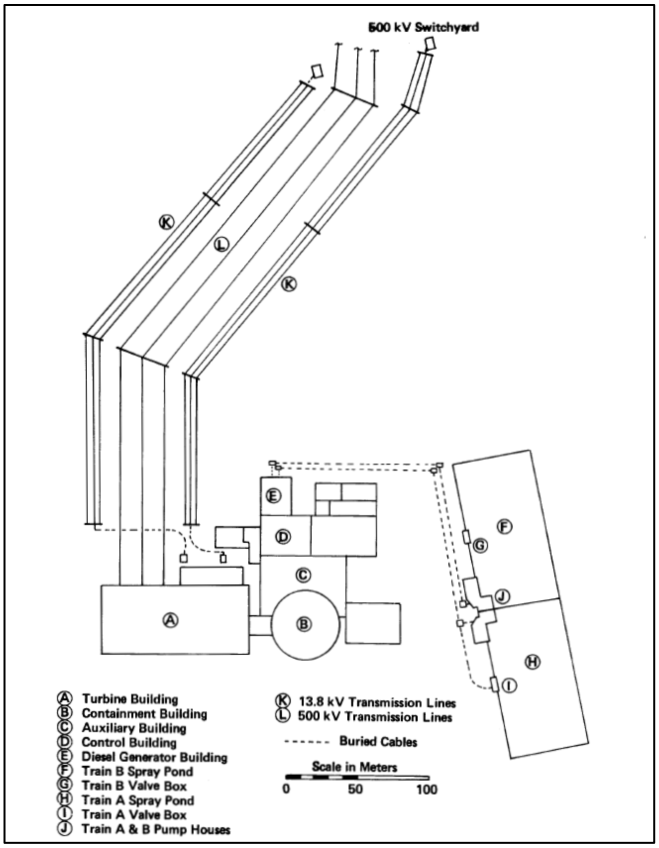

Figure 6.1 Plot plan of Palo Verde Nuclear Generating Station [20].

.

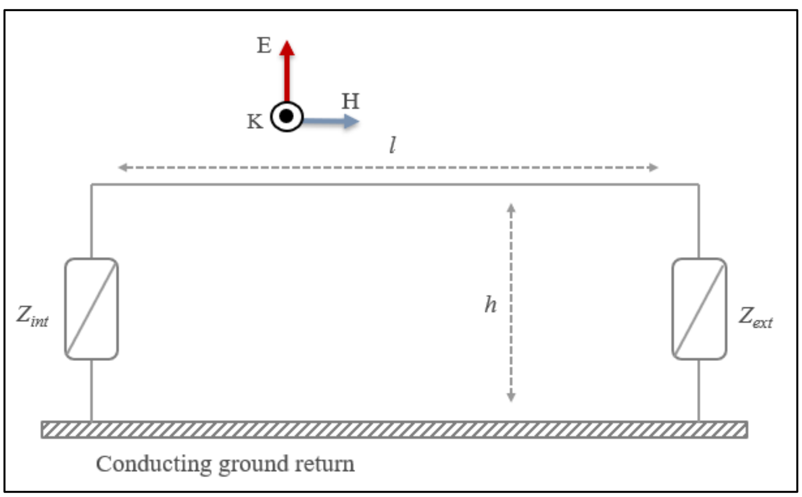

Figure 6.2 Single conductor earth return transmission line model illuminated by plane wave.

$$Z_0 = 60\log\left(\frac{2h}{a}\right) \quad (6.1)$$

The lines are excited by a plane wave excitation source defined similarly to prior simulations. This normalized plane wave is vertically polarized and propagates with an AoI of 75°. The direction of propagation, either parallel or perpendicular to the line enclosed area, is simulated to determine which constitutes the strongest coupling. For a 10 m line 1 m above the ground plane excited at 10 MHz, largest currents are induced when the incoming radiation is perpendicular to the line. However, results may vary for different frequencies. See Figure A5 in the Appendix for coupling current results. The frequency range and frequencies analyzed are maintained as previously in this thesis.

6.4 Structure Model

The building structure employed in all cable coupling simulations is the same 10 by 3 by 4 m rectangular structure. The model has 20 cm wall thickness and includes 5 cm diameter reinforcing bars in all six walls. The rebar is placed in the center of the concrete walls and each rebar is spaced approximately 61 cm apart in each direction. The rebar and the ground plane are modeled as PEC while the concrete is modeled as a frequency-independent dielectric. The penetrating line enters the structure wall through a small aperture, and exits the structure through a small aperture in the floor. Connectivity with the ground plane is made beneath the structure floor. The building model is pictured in Figure 6.3. A separate model with an aperture of such size, but without the penetrating line, is simulated to observe electromagnetic penetration through the aperture itself. The small apertures demonstrated negligible effect on field values inside the structure's interior.

6.5 Simulation Results

6.5.1 Base Case

The cable penetrating problem as outlined in the above sections, is complex because of the penetration into the structure. Many variables associated with the radiation, cable, and structure influence the coupling and radiated field results. A base case model is simulated and the results serve as a comparative control. The base case provides a means to discern meaningful results and draw conclusions. The 1 cm radius line rises to a height of 2.7 m above the ground plane. The point of penetration is also at 2.7 m which lies in the upper third region of the building structure. The horizontal portion of the line is 15 m in length and penetrates approximately 1 m into the structure's interior before turning downward towards the ground plane. Two line terminations exist at the

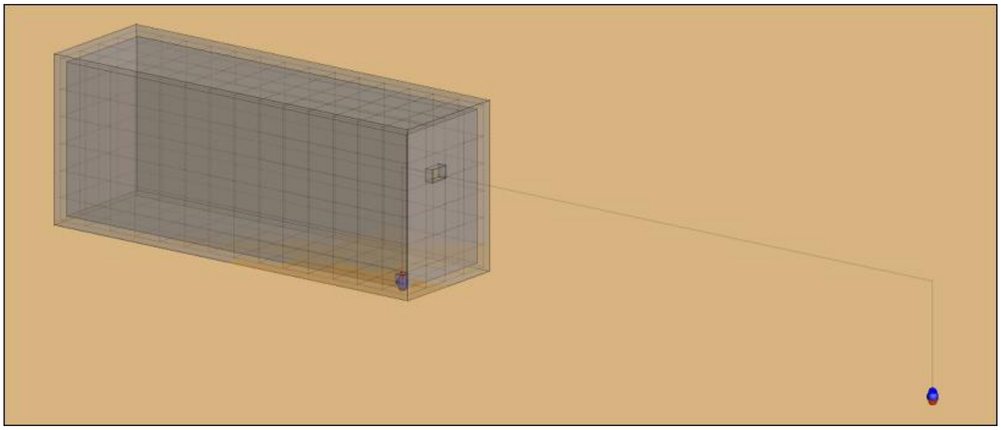

Figure 6.3 Rectangular building structure with penetrating cable.

ground plane connection points. A real impedance load is defined at each termination to equal the characteristic impedance defined by Equation 6.1. E and H field values and induced line currents are numerically calculated via MoM. Figure 6.4 displays the field results at 10 MHz excitation, which is the fundamental resonant frequency. In general, the fundamental resonance occurs at a frequency whose corresponding wavelength is double the line length. In this case, 30 m is double the line length and 10 MHz is the corresponding frequency. Figure 6.5 plots the maximum current magnitude for each analysis frequency. Figure 6.6 plots the structure's attenuation transfer function. For comparison, the transfer function is plotted with the transfer function of a building with no penetrating wire. It is also noteworthy, for this particular case and frequency, the maximum induced currents appear on the end portions of the line inside the structure. Appendix Figure A6 pictures the induced current visualization results.

6.5.2 Varying Line Height

Line height above the ground plane is the first variable associated with cable coupling studied. Different facilities may have penetrating lines at various heights serving various purposes. Height above the ground plane is an influential parameter associated with the line's coupling behavior. For instance, height is one of the two dependent parameters in the characteristic impedance calculation. Knowledge of Ampere's law of magnetic coupling tells us the larger the enclosed loop area, the more current is induced. A taller line implies a larger loop area confined by the line; thus, stronger coupling is expected. To test this theory, two line heights, 1 m and 3 m, are compared against the base case. The heights chosen account for low and upper portions of the structure. Both induced current magnitudes and the structure's transfer function are computed to obtain quantitative and qualitative results for comparison. Regarding the structure's attenuation, a 5 dB E field difference exists throughout the low frequency region between the lowest and tallest line heights. As expected, the taller the line, the more intense the electromagnetic coupling. A minimum attenuation peak is observed in both the E and H fields around 10 MHz, corresponding to the fundamental resonance. Results converge and line height appears to have little influence at frequencies above 20 MHz. This is due to the structure's high pass filter effect. At higher frequencies, the inherent E field shielding effectiveness of the structure's dielectric is reduced and the penetrating cable is no longer the primary means of radiation. Despite high induced current values at higher frequencies, the interior field values are dominated by diffused fields from the structure's walls. Figures 6.7 and 6.8 represent the transfer function and induced current magnitude results respectively.

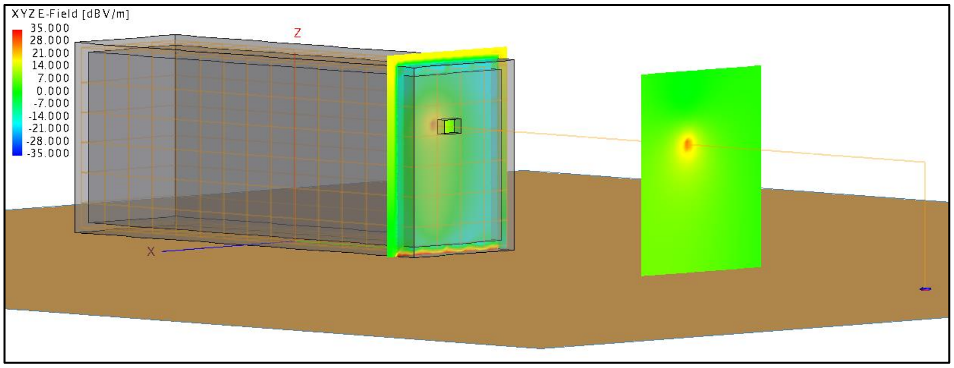

(a)

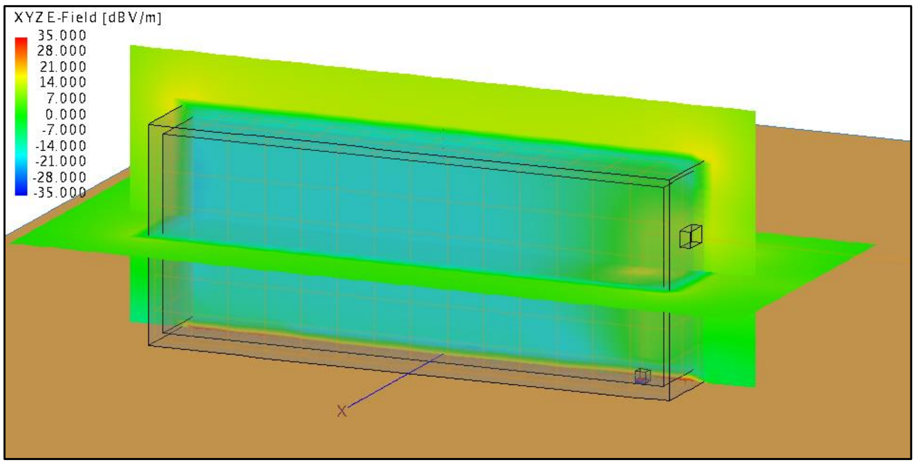

(b)

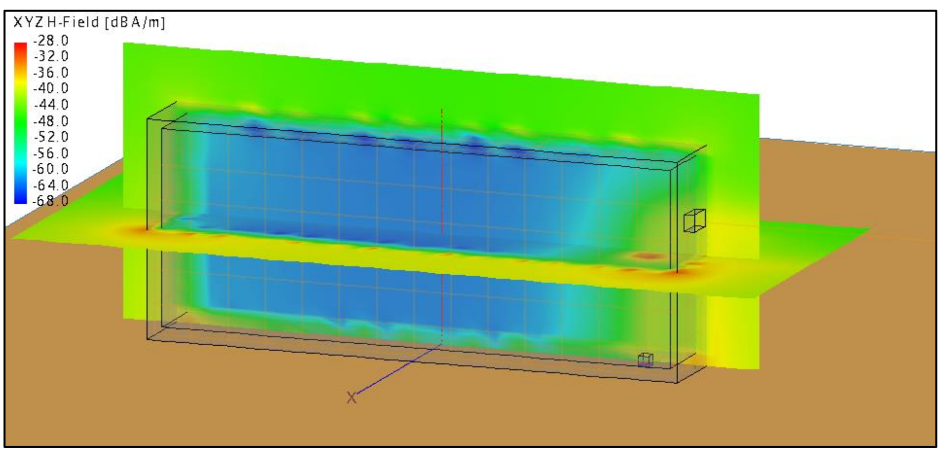

(c)

Figure 6.4 Base case field results: (a) Electric field at 10 MHz; (b) Alternate view Electric field at 10 MHz; (c) Magnetic field at 10 MHz.

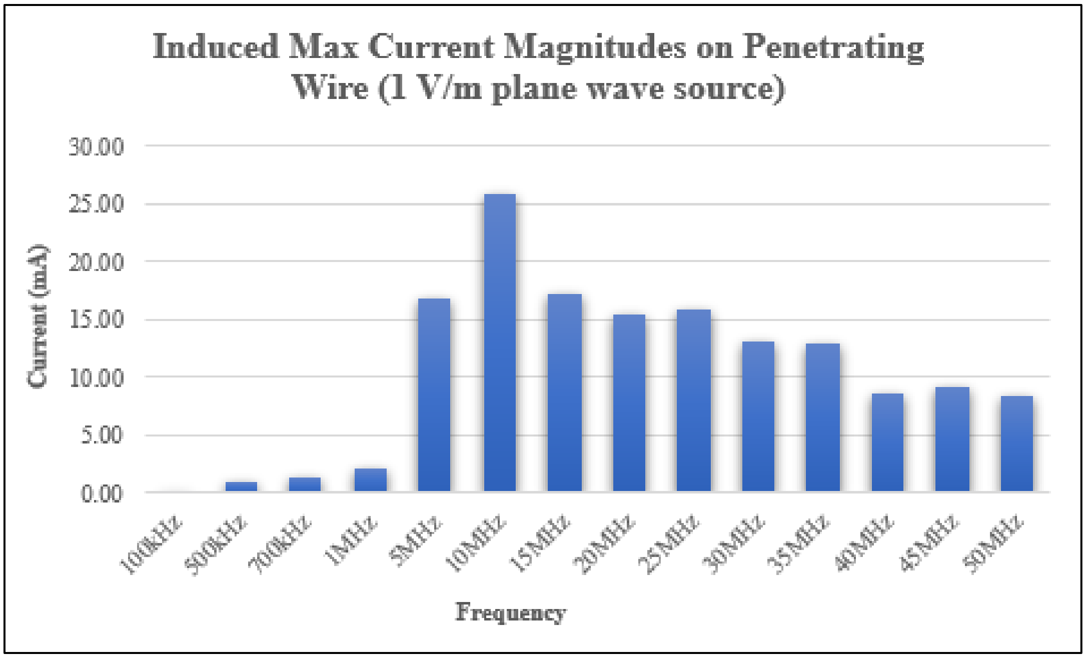

Figure 6.5 Maximum induced line current magnitudes for each analysis frequency.

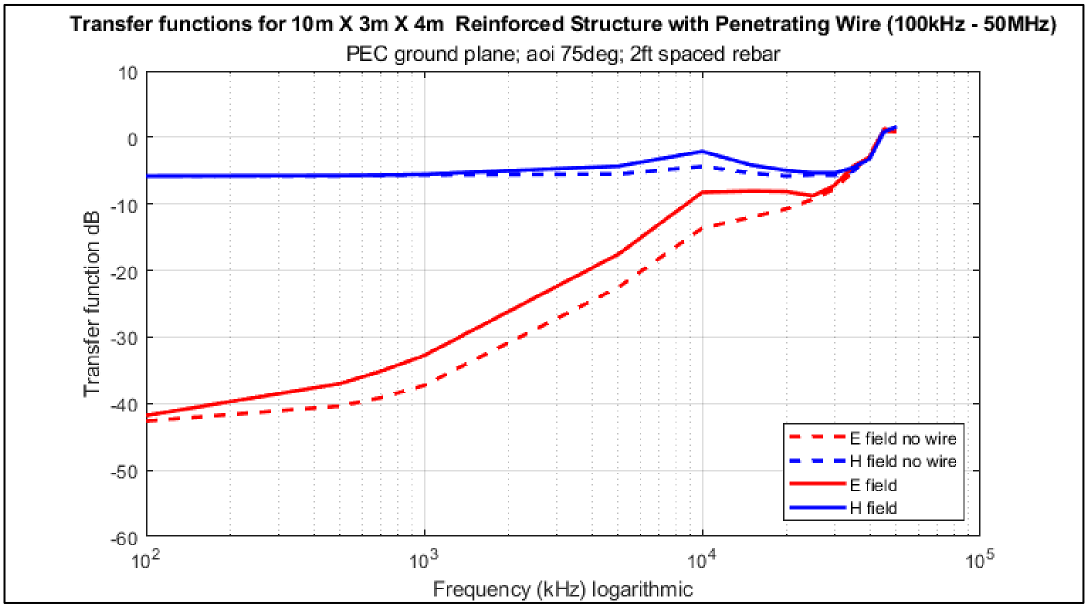

Figure 6.6 Base case structure attenuation transfer function.

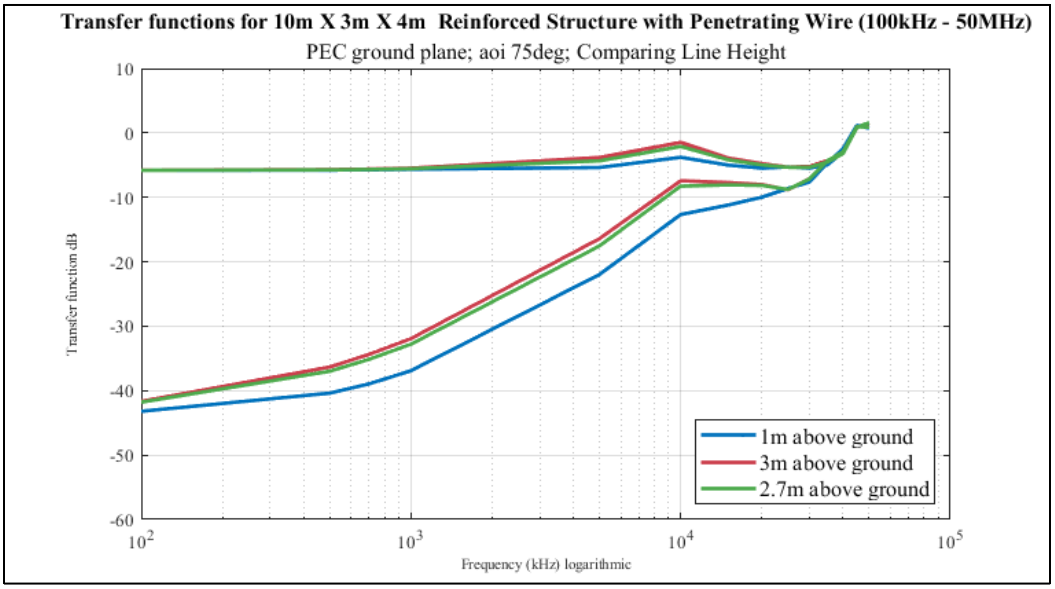

Figure 6.7 Structure transfer function comparing heights of penetrating line.

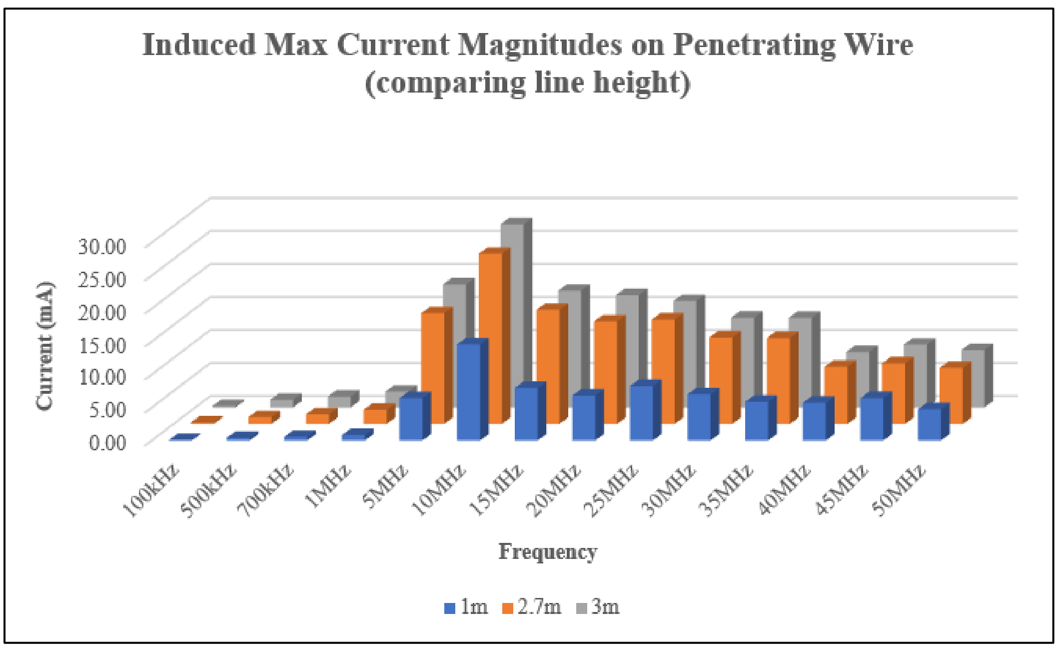

Figure 6.8 Maximum induced current magnitudes comparing line heights.

6.5.3 Varying Line Radius

The second of two dependent parameters in the characteristic impedance equation is the radius of the conductor. It is predicted to be a critical parameter. Possibly the most notable difference between power, communication, and instrumentation cables is the size of the line radius. Therefore, for this comparison it is vital to have a complete set of results. Size differences can even vary by orders of magnitude in some cases. To gather observations and characterize the associated trends of EMP coupling with penetrating cable size, the line radius is simulated over a range of 2 mm to 5 cm. Three sizes are tested starting from 2 mm and increasing by a factor of five to 1 cm and 5 cm. Information from EPRI's report on power plant cable specs [62] is used to define the cable size. As intuition tells us, the larger diameter line induces more energy. The intensified coupling response appears to increase with line size. For example, increasing the radius by a factor of 5, from 2 mm to 1 cm, results in an average 15% increase in maximum induced current. Alternatively, increasing the radius by a factor of 5 from 1 cm to 5 cm results in an average 33% increase in maximum induced current. A similar overall reduction of structure attenuation results for increasing line radius is observed as compared to increasing line height above the ground plane in Section 6.5.2. The transfer function results are plotted in Figure 6.9, and the current results are charted in Figure 6.10.

6.5.4 Varying Line Termination

When studying standard operation of transmission lines at standard power frequencies such as 60 Hz, transient phenomena such as propagation time, standing waves, and voltage reflections are not considered necessary in the calculations. However, when high frequency energy travels along the line attention must be paid to the aforementioned phenomena. Wavelengths of incident radiation from a HEMP event range from 3 to 3000 m, and thus are comparable to structure dimensions, including dimensions associated with the penetrating line. As the wavelength of the travelling signal becomes comparable with the length of the transmission line, current and voltages will not be the same at each point and the line terminations will have substantial impact on the signal reflection. This section documents results of simulations comparing the effects of different line terminations. Three cases are simulated for which the interior line termination is defined as open circuit, short circuit, and matched load. The exterior line termination is maintained as a matched load for each of the three cases. A matched load is simply the real characteristic impedance quantified by Equation 6.1. First looking at the radiated fields within the structure, the open circuit termination constitutes the strongest radiated fields. The structure's E field attenuation is reduced by as much as 10

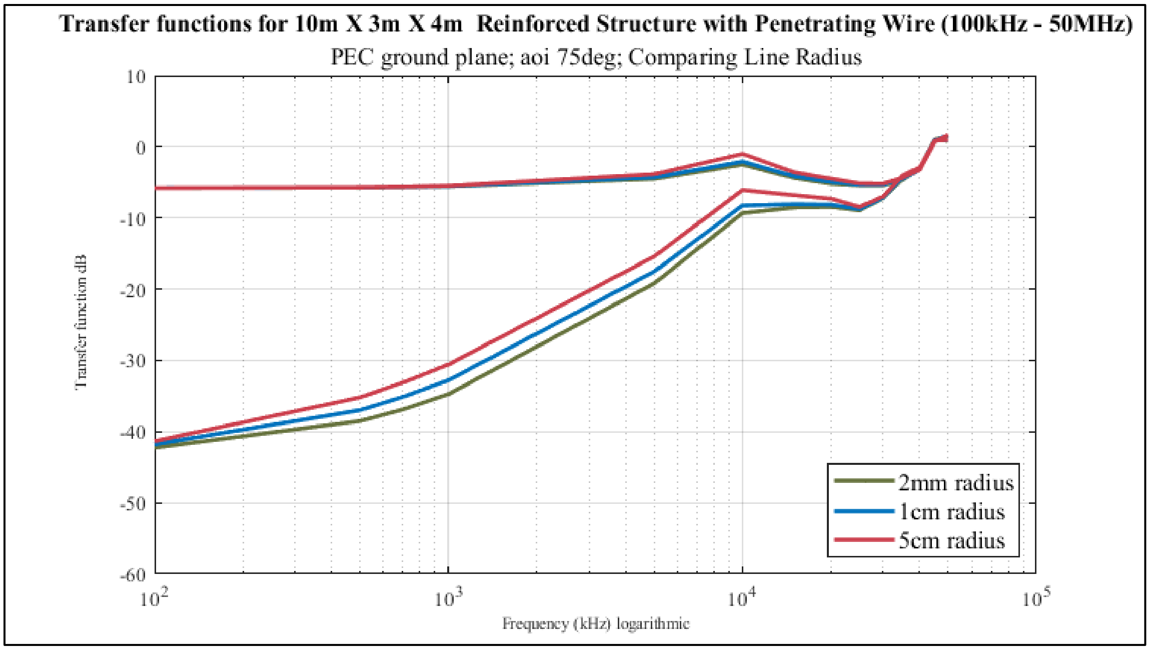

Figure 6.9 Structure transfer function comparing size of penetrating line.

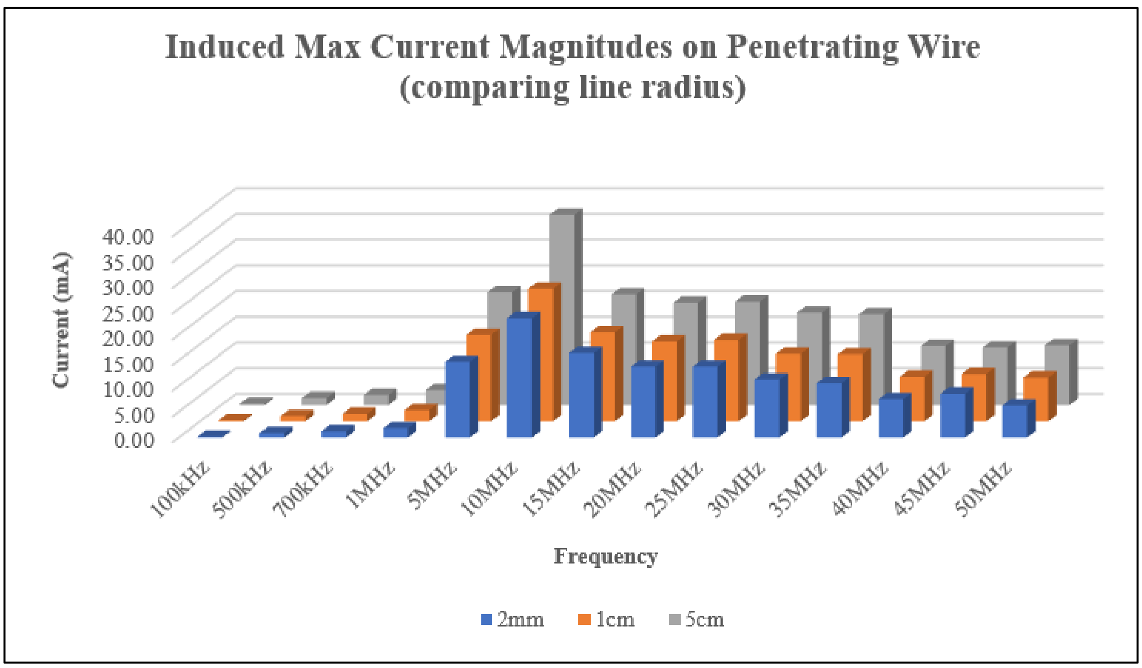

Figure 6.10 Maximum induced current magnitudes comparing line size.

dB relative to the short circuit case. In fact, the short circuit case constitutes the weakest radiated response, as the energy is directed to ground through the line. The short-circuited line appears to develop a strong radiated response at approximately 15 MHz. Transfer function results are displayed in Figure 6.11 below. Not only is the radiated energy a concern, but also the over-voltages induced at the termination. High overvoltage surges may threaten connected equipment and cause electrical breakdown damage. The line terminated in an open circuit induces the most intense over-voltage from E1 coupling. The voltage at the termination is observed as twelve times the normalized plane wave voltage. The termination voltage response is plotted in Appendix Figure A7.

6.5.5 Varying Line Penetration Distance

In the base case, a fixed length line penetrates a certain distance into a structure's interior before turning down towards the ground plane. It is reasonable to assume with more length of wire inside, more volume would be radiated. However, it is also reasonable to assume less coupling would take place if a lesser portion of the wire exists outside the facility. Two simulations are carried out to test these theories. First, the line penetration distance is extended from 1 m to 8 m while maintaining the overall line length at 15 m. This means 14 m of line exist outside of the facility in the 1 m penetration case, and 11 m in the 4 m penetration case. Secondly, the interior portion of the line is extended up to 8 m while maintaining the outside length portion at 15 m. In the second simulation case, the overall line length increases up to 23 m. Results from the overall fixed line length case indicate a slightly reduced attenuation characteristic when the line penetrates 2 m into the interior. The 4 and 8 m penetration lengths result in less of attenuation reduction despite radiating more interior volume. This is because less line exists in the free space exterior to induce large currents. In other words, the worst-case scenario occurs when the penetration distance is in the middle of the range, possibly around 3 m. The transfer function results at higher excitation frequencies differentiate more with the various penetration lengths. All simulated lengths worsen the structure's shielding effectiveness compared to the base case. The transfer functions are displayed in Figure 6.12 to better depict the results.

Secondly, the exterior portion of the line is maintained at 15 m while the interior penetrating distance is varied. Results from this simulation indicate a more severe reduction in the structure's attenuation. As the penetration distance increases the E and H field strengths inside the structure intensify, especially near the 10 MHz resonant frequency. Although the overall line length increases for each variation, the resonant point did not change. The fundamental resonance stayed consistent for the fixed 15 m length exterior portion of the line. Results are illustrated in Figure 6.13.

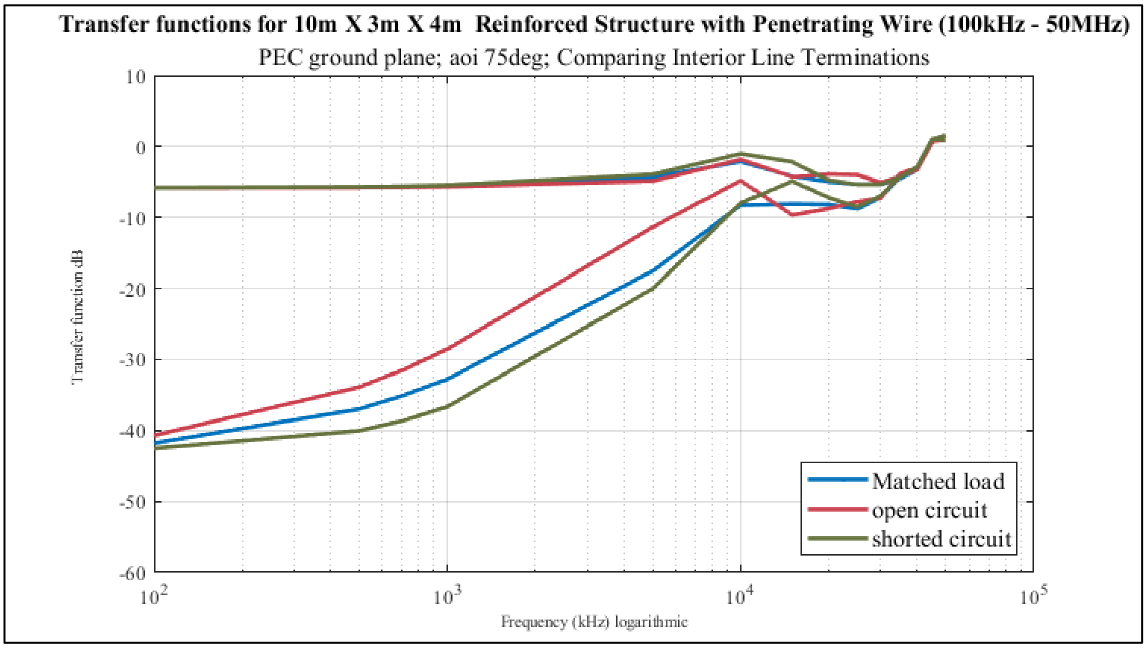

Figure 6.11 Structure attenuation transfer function comparing line terminations.

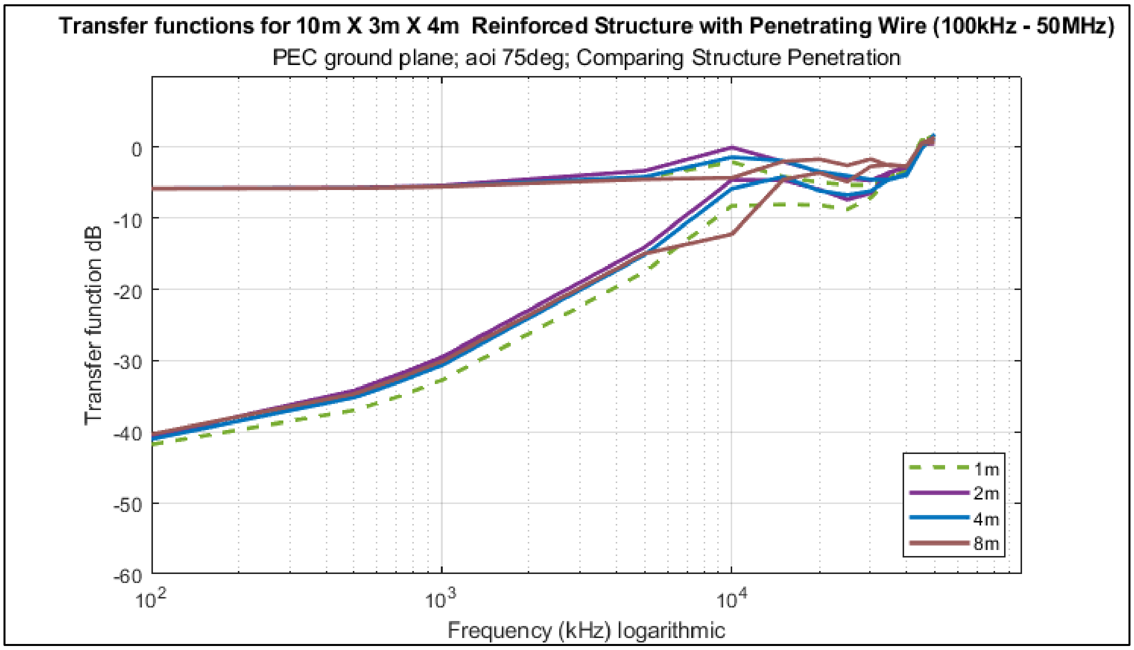

Figure 6.12 Structure attenuation transfer function comparing penetration distances of a fixed length line.

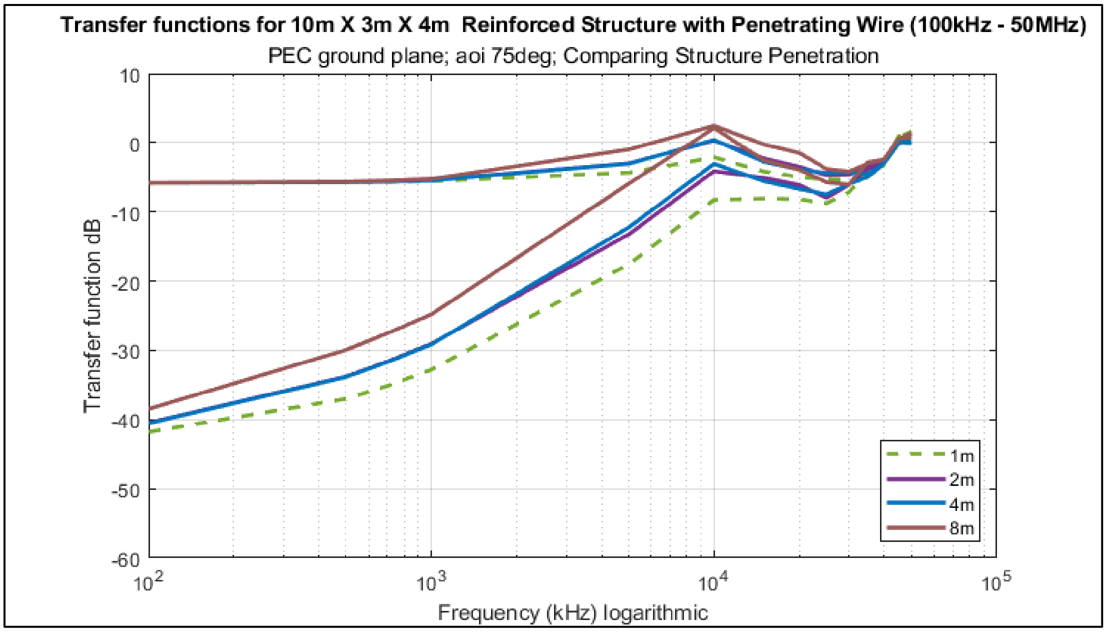

Figure 6.13 Structure attenuation transfer function comparing penetration distances of a variable length line.

6.5.6 Varying Line Length

The last, but arguably one of the most important, parameters studied is line length. Length dictates the resonant frequencies at which the most energy is coupled. In general, longer lines are able to couple more energy at lower frequencies. Line length is also directly related to magnetic coupling corresponding to the loop area defined in Ampere's law. Also, as illustrated in Figure 6.1, plant cables can vary significantly in length. For example, power cables connecting to the transmission grid or instrumentation cables spanning from building to building within the plant. To analyze the effect of line length, the horizontal portion of the line is elongated outside of the structure while maintaining all other parameters as fixed, including the length of the interior portion of the line, at 1 m. Lengths of 30 m, 45m, and 150m are compared against the 15 m base case. The results obtained indicate overall line length as the most dominant parameter tested in this line coupling study. Induced currents increase significantly as length increases, and consequently, the interior field values also intensify. Average E field shielding effectiveness is reduced by up to 20 dB when a long line is penetrating a facility's walls; and up to 5 dB for H field attenuation. As with other line parameters, the effect is most noticeable at lower excitation frequencies especially at resonant frequencies. The largest induced current magnitudes are observed at frequencies corresponding to a wavelength which is twice the geometrical line length. These results signify the penetrating line behaving as a half wave antenna system. By analyzing induced current results in Figure 6.14, one can deduce the half wave resonant frequency of a 30 m line is 5 MHz. The maximum induced current at 5 MHz for the 30 m line is significantly larger than current induced at nearby frequencies. If reading the magnitude values in tabular format is beneficial for the reader, then Table A1 should be reviewed in the Appendix.

The resonant frequencies are also observed in the transfer function and field visualization results. Highest induced currents directly correspond to strongest radiated fields. Thus, the different resonant points for the lines can be observed as 'mountain peaks' in the structure's transfer function results. The effect of line length on the structure's attenuation characteristic can easily be observed in Figure 6.15 below. The 150 m line dramatically changes the E field attenuation in the low frequency region. High intensity fields illuminate nearly half of the structure's interior at the 1 MHz resonant frequency.

Additional analysis is done for the longer line 150 m in length. Behavior of the 150 m line is consistent with the shorter length lines. The fundamental resonance is observed at 1MHz which corresponds to a 300 m wavelength (twice the line length). Also, the structure's attenuation transfer function trend is similar to previously studied cases. More

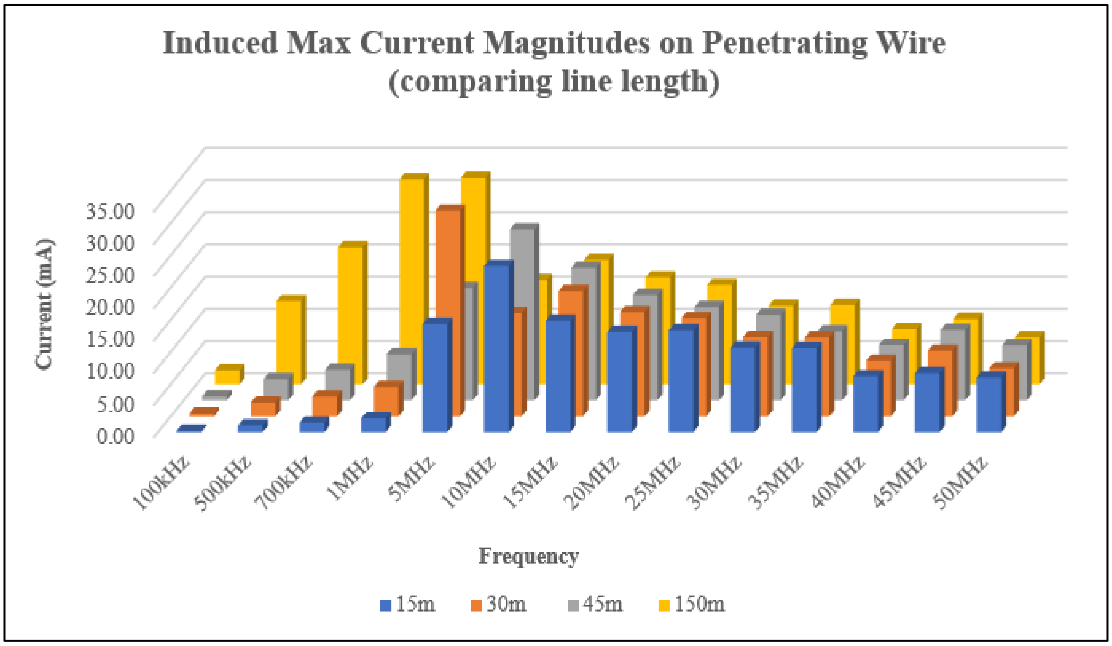

Figure 6.14 Maximum induced current magnitudes comparing line length.

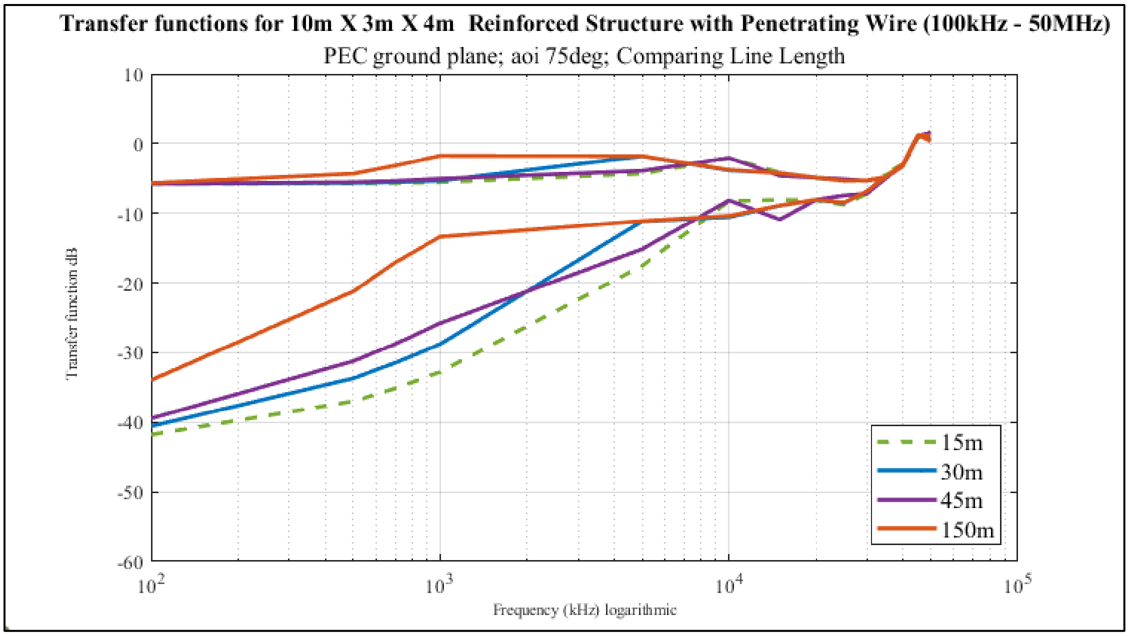

(a)

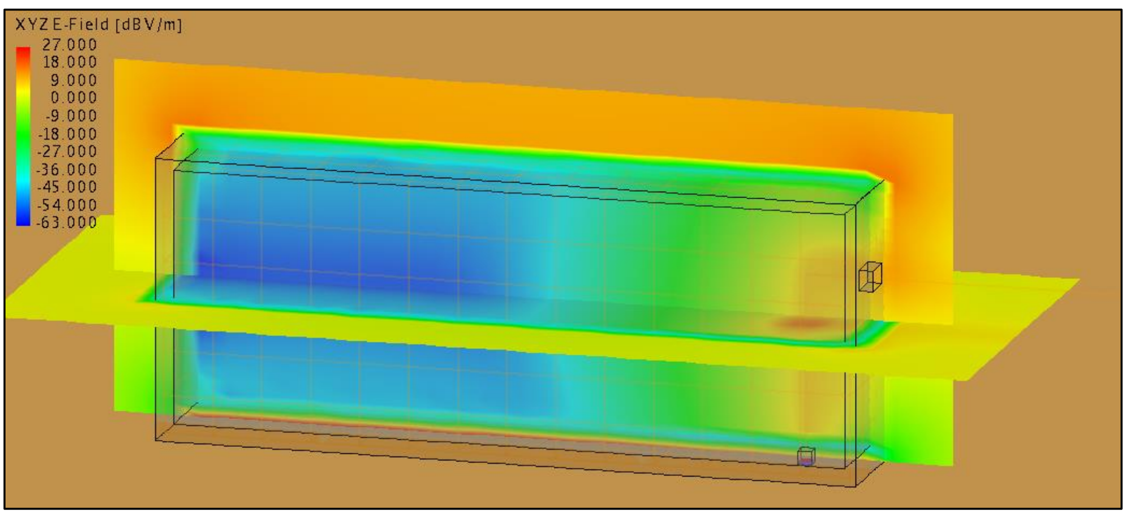

(b)

Figure 6.15 Structure attenuation transfer function comparing line length (a); E field visualization at 1 MHz excitation (b).

computationally intensive simulation is required for lines of even longer length. As the fundamental resonant frequency becomes smaller for longer lines, the resonant multiples also become closer together. In simple terms, more frequency analysis points are required to study very long lines. Also, simulation at low frequencies requires special attention as accuracy and convergence may become an issue.

6.5.7 Combined Parameters for Worst Case

Up to this point, the cable coupling parameters have been simulated individually. Although discrete simulations provide detailed insight into each parameter's effect, one of this work's themes is to analyze worst-case scenarios. Penetrating lines at real world power generation facilities may be large, high off the ground, and long. It is helpful to observe the combined effect from extreme cases, and thus a worst-case simulation is carried out. The worst-case model employs 5 cm radius, 3.35 m tall, and open circuited line with various overall lengths. Additionally, the line penetrates further into the facility interior to radiate more volume. In the worst-case model, the line penetrates 8 m into the interior compared to 1 m in the base case model. Results indicate a severe reduction in shielding effectiveness, especially for the E field at low frequencies. The reduction of H field attenuation is more significant at resonant frequencies. A moderate reduction in shielding effectiveness is observed for both E and H fields up to 30 MHz. The worst-case line at 10 m length reduced the E field attenuation by 10+ dB for most of the frequency range when compared to the base case; and the effect is even more profound for longer length lines. Figure 6.16 pictures the worst-case model simulation results.

The interior termination voltage results are compared for the three line lengths parameterized for the worst-case scenario. The termination of longer lines develops higher magnitude over voltages. Also, the longer lines possess many more resonance points as their fundamental resonant frequency is much lower. The interior termination voltage is plotted against frequency in Figure 6.17.

6.6 Shielded Cables

Extending the analysis from plain wires to shielded cables is of interest. The hybrid MoM MTL solution method is utilized for cable simulations to reduce total computational time. The structure and line are discretized; however, the line is solved with MTL and the external fields are solved with MoM. The hybrid method is validated against pure MoM for the standard frequency range of this thesis work. Termination voltage as a function of frequency is plotted for both solution methods in Appendix Figure A8.

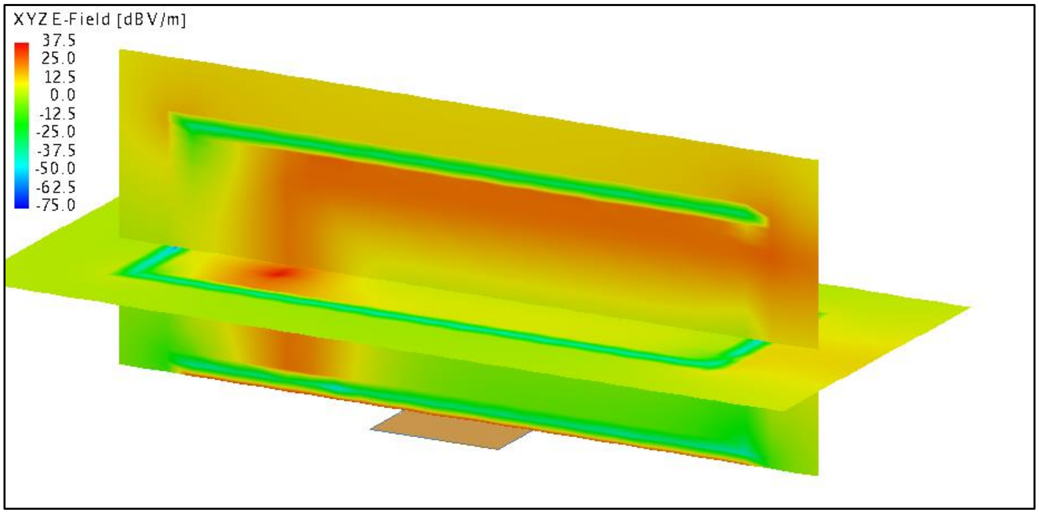

(a)

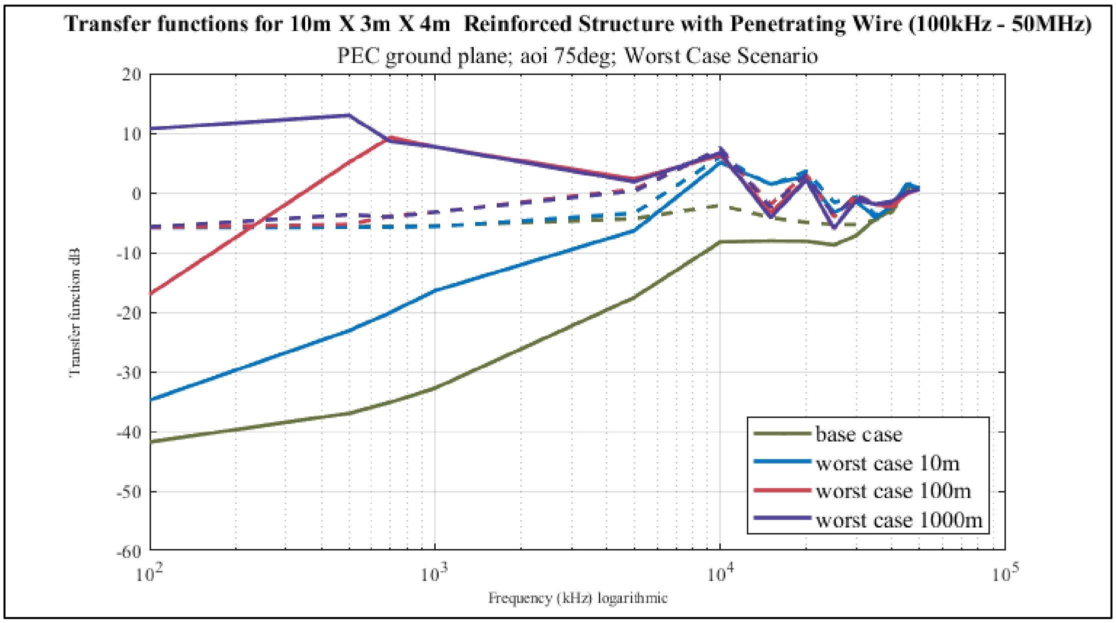

(b)

Figure 6.16 Worst case field results: (a) Electric field at 500 kHz, 1000 m line; (b) Transfer function E field solid lines, H field dashed lines.

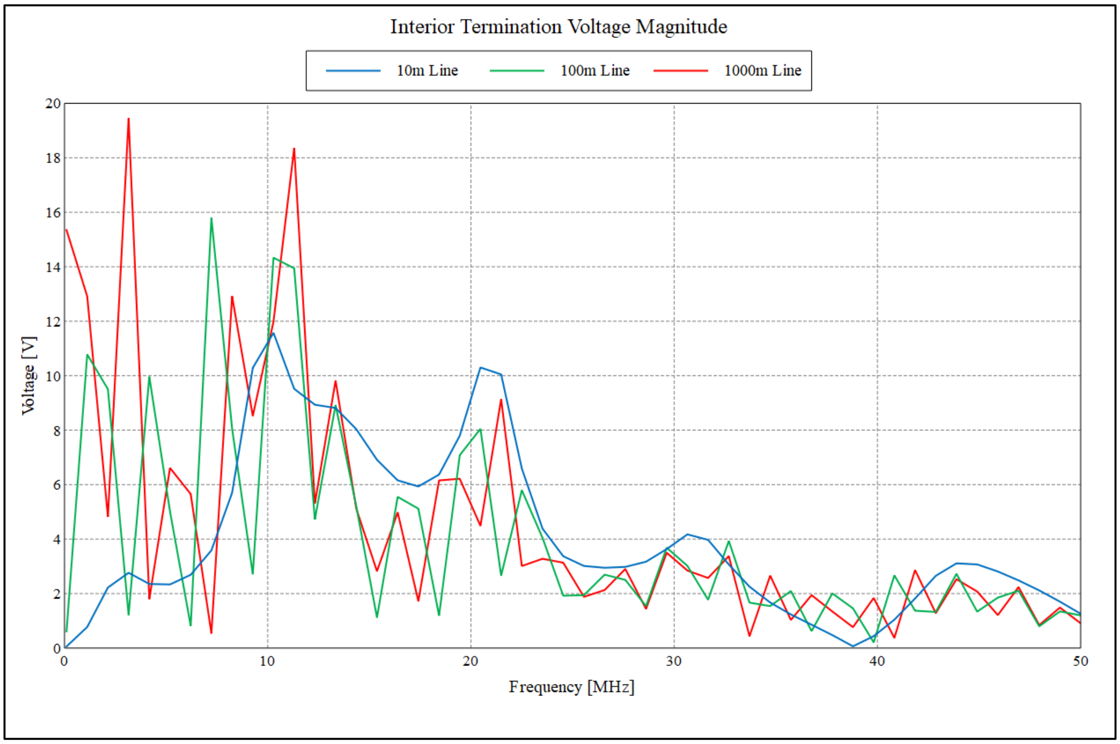

Figure 6.17 Worst case termination voltage vs. frequency for various line lengths.

With validation of the hybrid solution method, research questions regarding the effectiveness of cableshield as protection against E1 coupling can be answered. The insulation and/or braided shielding around cables is the differentiating factor as compared to wires and lines. Also, many cables may be placed together within a conduit, which may be metallic or non-metallic. The insulation around the cable is typically a dielectric such as oil/paper, cloth, or plastic. Some cable insulations include a metallic sheath, referred to as a cable shield. The function of the dielectric insulation is to electrically insulate the wires from each other, while the cableshield prevents electrical noise and electromagnetic interference (EMI) from penetrating or leaking into the wire. Various types of cable shields exist, with the two primary types being solid shields and braided shields. Two prominent researchers, Kley and Vance, have outlined definitions and parameters to characterize braided cable shields and their shielding performance [63], [64]. The FEKO software includes three different cable shield models: a solid shield, a braided shield defined by the Kley model, and a braided shield defined by the Vance model. Simulations are conducted to evaluate and compare the shielding effectiveness of the different models. A simple model including a 10 m long single conductor above the ground plane is shielded with the various cableshields as well as plain dielectric insulation. The inner conductor has a radius of 10 mm, the insulation is 2 mm thick, and each cableshield is approximately 2 mm thick. Two signal paths are defined in the cable: one for the conductor and the other for the shield. The conductor signal, traveling through pin1_1 and pin2_1, is terminated with impedance loads. The shield signal is grounded at pin1_2 and pin2_2. Figure 6.18 pictures the cable schematic.

The cables are illuminated by plane wave radiation at HEMP range frequencies, and the induced termination voltage is measured and compared. Of course, the solid shield, which is basically a cylinder around the entire length of the conductor, prevents virtually all electromagnetic coupling, and a near zero voltage appears at the termination. The cable with pure dielectric insulation couples as much energy as wire with no insulation, and 1.8 V is induced across the termination at the fundamental resonant frequency of 15 MHz. For reference the base test is at 1.0 V. The solid shield and plain insulated cable results are cross validated with both the MTL and MoM solution methods. The braided cable shields are a much more complex geometry and thus only MTL method is utilized. The braided shield effectiveness is comparable to the solid shield at all frequencies except those near the resonances. At frequencies near the resonance, the cable shield’s performance is highly dependent upon the geometrical construction of the braid. Geometrical parameters include individual shield wire diameter, number of carriers, number of wires in each carrier, and weave angle. Overall a braided shield can be characterized by its optical coverage K, which is how much surface area of the conductor is covered per unit length [64]. The higher the K value, the better the shielding

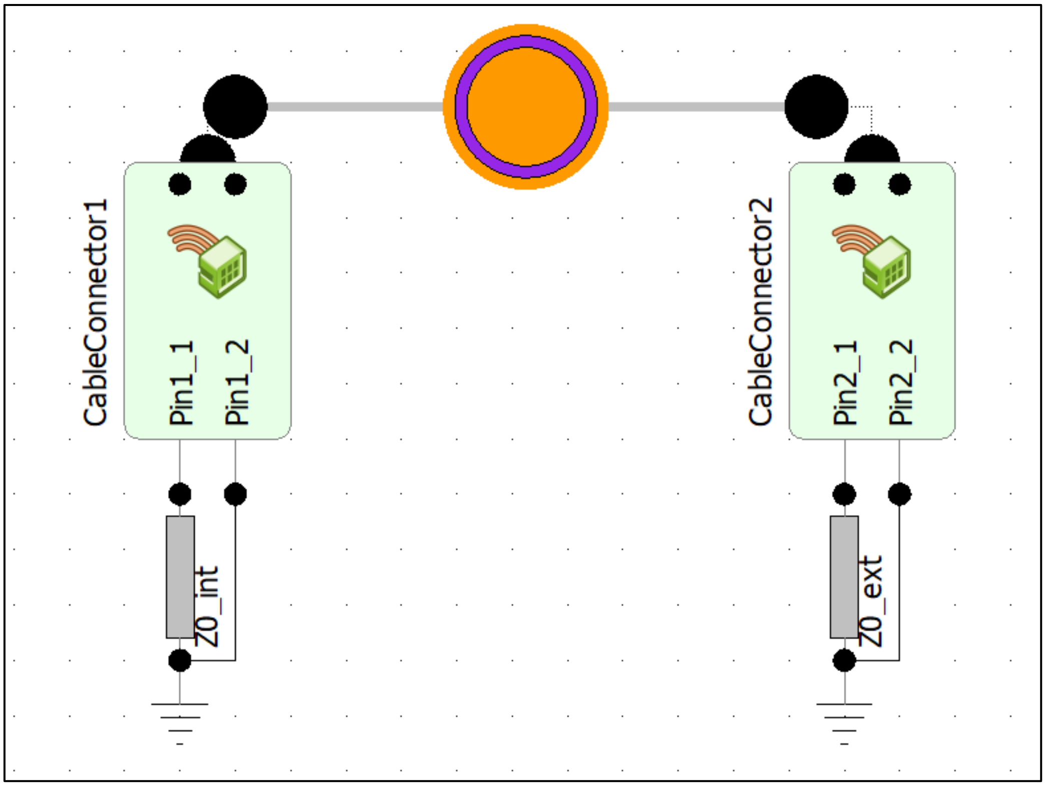

Figure 6.18 Cable signal circuit schematic.

effectiveness near resonant frequencies. The induced voltage is kept below 400 mV when *K* is 80%. Interestingly, the induced voltage at resonant frequencies for the braided shields with *K* at 50% is higher than an unshielded cable. Induced voltage results for the 50% covered cable can be found in Figure A9 of the Appendix, and results for an 80% covered cable are plotted below in Figure 6.19.

Next, the cable structure interaction is analyzed. The cable penetrates the reinforced concrete rectangular structure in a manner similar to the line simulations in prior sections. The conductor is 3 m above the ground and penetrates approximately 2 m into the structure's interior. The inner conductor radius is 5 cm and is separated from the shield with a 10 mm thick polyethylene dielectric insulation. The shield is modeled as PEC with a 10 mm thickness. The schematic in Figure 6.18 is also applicable to this set of simulations. Presence of an unshielded cable, regardless of insulation, reduces structure shielding by roughly 10 dB for most of the frequency range, excluding the low and high ends. The same model is simulated again except a solid cableshield is introduced. The conductor itself does not induce energy from the E1 pulse, and therefore connected equipment is safe from conducted electromagnetic threats. This also means the termination loads will not affect conducted and radiated energy. However, the metallic cableshield induces energy and acts as a separate conductor carrying coupled energy. When comparing with both an unshielded cable and a case without any cable present, the structure shielding is slightly improved at very low frequencies. More energy is transferred to the structure's interior from the shielded cable at frequencies above 6 MHz. The resonant effect is intensified when employing the shielded cable. For completeness, results from the two braided shield models are compared with the solid shield, and there is no difference regarding the energy carried by the shield into the building interior. Therefore, while the induced signal on the conductor depends on cable shield, the radiated fields inside structure do not. Figure 6.20 plots transfer function results for all the shielded cables.

It is common for the cableshield to be electrically grounded outside of the facility. Ideally, any induced signal would be directed to ground before entering the building interior. A few grounding methods are simulated to determine their respective effectiveness at preventing energy from entering the facility. A 10 m long solid shielded cable is simulated via the MoM. To reduce computational memory demand, the structure is modeled as a 3 m cube with 10 cm thick concrete walls. The first ground is modeled as a solid PEC wire which connects directly from the cableshield to the ground plane. This ground wire is placed right outside the building wall. The exterior grounding method is compared against cases where the cableshield is grounded at the ends of the line directly,

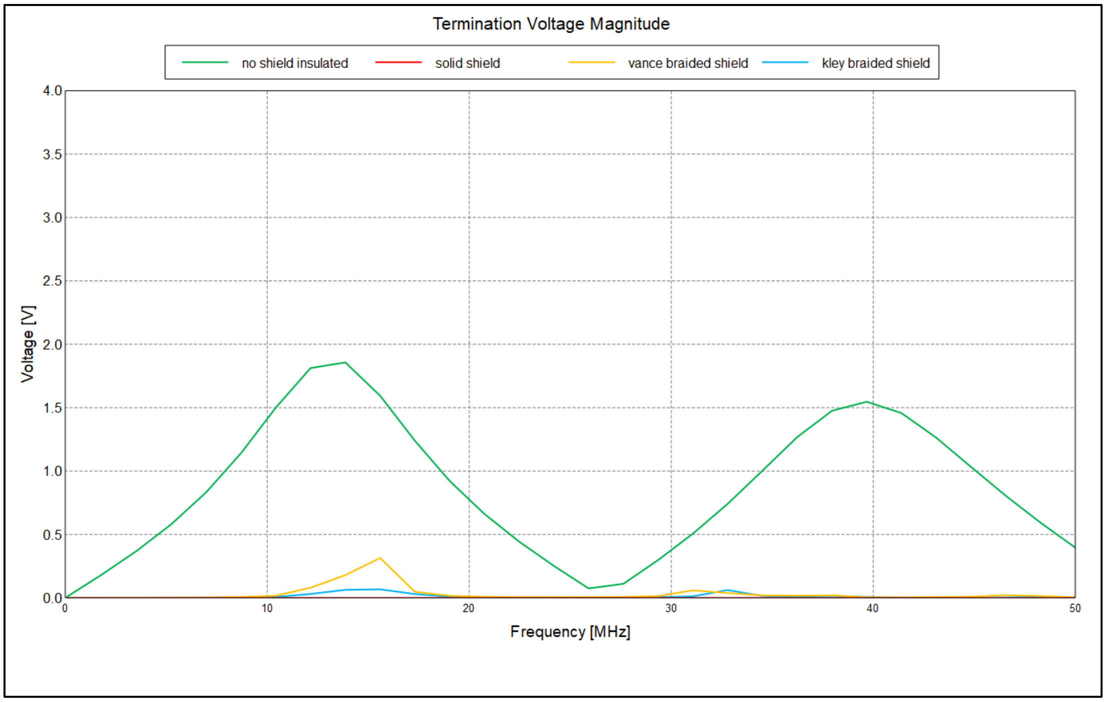

Figure 6.19 Induced cable voltage comparing effectiveness of different cableshields.

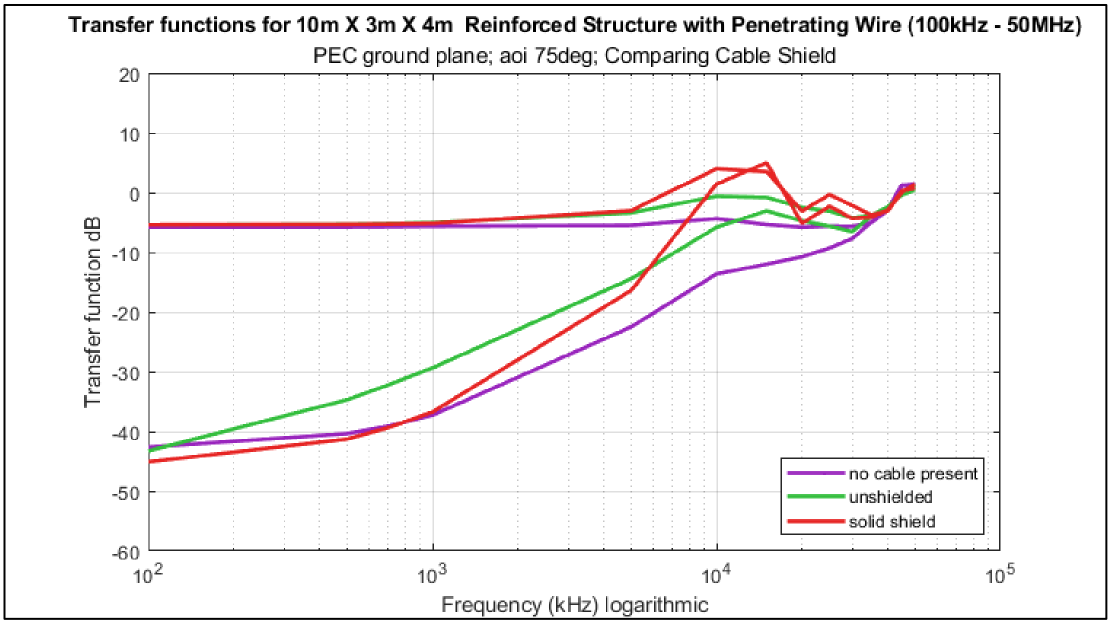

(a)

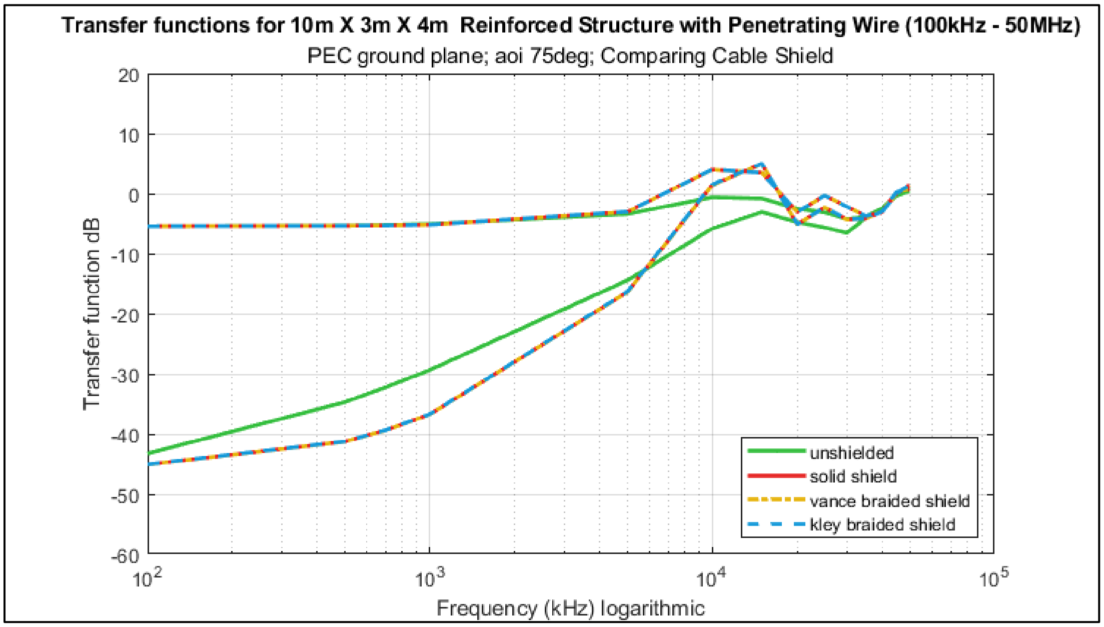

(b)

Figure 6.20 Structure attenuation transfer function comparing penetrating shielded vs. unshielded cables (a) and various cableshield types (b).

and where the cable shield is both terminated and grounded externally. For the latter, the unshielded cable continues to penetrate the structure. Results from the structure transfer function illustrate the cableshield termination location has little influence on average internal field strengths. Only at resonant frequencies does the exterior terminated cableshield mitigate interior field strength. For frequencies below 10 MHz, the grounding method constitutes no difference in average internal field strengths. However, the results indicate the exterior ground helps mitigate the intense energy from the fundamental resonance from entering the facility. In fact, the resonance is slightly shifted from ~12 MHz to ~15 MHz as the external ground effectively changes the length of the cable. Figure 6.21 displays the transfer function results, where the black lines represent the model where the cableshield is only grounded at the ends, colored lines represent the model with an extra external ground, and the dashed lines represent the model where the cable shield is also terminated outside of the structure. Figure 6.22 compares the induced current and field intensities for the models with an interior and exterior terminated cableshield both including the external ground. As previously mentioned, when the cableshield is terminated outside the facility, interior field strengths at resonant frequencies are reduced.

Proper grounding is very important for all electrical networks from the standpoint of safety, operating performance, and protection. Thus, further investigation of the simulated grounding methods and their performance is appropriate. As discussed previously in this work, the structure itself behaves as a high pass filter and the transfer function is dominated by the diffused field radiation. Conducted radiation contributes less. Therefore, to study the impact of cableshield grounding more thoroughly, the conducted radiation contribution should be increased. Results from section 5.3.2 indicate a near complete elimination of diffused field radiation when the structure exterior is plated with metal. If a penetrating cable is incorporated, any interior radiation will have resulted from such a cable. Simulation is conducted for a PEC plated cubical structure where a shielded cable penetrates a wall. Due to the plated walls, shielding effectiveness drastically improved, especially against the low frequency H field. Without the influence of diffused fields, the results are primarily dictated by the penetrating line and thus the resonance effects are dramatized. Throughout the low frequency region, the external ground reduces field intensity developed inside the structure, especially the H field. Overall, the performance of the external ground is more easily observed when conducted radiation is the dominant effect appearing in the transfer function results. Figure 6.23 plots the transfer functions for this special case.

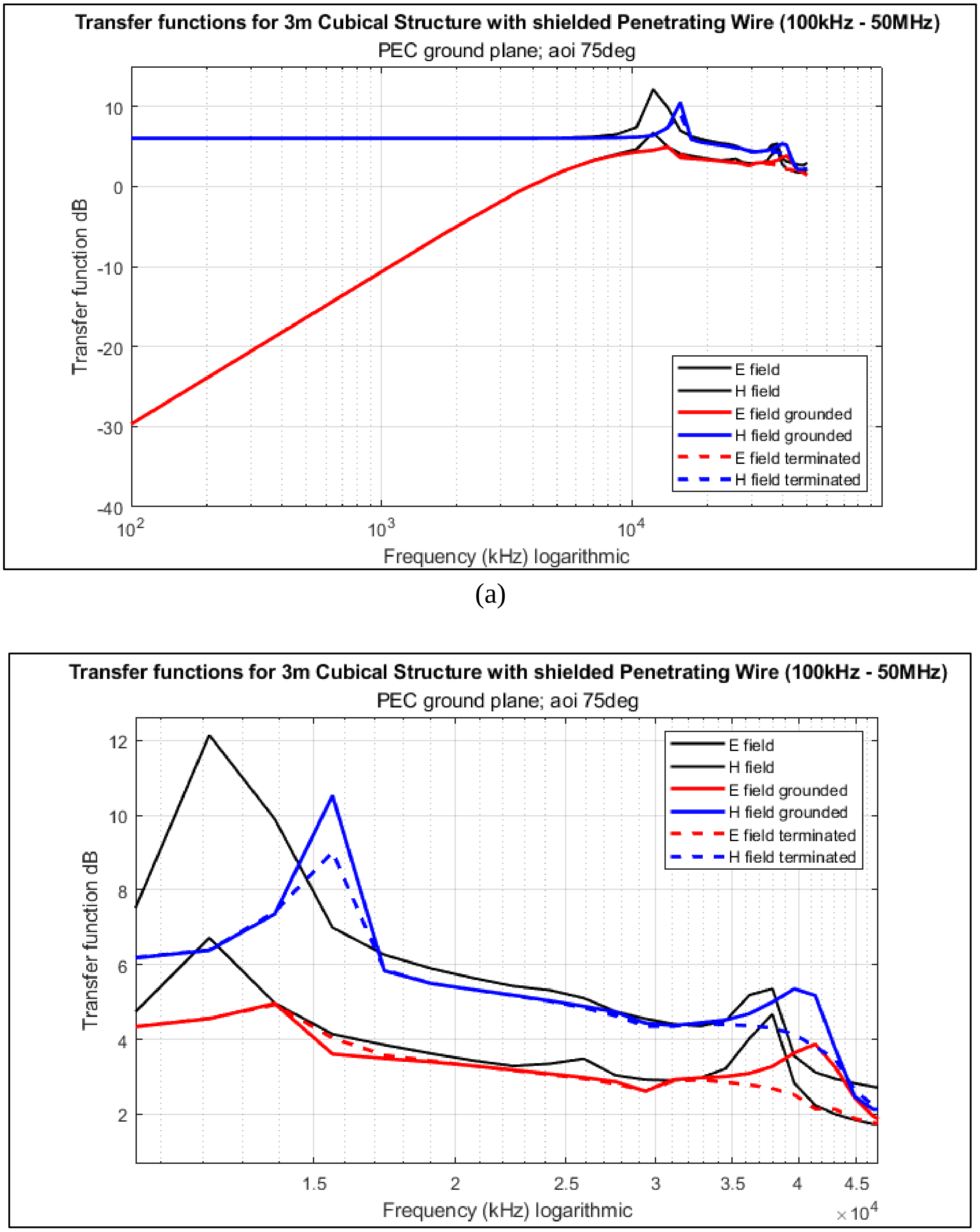

(a)

(b)

Figure 6.21 Structure transfer function comparing grounding locations; entire frequency range (a), resonance region (b).

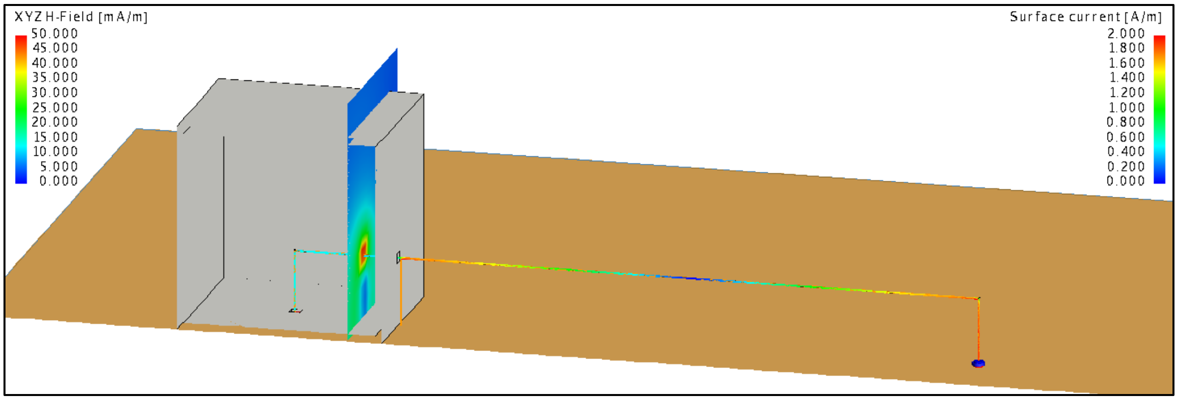

(a)

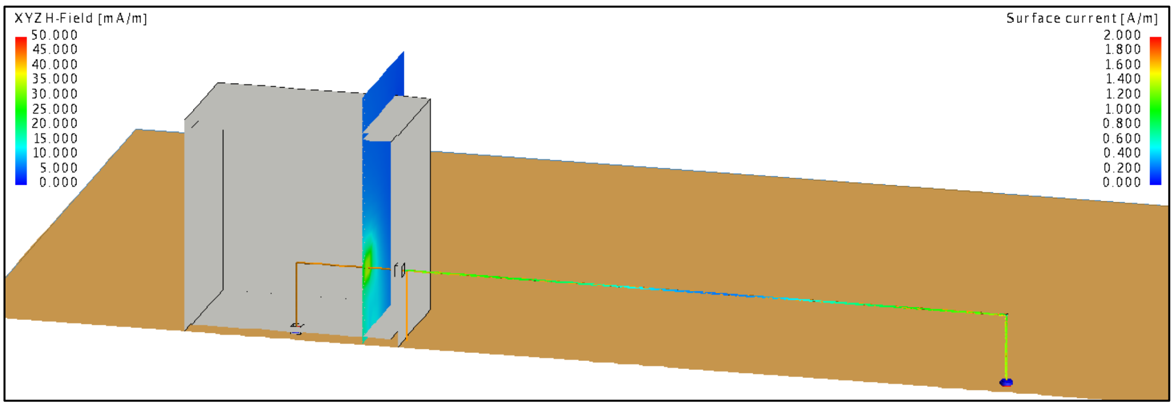

(b)

Figure 6.22 Interior H field intensities and induced cableshield currents for 15 MHz excitation frequency; interior terminated cableshield (a), exterior terminated cableshield (b).

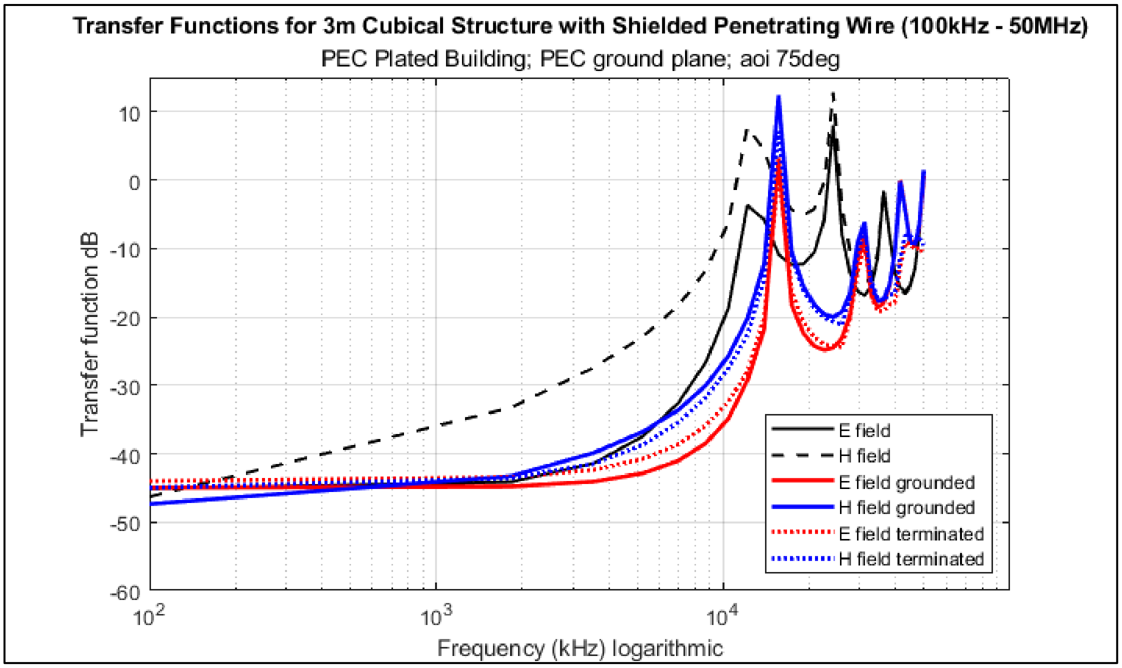

Figure 6.23 Shielded structure transfer functions comparing grounding methods.

Chapter 7

Conclusions

7.1 Conclusions from EMP Building Interactions

This work has studied several variables and their influence on electromagnetic penetration of structures associated with high-altitude electromagnetic pulse. Variation with the angle of incidence of the incoming radiation has little influence on the fields observed inside the structure when considering an averaged angle in the middle of the range. In general, higher AoI correlates to stronger induced fields. Strongest coupling effects are expected when the incoming radiation is vertically polarized because of the total magnetic field excitation. It was also observed for lower frequencies the excitation behavior replicated that of surface boundary condition behavior. When considering a structure's wall material, frequency dependence of the electrical properties does not constitute significant differences in structure's transfer function results. Using a frequency-independent model or a software defined media is reasonable. The same statement can be made regarding dielectric ground planes. No significant difference was observed when comparing a perfect electric conductor and dielectric ground plane, especially in the low frequency region. It is worthwhile to note the H field remains roughly constant throughout the low frequency region. However, the E field attenuation decreases quadratically as a function of frequency. This general behavior serves as a baseline for future studies. Overall, these results provide reasonable assumptions which can be applied as simplifications when studying more complex cases. The key conclusions from EMP building interaction studies are listed below.

- Polarized radiation induces the strongest fields.
- A concrete structure may accurately be modeled as a frequency-independent dielectric for simulation work.
- MoM may exhibit inaccuracies when modeling the ground plane as a dielectric.
- A structure's electric field attenuation transfer function highly depends on frequency and decreases with increasing frequency. Therefore, the structure behaves as a high pass filter.

7.2 Conclusions from Structure Design Characteristics

The initial findings from EMP building interaction fundamentals are applied in more complicated cases with more detailed models. The extra complexity regards variables associated with a structure's design and architecture. Characteristics such as apertures, composite construction, and geometrical layouts are studied. Glass windows diminish a structure’s shielding effectiveness, especially at lower frequencies. Locations near and perpendicular to the window’s surface are most susceptible to intense fields. No significant difference is observed for different types of glass with various conductivities. Even further diminished attenuation is observed at the lower frequencies when the windows are open. The average penetrating radiation is a function of total aperture surface area and not necessarily individual aperture placement or size. Therefore, a building’s reduction in attenuation for the diffused fields can be estimated by window surface area. The other aperture considered in this work is a large metallic bay garage door. The overall shielding is reduced; however, when the metallic door is closed, the vicinity immediately behind the wall is better shielded as compared to an open door. Any small gaps around the edge of the door serve as points of infiltration for radiation at higher frequencies due to diffraction. The most influential structure design characteristic is the incorporation of reinforcing bars into the concrete. Reinforced concrete composite construction constitutes significant shielding improvement for the both the electric and magnetic fields throughout the entire frequency range. The more closely the rebar is placed together, the better the attenuation. A metallic roof provides slightly improved shielding at the lowest frequencies, but due to surface waves and scattering effects, the edges of the metallic roof intensely radiate energy. A structure’s shielding effectiveness is immensely reduced if the roof edges are exposed to the interior. Finally, basic geometrical considerations were evaluated. Thicker walls enable better shielding throughout the frequency range as expected. A rectangular structure exhibits slightly better shielding at frequencies below 10 MHz, while a cubical structure exhibits improved shielding at higher frequencies. Attenuation is nearly unaffected when considering the direction of incident radiation upon the rectangular structure. Validation of the results is achieved by both convergence tests and, in some cases, time domain simulation. It is important to note, shielding against the magnetic field is very difficult, especially at lower frequencies. The only design characteristic which provided H field attenuation is the reinforcing bars. Therefore, buildings constructed to higher structural integrity standards and seismic classes will consequently possess better E1 shielding characteristics. More rebar, more concrete, fewer windows, and sealed doors are all characteristics which improve a structure’s shielding effectiveness against HEMP E1 diffused fields. To summarize, key conclusions are expounded in the bulleted list below.

- Critical equipment near the vicinity of large windows, doors, and other apertures is at risk of intensified fields.
- Diminished structure attenuation due to windows may be estimated by total window surface area.
- Tightly spaced reinforcement bars provide excellent shielding for both the electric and magnetic fields over a wide frequency band. The more rebar and concrete construction material the better.

7.3 Conclusions from Line/Cable Coupling

Conducted electromagnetic energy is one of the hazardous effects of HEMP. An exposed line or cable will conduct energy via the magnetic coupling effect, and the conducted energy will travel as an electrical transient. The transient may induce dangerously high voltages and currents to connected equipment and may re-radiate energy into a space where the cable enters. Variables associated with a structure-penetrating line were simulated to determine their influence. The penetrating line's electromagnetic response replicated that of a half wave antenna. Stronger coupling, which results in larger induced currents, is observed when the line is higher off the ground. A similar observation is made for lines with a larger radius. If an open circuit termination exists within the structure's interior, a significant voltage reflection occurs resulting in a significant amount of re-radiated energy. Such energy reduces the structure's electric field shielding by as much as 10 dB. Length of the penetrating line is the most influential parameter. Significantly larger currents are induced for longer lines (where the length is exposed to open air). Additionally, more energy at lower frequencies is coupled as the line length increases. Shielded cables are deemed effective to protect against conducted HEMP transients if the cableshield coverage exceeds 80%. Also, the grounding of the cableshield has influence on the energy carried into the structure's interior. It is recommended a proper ground be installed outside, before the cable penetrates a facility. The cableshield itself becomes a conductor of transients and thus shall be designed appropriately. Several conclusions from the cable coupling studies, which warrant caution, are listed below.

- High off the ground, large diameter wires such as power lines, induce larger currents and are more susceptible to stronger HEMP coupling in comparison to smaller lines.
- Single conductor above ground transmission networks couple energy from HEMP as half wave antennas where the fundamental resonance occurs at a wavelength which is double the physical line length.
- Radiative effects from penetrating lines are more significant at lower frequencies due to the structure's high pass filter characteristic.
- A structure which may exhibit excellent shielding by itself, could be vulnerable to electromagnetic threats if improperly grounded, or unshielded penetrating cables are present.

7.4 Overall Conclusions

Nuclear power plants erected with stricter construction standards are generally better shielded against HEMP. More rebar and concrete material aids in the structure's attenuation. In general, hydro power plants are relatively safe from HEMP because a large fraction of the infrastructure is placed deep within reinforced concrete which shields against E1 effectively. Regardless of fuel source, the electrical generator room may be constructed separate to the dam or reactor and thus could be more exposed to HEMP radiation. Generation facilities which are constructed with less material, such as gas or renewables, are relatively more susceptible to EMP hazards. Significant vulnerabilities exist for interior equipment placed near large apertures such as windows and doors. Equipment placed in complete exposure outside buildings is of course most vulnerable. Also, if penetrating cables exist, which are not shielded and grounded appropriately, significant amounts of EM energy can be coupled into the structure's interior. Considering the worst-case radiation scenario with peak field intensities, and illuminating a structure with apertures and penetrating cables, abnormal levels of EM radiation, in addition to electrical surges, are expected to develop inside a structure's interior. Different locations within the interior will experience various levels of EM intensity. Depending on the location, protection, and damage threshold of interior equipment, normal facility operations could be hindered.

7.5 Recommendations for Future Work

Mitigation and protection against HEMP is another area of study with great interest. It is possible that existing protection equipment, designed for other electromagnetic hazards and power system transients, may provide some mitigation against HEMP. Alternatively, after the E1 pulse, arresting equipment may be compromised, leaving a large vulnerability against the following E2 pulse. Ongoing work is being carried out to evaluate the performance of surge protection devices (SPD) against very fast transients. MoM is utilized to evaluate the EM coupling effects from HEMP and characterize the electrical surge, while circuit simulation is utilized to study a surge arrester's non-linear response in the time domain. The difficulty associated with this study is translating the frequency domain impedance of the coupling network into the time domain circuit. Expanding further to evaluate a variety of mitigation options is highly recommended so the industry can harden their systems effectively.

To reiterate, many of the results presented in this thesis serve as a collection of generalized observations. Such observations can be extended to more specific and complex study scenarios, and the simulation approach can be utilized for this future work. Additionally, the results from this work may be compared against. However, specific facilities may exhibit unique attenuation characteristics or excite different resonances, and therefore, it is of great interest to obtain results for detailed models. For example, modeling and simulating a specific structure in great detail including interior equipment, complex geometries, and protection may provide many insights. New vulnerabilities or securities may be realized upon simulation of a detailed model. More computational power and memory is required for detailed models.

The contents of this paper focus on EM radiation from the early time component (E1) of a high-altitude nuclear detonation represented as a plane wave. However, an EM pulse could also be generated from a non-nuclear device carried by a missile, aircraft, drone, or even land-based equipment producing a more localized effect. Radiation from non-nuclear EMP is commonly classified as intentional electromagnetic interference (IEMI) or high-power electromagnetic weaponry (HPEM). Although the radiation from IEMI does not threaten wide areas, serious hazards remain for individual facilities or substations which are targeted. Such EM sources typically operate at higher frequencies (microwave frequency range) compared to HEMP (radio frequency range). The non-nuclear EM attack vectors are a more probable avenue for adversaries in comparison to a nuclear event. The aforementioned information warrants further research, including simulations designed to study EM radiation from IEMI, to be conducted. Numerical methods such as ray launching geometric optics and other high frequency methods must be utilized to study IEMI.

List of References

[1] J. S. Foster, et al., "Report of the commission to assess the threat to the united states from electromagnetic pulse (EMP) attack. volume 1: Executive report", *National Research Council, Committee on Electromagnetic Pulse Environment*, Washington DC, 2004.

[2] Conrad L. Longmire, "On the Electromagnetic Pulse Produced by Nuclear Explosions", *IEEE Transactions on Antennas and Propagation*, Vol. AP-26, No. 1, January 1978.

[3] Conrad L. Longmire, "Justification and Verification of High-Altitude EMP Theory Part 1, LLNL-9323905, June 1986.

[4] E. Savage, J. Gilbert, and W. Radasky, "The early-time (E1) high-altitude electromagnetic pulse (HEMP) and its impact on the US power grid." Report Metatech, Goleta, CA, Meta-R-320, 2010.

[5] E. Conrad, et al., "Collateral Damage to Satellites from an EMP Attack", *United States Defense Threat Reduction Agency*, DTRA-IR-10-22, Fort Belvoir, VA, 2010.

[6] W. Radasky, "Generation of High-altitude Electromagnetic Pulse (HEMP)," *IEEE International Symposium on Electromagnetic Compatibility*, 2008.

[7] W. Karzas, and R. Latter, "Detection of the Electromagnetic Radiation from Nuclear Explosions in Space," *Physical Review*, vol. 137, no. 5B, pp. B1369-B1378, 1965.

[8] F. M. Tesche, "Continuous Wave Test Manual," NEMP Laboratory Measurement Note 64, 1994.

[9] R. Przesmycki, and M. Wnuk, "Susceptibility of it devices to HPM Pulse," *International Journal of Safety and Security Engineering*, vol. 8, no. 2, pp. 223-233, 2018.

[10] C. E. Baum, "From the electromagnetic pulse to high-power electromagnetics," *Proceedings of the IEEE*, vol. 80, no. 6, pp. 789-817, 1992.

[11] K. T. Bainbridge, "Trinity," Los Alamos Scientific Laboratory, Los Alamos, NM (USA), LA-6300-H, 1976.

[12] C. E. Baum, "EMP simulators for various types of nuclear EMP environments: An interim categorization," *IEEE transactions on antennas and propagation*, vol. EMC-20, no. 1, pp. 35-53, 1978.

[13] K. S. H. LEE, "EMP interaction: principles, techniques, and reference data: a handbook of technology from the EMP interaction notes," Dikewood Industries Inc., Albuquerque, NM, DC-EH-1289, 1980.

[14] S. Glasstone and P. J. Dolan, "The Effects of Nuclear Weapons," *United States Department of Defense*, 1977.

[15] D. Wang, et al., “Power Grid Resilience to Electromagnetic Pulse (EMP) Disturbances: A Literature Review,” *North American Power Symposium (NAPS)*, 2019.
[16] A. Wraight, W. D. Prather, and F. Sabath, "Developments in Early-Time (E1) High-Altitude Electromagnetic Pulse (HEMP) Test Methods," *IEEE transactions on electromagnetic compatibility*, vol. 55, no. 3, pp. 492-499, 2013.
[17] R. Horton, et al., "High-altitude electromagnetic pulse and the bulk power system potential impacts and mitigation strategies," Electric Power Research Institute, Palo Alto, CA, 3002014979, 2019.
[18] P. Barnes and J. Marable, “Transient response of nuclear power plant cables to high-altitude nuclear electromagnetic pulse (EMP),” Oak Ridge National Laboratory, TN (USA), ORNL-5152, 1976.
[19] P. Barnes, R. W. Manweller, and R. R. Davis, “The effects of nuclear electromagnetic pulse (EMP) on nuclear power plants,” Oak Ridge National Laboratory, TN (USA), ORNL-5029, 1977.
[20] D. M. Ericson, et al., “Interaction of electromagnetic pulse with commercial nuclear-power-plant systems,” Sandia National Laboratories, Albuquerque, NM, SAND82-2738, 1983.
[21] A. Aragon-Zavala, “Indoor Wireless Communications: From Theory to Implementation,” Wiley, 2017.
[22] A. A. Ayeni, A. A. Yusuf, and S. O. Onidare, "Correlation Between the Electromagnetic Properties of Building Materials and Wireless Signal Penetration Loss," *IEEE Transactions on Antennas and Propagation*, vol. 70, no. 12, pp. 12040-12048, 2022.
[23] “High Altitude Electromagnetic Pulse Protection for Ground-Based Facilities Performing Critical, Time-Urgent Work,” United States Department of Defense Interface Standard, MIL-STD-188-125-1, 1998.
[24] R. F. Harrington, "Matrix methods for field problems," *Proceedings of the IEEE*, vol. 55, no. 2, pp. 136-149, 1967.
[25] R. Garg, “Analytical and computational methods in electromagnetics,” Artech House, 2008.
[26] W. C. Gibson, “The method of moments in electromagnetics,” Chapman & Hall/CRC. 2007.
[27] Altair HyperWorks, User Manual for FEKO 14.0, 2015.
[28] LibreTexts Physics, “University Physics II” Chapter 16 Electromagnetic Waves, https://phys.libretexts.org/Bookshelves/University_Physics/University_Physics_(OpenStax)/Book%3A_University_Physics_II_-_Thermodynamics_Electricity_and_Magnetism_(OpenStax)/16%3A_Electromagnetic_Waves

[29] F. T. Ulaby, E. Michielssen, and U. Ravaioli, “Fundamentals of applied electromagnetics,” Boston: Prentice Hall, 2010.

[30] E. M. Purcell, “Electricity and magnetism,” Cambridge University Press, 2013.

[31] A. K. Kamra, and M. Ravichandran "On the assumption of the Earth's surface as a perfect conductor in atmospheric electricity," *Journal of Geophysical Research: Atmospheres*, vol. 98, no. D12, pp. 22875-22885, 1993.

[32] D. P. Mignardot, et al., “Electromagnetic Penetration of Structures with Applications in Vulnerability Assessment,” *International Conference on Innovations in Energy Engineering and Cleaner Production*, 2023.

[33] “IEEE Standard Method for Measuring the Effectiveness of Electromagnetic Shielding Enclosures,” Standards Committee of the IEEE Electromagnetic Compatibility Society, IEEE-STD-299-1991, 1991.

[34] “Chickamauga,” Tennessee Valley Authority, https://www.tva.com/energy/our-power-system/hydroelectric/chickamauga

[35] R. G. Olsen, and P. S. Wong "Characteristics of low frequency electric and magnetic fields in the vicinity of electric power lines." *IEEE Transactions on Power Delivery*, vol. 7, no 4, pp. 2046-2055, 1992.

[36] F. T. Ulaby, E. Michielssen, and U. Ravaioli, “Maxwell’s equations for time-varying fields,” in *Fundamentals of Applied Electromagnetics*, 6th ed., Boston: Prentice Hall, 2010, pp. 301.

[37] D. Cavka, N. Mora, F. Rachidi, and D. Poljak, “On the application of frequency dependent soil models to the transient analysis of grounding electrodes,” *Proceedings of the International Symposium of Electromagnetic Compatibility*, Brugge, Belgium, 2013.

[38] E. F. Vance, “Wave interaction with the soil,” in *Coupling to Shielded Cables*, Wiley, 1978.

[39] G. V. Keller and F.C. Frischknecht, “Electrical methods in geophysical prospecting,” New York: Pergamon Press, 1966.

[40] R. J. Lytle, "Measurement of earth medium electrical characteristics: techniques, results, and applications," *IEEE Transactions on Geoscience Electronics*, vol. 12, no. 3, pp. 81-101, 1974

[41] E. I. Parkhomenko, “Electrical properties of rocks,” Plenum Publishing Corp, 1967.

[42] USGS, Tennessee Geologic Map Data, Retrieved November 8, 2022, from https://mrdata.usgs.gov/geology/state/state.php?state=TN

[43] U.S. Department of the Interior, National Parks Service, Geology, November 8, 2022, from https://nps.gov/grsm/learn/nature/geology

[44] F. A. K. Kakar, K. A. Sani, and F. Elahi, “Essential factors influencing building penetration loss,” *Proceedings of the IEEE International Conference on Communication Technology*, 2008.

[45] M. M. Ibrahim, et al., "Optical, FTIR and DC Conductivity of Soda Lime Silicate Glass Containing Cement Dust and Transition Metal Ions." *Silicon*, vol. 8, pp. 443-453, 2016.

[46] M. Sołtys, et al., "Electrical and optical properties of glasses and glass-ceramics," *Journal of Non-Crystalline Solids*, vol. 498, pp. 352-363, 2018.

[47] L. D. Pye, H. J. Stevens, and W. C LaCourse, “Introduction to Glass Science,” United States: Springer, 2012.

[48] E. J. Fagan, and R. H. Lee, "The Use of Concrete-Enclosed Reinforcing Rods as Grounding Electrodes. "*IEEE Transactions on Industry and General Applications*, vol. IGA-6, no. 4, pp. 337-348, 1970.

[49] K. Majcher, et al., “Methods of Protecting Buildings against HPM Radiation—A Review of Materials Absorbing the Energy of Electromagnetic Waves,” *MDPI Journal on Materials*, vol. 13, 2020.

[50] Mignardot et al., “Effects on Structure’s Electromagnetic Shielding Effectiveness Considering Penetrating Cables Coupling Energy from HEMP Event,” *IEEE PES ISGT Conference*, 2024.

[51] F. M. Tesche, J. M. Keen, and C. M. Butler, "Example of the use of the BLT equation for EM field propagation and coupling calculations," *URSI Radio Science Bulletin*, no. 312, pp. 32-47, 2005.

[52] R. G. Olsen, and A. G. Tarditi, "EMP coupling to a straight conductor above ground: Transmission line formulation based on electromagnetic reciprocity," *IEEE Transactions on Electromagnetic Compatibility*, vol. 61, no. 3, pp. 919-927, 2018.

[53] A. G. Tarditi, et al., “High Voltage Modeling and Testing of Transformer, Line Interface Devices, and Bulk System Components Under Electromagnetic Pulse, Geomagnetic Disturbance, and other Abnormal Transients,” Oak Ridge National Laboratory (ORNL), Oak Ridge, TN (United States), 2019.

[54] F. M. Tesche and P. R. Barnes, "The HEMP response of an overhead power distribution line," *IEEE Transactions on Power Delivery*, vol. 4, no. 7, pp. 1937-1944, 1989.

[55] J. H. Marable, P. R. Barnes, and B. B. Nelson, “Power system EMP Protection,” Oak Ridge National Laboratory (ORNL), Oak Ridge, TN (United States), 1975.

[56] S. K. Pukkalla, and B. Subbarao, “Study on Modeling & Simulation Analysis of Electromagnetic Pulse (EMP) Coupling to Cables,” *15th International Conference on Electromagnetic Interference & Compatibility (INCEMIC)*, 2018.

[57] J. Wang, et al., "Transient responses of coaxial cables in an electrically large cabin with slots and windows illuminated by an electromagnetic pulse," *Progress in Electromagnetics Research*, vol. 106, pp. 1-16, 2010.

[58] W. Weeks, "Multiconductor transmission-line theory in the TEM approximation," *IBM Journal of Research and Development*, vol. 16, no. 6, pp. 604-611, 1972.

[59] Baum, C. E, T. K. Liu, and F. M. Tesche, "On the analysis of general multiconductor transmission-line networks," *Interaction Note 350*, 1978.
[60] F. M. Tesche, and C. M. Butler, "On the addition of EM field propagation and coupling effects in the BLT equation," *Interaction Note 588*, 2003.
[61] E. F. Vance, *Coupling to Shielded Cables*, New York: Wiley, 1978, pp. 45.
[62] G. J. Toman, and L. P. Gradin, “Power plant practices to ensure cable operability.” Electric Power Research Institute, Palo Alto, CA, 1992.
[63] T. Kley, "Optimized single-braided cable shields," *IEEE Transactions on Electromagnetic Compatibility*, vol. 35, no. 1, pp. 1-9, 1993.
[64] E. F. Vance, "Shielding Effectiveness of Braided-Wire Shields," *IEEE Transactions on Electromagnetic Compatibility*, vol. EMC-17, no. 2, pp. 71-77, 1975.

Appendix

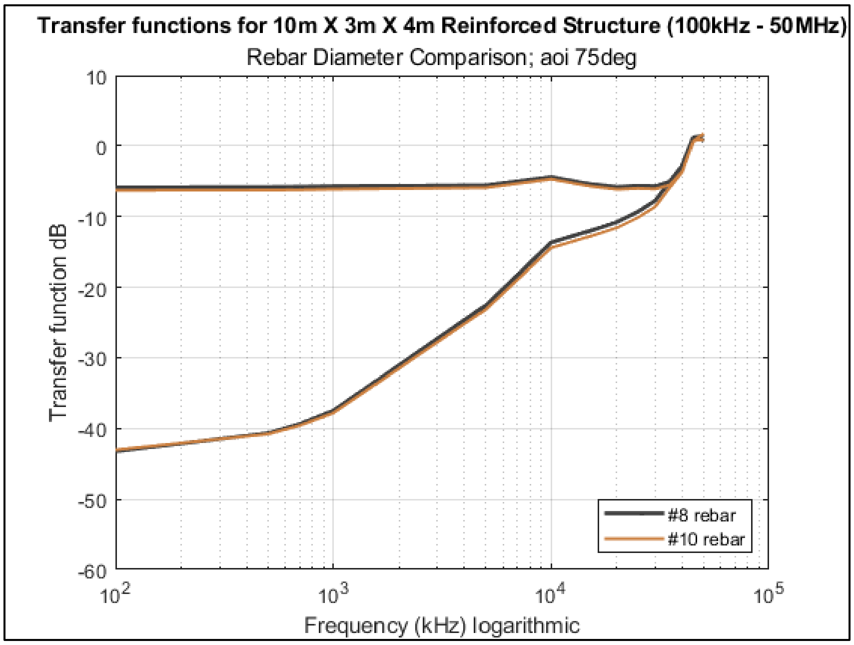

Figure A1. Reinforced structure transfer functions comparing rebar size.

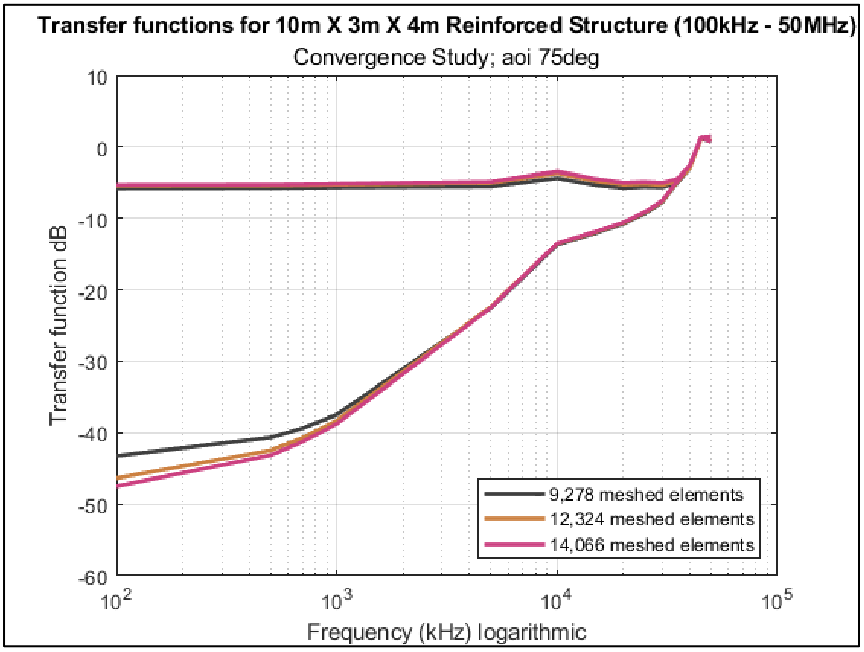

Figure A2. Reinforced structure transfer functions convergence study.

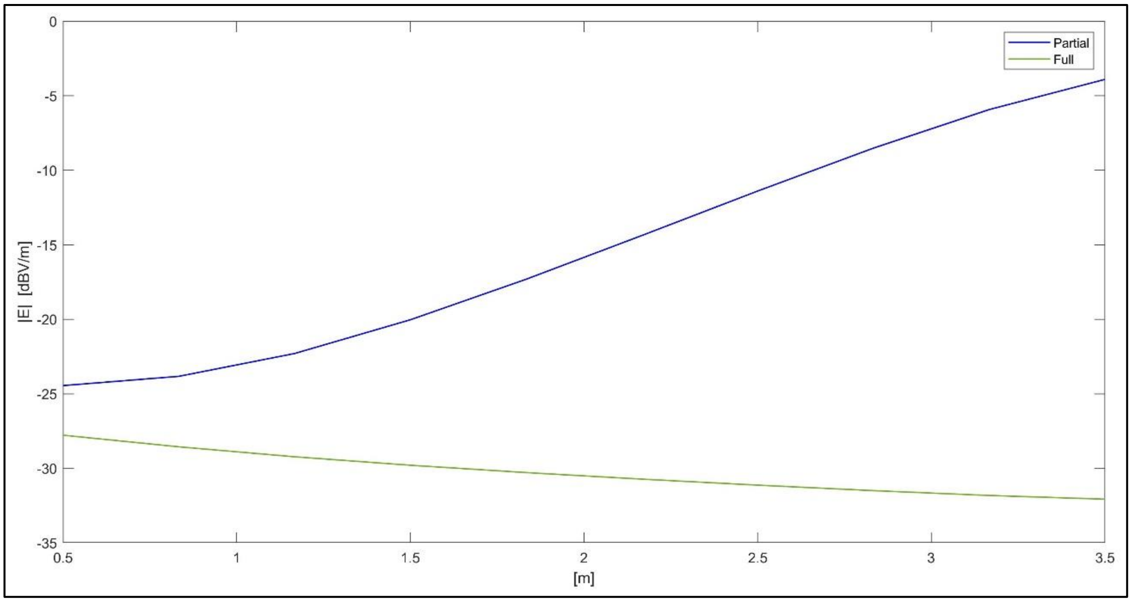

Figure A3. FDTD simulation results of E field vs. height above ground comparing a full coverage and partial coverage metallic roof.

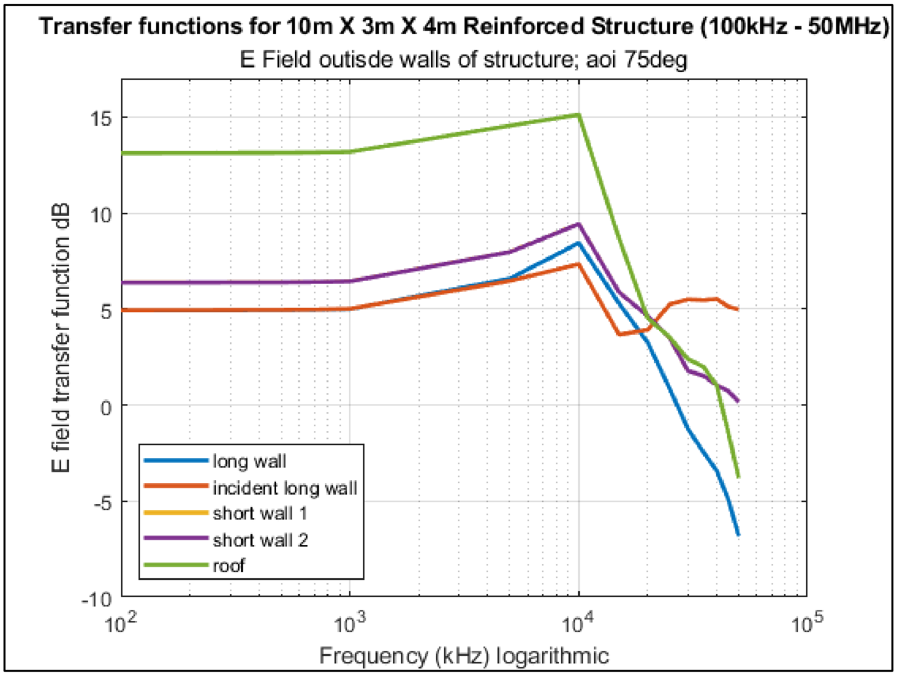

(a)

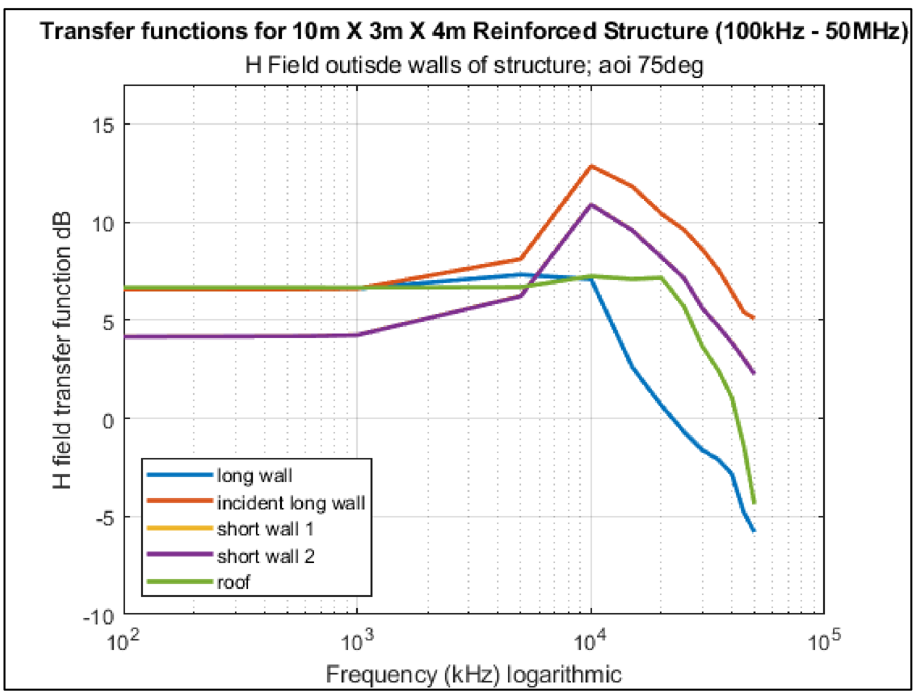

(b)

Figure A4. Field strength transfer functions, E field (a), H field (b), for volumes exterior to the structure.

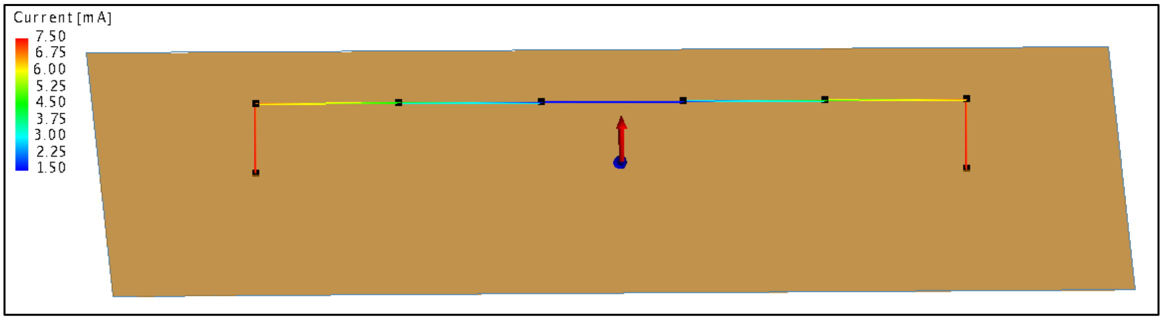

(a)

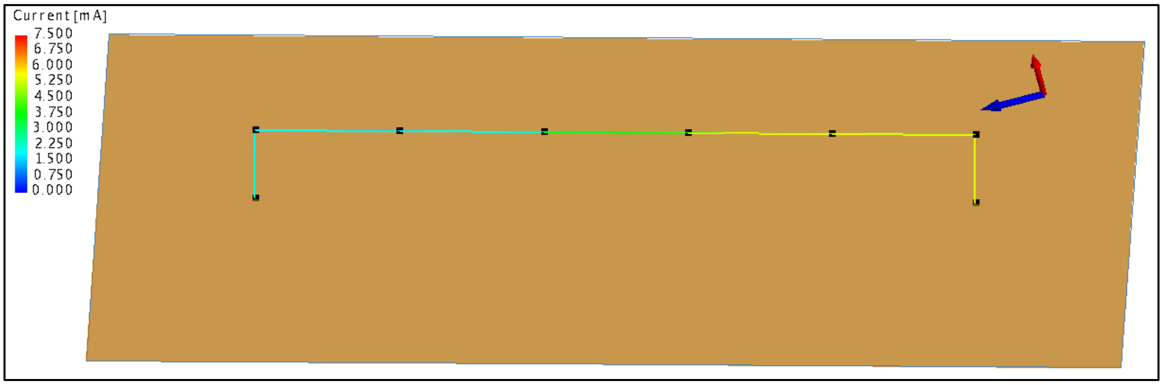

(b)

Figure A5. Induced currents when excitation is perpendicular to loop area (a), and parallel to loop area (b).

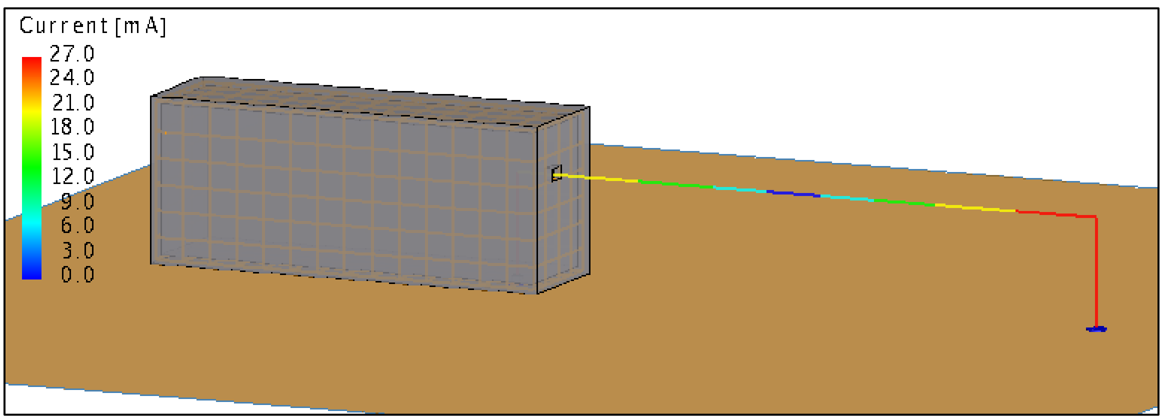

Figure A6. Induced currents at 10 MHz normalized excitation.

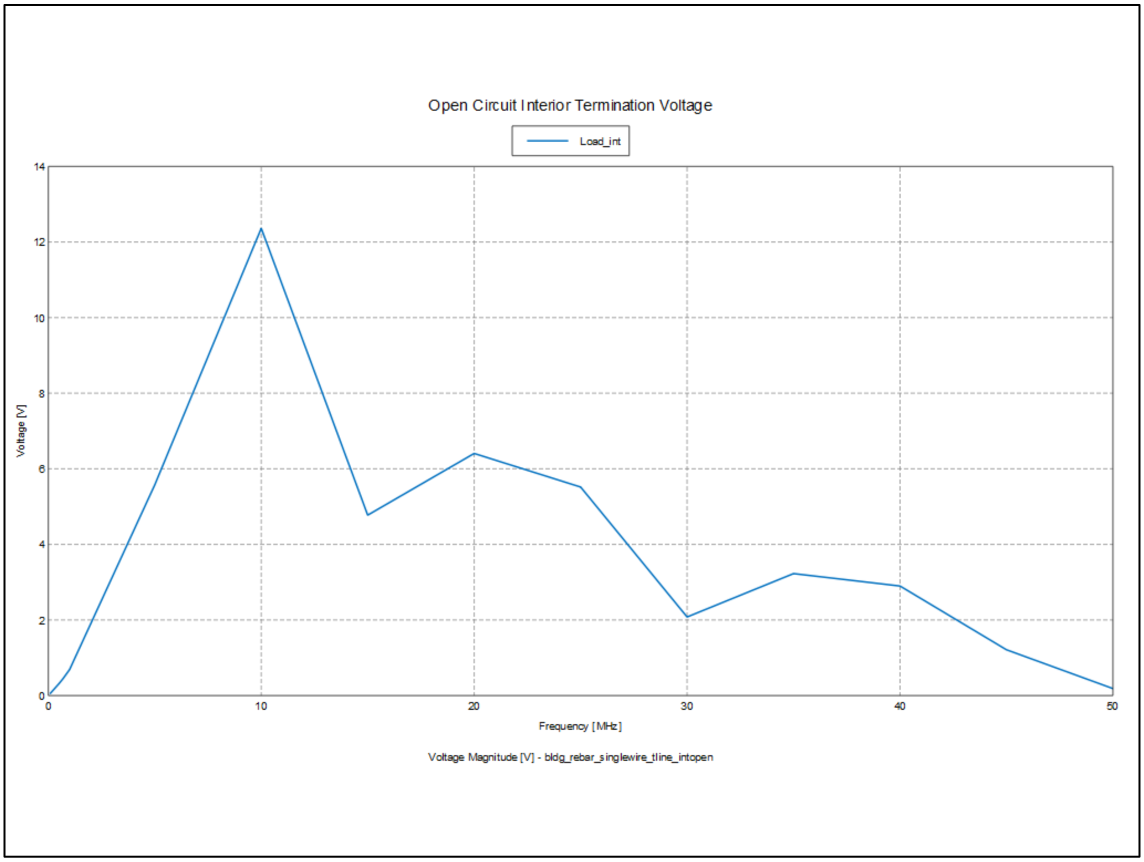

Figure A7. Interior termination voltage response when open circuited.

Table A1. Induced current magnitudes for various line lengths (normalized excitation).

Induced Max Current Magnitudes (mA) on Penetrating Wire (Comparing Line Lengths)														
Frequency	100kHz	500kHz	700kHz	1MHz	5MHz	10MHz	15MHz	20MHz	25MHz	30MHz	35MHz	40MHz	45MHz	50MHz
15m	0.20	1.03	1.46	2.15	16.77	25.79	17.29	15.54	15.81	13.10	13.02	8.66	9.18	8.50
30m	0.42	2.15	3.07	4.55	31.90	16.01	19.40	16.16	15.24	12.29	12.25	8.62	10.13	7.45
45m	0.64	3.29	4.75	7.13	17.44	26.51	20.58	16.34	14.46	13.24	10.68	8.60	10.94	8.56
150m	2.17	12.93	21.25	31.82	32.10	16.20	19.33	16.60	15.41	12.20	12.32	8.59	10.16	7.30

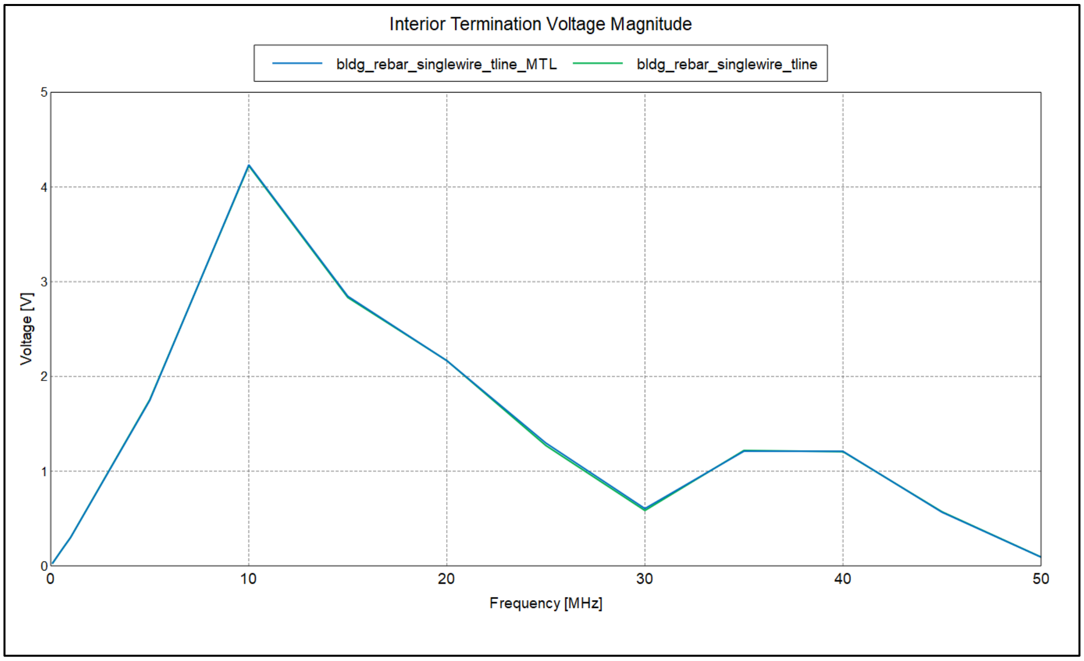

Figure A8. Termination voltage magnitude vs. frequency comparing MTL (blue) and MoM (green) methods.

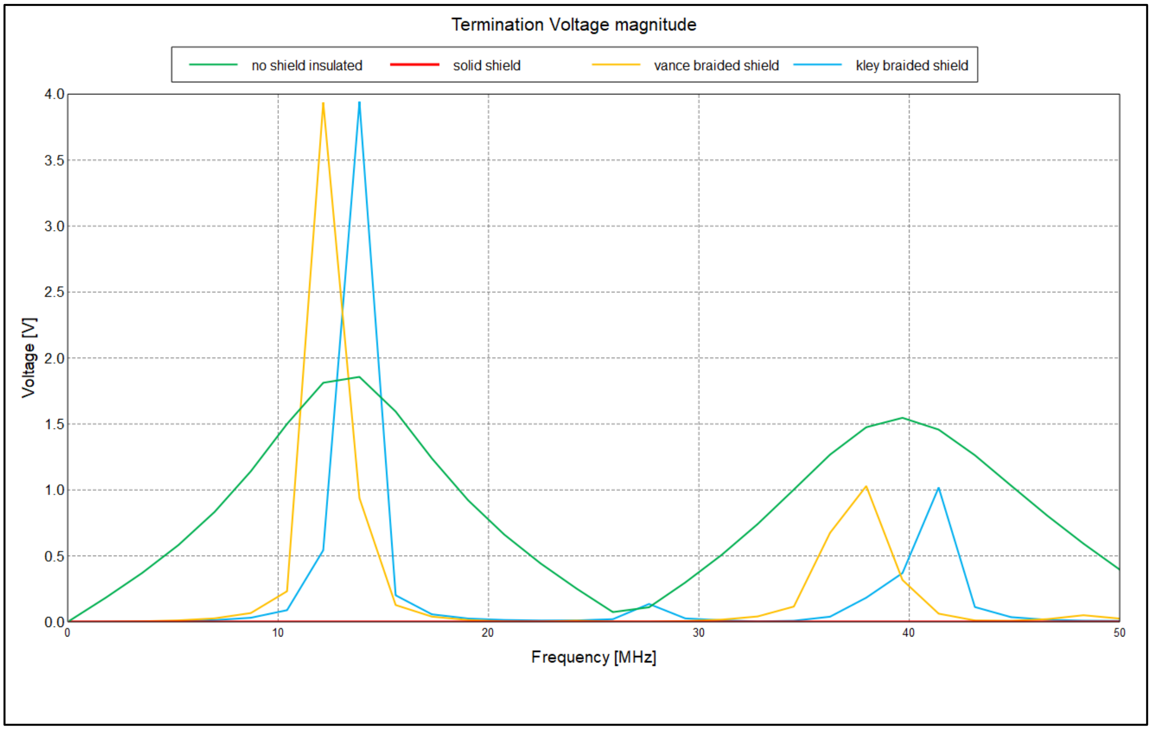

Figure A9. Induced cable voltage where cableshield coverage *K* is 50%.

Vita

David Mignardot, originally from Santa Fe, New Mexico, is currently a graduate student at the University of Tennessee Knoxville studying electrical power engineering. He is working as a student research assistant for the Center for Ultra-Wide-Area Resilient Electric Energy Transmission Networks (CURENT) research center. David received his Bachelor's of Science in Mechanical Engineering from New Mexico State University in May of 2022. He has worked two internships for Los Alamos National Laboratory as a Research and Development Engineer designing and testing equipment for high voltage pulsed power and particle accelerator systems. David hopes to pursue a career designing, maintaining, and operating electric power infrastructure and control systems.